

National Library of Canada

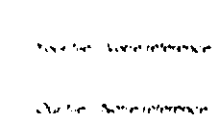
Acquisitions and

395 Wellington Street Ottawa, Ontano K1A 0N4

Bibliothèque nationale du Canada

Direction des acquisitions et Bibliographic Services Branch des services bibliographiques

> 395, rue Wellington Ottawa (Ontano) KIA ON4



#### NOTICE

The quality of this microform is heavily dependent upon the quality of the original thesis submitted for microfilming. Every effort has been made to ensure the highest quality of reproduction possible.

La qualité de cette microforme dépend grandement de la qualité la de thèse soumise microfilmage. Nous avons tout fait pour assurer une qualité supérieure de reproduction.

**AVIS** 

If pages are missing, contact the university which granted the degree.

S'il manque des pages, veuillez communiquer avec l'université qui a conféré le grade.

Some pages may have indistinct print especially if the original pages were typed with a poor typewriter ribbon or if the university sent us an inferior photocopy.

d'impression qualité certaines pages peut laisser à désirer, surtout si les pages été originales ont dactylographiées à l'aide d'un ruban usé ou si l'université nous a fait parvenir une photocopie de qualité inférieure.

Reproduction in full or in part of this microform is governed by the Canadian Copyright Act, R.S.C. 1970. C. C-30, and subsequent amendments.

La reproduction, même partielle, de cette microforme est soumise à la Loi canadienne sur le droit d'auteur, SRC 1970, c. C-30, et ses amendements subséquents.

# ( anada

# FINITE ELEMENTS AND VECTOR ABSORBING BOUNDARY CONDITIONS IN 3-D

by

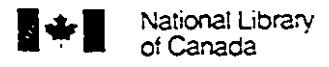
Vassilios N. Kanellopoulos, B.Sc.Physics, M.Eng.

A thesis submitted to the Faculty of Graduate Studies and Research in partial fulfillment of the requirements for the degree of Doctor of Philosophy



Electrical Engineering Department
McGill University
Montréal, Québec, Canada
December, 1991

© Vassilios N. Kanellopoulos



Acquisitions and Bibliographic Services Branch

395 Weilington Street Ottawa, Ontano K1A 0N4 Bibliothèque nationale du Canada

Direction des acquisitions et des services bibliographiques

395, rue Wellington Ottawa (Ontano) K1A 0N4

Note that Soften references

Orbin Actinizationen

The author has granted an irrevocable non-exclusive licence allowing the National Library of Canada to reproduce, loan, distribute or sell copies of his/her thesis by any means and in any form or format, making this thesis available to interested persons.

L'auteur a accordé une licence irrévocable et non exclusive à la Bibliothèque permettant nationale dи Canada reproduire, prêter, distribuer ou vendre des copies de sa thèse de quelque manière et sous quelque forme que ce soit pour mettre des exemplaires de cette thèse à la disposition des personnes intéressées.

The author retains ownership of the copyright in his/her thesis. Neither the thesis nor substantial extracts from it may be printed or otherwise reproduced without his/her permission. L'auteur conserve la propriété du droit d'auteur qui protège sa thèse. Ni la thèse ni des extraits substantiels de celle-ci ne doivent être imprimés ou autrement reproduits sans son autorisation.

ISBN 0-315-87567-4



Στους γονεις μου

To my parents

#### Abstract

The use of the Finite Element Method (FEM) for the numerical solution of electromagnetic scattering in unbounded regions requires proper boundary conditions on the outer surface that truncates the infinite three-dimensional space. In this work new vector absorbing boundary conditions are proposed that: a) cause almost no reflection on the outer surface for the outward radiation, and b) preserve the symmetry and sparsity of the finite element matrices.

A computer program was written to implement the new boundary condition. The program uses curvilinear finite elements which do not introduce spurious corruptions. The errors due to incomplete absorption decrease as the outer surface is moved further away from the scatterers. An error of about 1% in near-field values was obtained with the second order-absorbing boundary condition, when the outer surface was less than half a wavelength from the scatterer.

Abstract ii

#### Résumé

L'utilisation de la Méthode des Eléments Finis (MEF) pour la résolution numérique des problèmes de diffusion d'ondes électromagnétiques en milieux ouverts nécessite la définition de conditions aux limites propres sur la surface externe tronquant l'espace tridimensionnel infini. Le travail présenté dans cette thèse a conduit à proposer de nouvelles conditions vectorielles aux limites absorbantes qui a) n'occasionnent quasiment aucune réflexion du rayonnement progressif sur la surface extérieure et, b) conservent aux matrices d'éléments finis leur caractère symétrique et creux.

Un programme informatique a été élaboré pour mettre en oeuvre les nouvelles conditions aux limites. Ce programme utilise des éléments finis curvilignes qui ont l'avantage de ne pas introduire des solutions parasites. On observe une diminution de la marge d'erreur résultant de l'absorption incomplète à mesure que l'on déplace la surface externe à une distance croissante de la source de diffusion. Un taux d'erreur d'environ 1% dans les valeurs du champ proche a été obtenu avec les conditions aux limites absorbantes de second ordre lorsque la surface externe était placée à une distance inférieure à une demie longueur d'onde de la source de diffusion.

Résumé iii

#### Περιληψη

των πεπεδασίτενων στοιχειών.

Η χρήση της Μεθοδου των Πεπεδασίτενων Στοιχειών (ΜΠΣ) για την αριθμητική επιλυσή Απόρο. Σ' αυτήν την διατριβή προτεινονται νεες διανυσίτατικες απορροφητικές οριακές συνθήκες οριακές συνθήκες επι της εξωτερικής επιφανείας που αποκοπτεί τον απείδο τρισδιαστάτο οριακές αυνθήκες επι της εξωτερικής επιφανείας που αποκοπτεί τον απείδο τρισδιαστάτο απόροβληματών ηλεκτρομαγνητικής σκεδασής σε ανακλάσεις επι της εξωτερικής επιφανείας στην προβληματών ηλεκτρομαγνητικής σκεδασής σε ανακλάσεις επι της εξωτερικής επιφανείας στην απόροβληματών ηλεκτρομαγνητικής σκεδασής σε ανακλάσεις επι της εξωτερικής επιφανείας στην προβληματών ηλεκτρομαγνητικής σκεδασής σε ανοικτές περιοχές, χρειαζεται καταλλήλες απόροβληματών ηλεκτρομαγνητικής σκεδασής σε ανακλάσεις επι της εξωτερικής επιφανείας στην προβληματών ηλεκτρομαγνητικής σκεδασής σε ανακλάσεις επι της εξωτερικής επιφανείας στην απόροβληματών ηλεκτρομαγνητικής σκεδασής σε ανακλάσεις επι της εξωτερικής επιφανείας στην απόροβληματών ηλεκτρομαγνητικής σκεδασής σε ανακλάσεις επι της εξωτερικής επιφανείας στην προβληματών ηλεκτρομαγνητικής σκεδασής ανακλάσεις επι της εξωτερικής επιφανείας στην απόροβληματών ηλεκτρομαγνητικής σκεδασής ανακλάσεις επι της εξωτερικής επιφανείας στην απόροβληματών ηλεκτρομαγνητικής σκεδασής ανακλάσεις επι της εξωτερικής επιφανείας στην απόροβληματών ηλεκτρομαγνητικής σκεδασής ανακλάσεις επι της εξωτερικής επιφανείας στην απόροβληματών ηλεκτρομαγνητικής ανακλάσεις επι της εξωτερικής επιφανείας στην απόροβληματών ηλεκτρομαγνητικής ανακλάσεις επι της εξωτερικής επιφανείας στην απόροβληματών ηλεκτρομαγνητικής ανακλάσεις επι της εξωτερικής επιφανείας στην απόροβληματών ηλεκτροματών στην απόροβληματών ηλεκτροματών επιφανείας στην απόροβληματών ηλεκτροματών στην απόροβληματών ηλεκτροματών απόροβληματών στην απόροβληματών στην απόροβληματών 

μικροτερή του μισου μήκους κυματος απο τον σκεδαστή.

Οι νεες αυτες οριακες συνθήκες, οταν η εξωτερική επιφανεια βρισκοταν σε αποστασή απορροφήτικες οριακες συνθήκες, οταν η εξωτερική επιφανεια απομακρινεται απο τους σκεδαστες. Σφαλματα της ταξής του 1% στις τιμές του κοντίνου πεδίου παρατηρήθηκαν με δευτέρου βαθμου βαθμου ταξής του 1% στις τιμές του κοντίνου πεδίου παρατηρήθηκαν με δευτέρου βαθμου βαθμου 1% στις τιμές του κοντίνου πεδίου παρατηρήθηκαν με δευτέρου βαθμου βαθμου 1% στις τιμές του κοντίνου πεδίου παρατηρήθηκαν με δευτέρου βαθμου βαθμου 1% στις τιμές του κοντίνου πεδίου παρατηρήθηκαν με δευτέρου βαθμου βαθμου 1% στις τιμές του κοντίνου πεδίου παρατηρήθηκαν με δευτέρου βαθμου βαθμου 1% στις τιμές του κοντίνου πεδίου παρατηρήθηκαν με δευτέρου βαθμου βαθμου 1% στις τιμές του κοντίνου πεδίου παρατηρήθηκαν με δευτέρου βαθμου βαθμου 1% στις τιμές του κοντίνου πεδίου παρατηρήθηκαν με δευτέρου βαθμου 1% στις τιμές του κοντίνου πεδίου παρατηρήθηκαν με δευτέρου βαθμου 1% στις τιμές του κοντίνου πεδίου παρατηρήθηκαν με δευτέρου βαθμου 1% στις τιμές του κοντίνου πεδίου παρατηρήθηκαν με δευτέρου βαθμου 1% στις τιμές του κοντίνου πεδίου παρατηρήθηκαν με δευτέρου βαθμου 1% στις τιμές του κοντίνου πεδίου παρατηρήθηκαν με δευτέρου βαθμου 1% στις τιμές τι

# Contributions to Original Knowledge

- a) New n th order Absorbing Boundary Conditions have been developed for the 3-D vector wave equation.
- b) A new functional has been derived implementing the second order Absorbing Boundary Conditions (ABC). The functional leads to a symmetric matrix problem, which was previously not possible.
- c) It has been shown how the new functional can be used with tangentially-continuous finite elements of mixed order the kind necessary to eliminate the effects of spurious corruptions. In particular, it has been shown that additional, normal continuity of the field is needed on the Absorbing Boundary Surface (ABS).
- d) Computational results have confirmed what was until now a theoretical conjecture: that the second-order ABC gives significantly more accuracy than first-order, at no extra cost. Field values of about 1% error where obtained with the second-order ABC when the ABS was placed less than a half wavelength away from the scatterer.

### Acknowledgements

First of all I would like to express my sincere respect and appreciation to my supervisor Dr. J.P. Webb for his acute counselling and guidance, his invaluable mathematical enlight-enments throughout my research, and his determination to go on at critical times. I thank him for his loyalty to the principle: originality can never be something that only looks good.

I am also deeply grateful to Dr. D.A. Lowther and Dr. P.P. Silvester for their fruitful discussions and comments and for the facilities they provided, Dr. T.J.F. Pavlásek for sharing with me elements of his life-time research experience, Dr. Steve McFee for his valuable contribution and Dr. Nick Chepurniy from Cray Research Canada for his patience and willingness to provide computer time and efficient software tools on the Cray computers.

To my parents Nikolaos and Maria in Thessaloniki-Greece I owe the most. Their love, faith, continuous interest and constant care, were strongly felt at all times regardless the distance. I thank them from the bottom of my heart. Special thanks are addressed to Valérie in Paris-France for her affection and devotion.

I also thank my uncles Dino and Billy in Montréal-Canada for their help and encouragement during the long years of my research at McGill university and the members and ex-members of the CADLab for their cooperation and friendship.

Financial support from the Natural Sciences and Engineering Research Council (NSERC) of Canada and the Centre de Recherche Informatique de Montréal (CRIM) is gratefully acknowledged.

#### Ευχαριστιες

Εν πρωτοις θα ηθελα να εκφρασω τον ειλικρινή σεβασμο και εκτιμήση μου στον επιβλεποντα καθηγήτη μου, διδακτορα J.P. Webb για την οξυδερκή επιβλεψή και καθοδήγηση του, τις ανεκτιμήτες μαθηματικές διαφωτίσεις του καθ' όλη τη διαρκεία της ερευνής μου, και για την αποφασιστικότητα του να προχωρεί στις κρισίμες στίγμες. Τον ευχαρίστω για την πίστη του στην αρχή η πρωτοτυπία πότε δεν μπόρει να είναι κατί που μόνο φαίνεται ομόρφο.

Επισης ειμαι βαθυτατα ευγνωμων στους διδακτορες D.A. Lowther και P.P. Silvester για τις γονιμες συζητησεις και σχολια τους, και για τις διευκολυνσεις που μου παρειχαν, στον διδακτορα T.J.F. Pavlásek που μοιραστηκε μαζι μου στοιχεια απο την δια βιου ερευνητική του πειρα, στον διδακτορα Steve McFee για την πολυτιμή συμβολή του και στον διδακτορα Nick Chepumiy απο την Cray Research Canada για την υπομονή του και προθυμια του να παρασχει υπολογιστικό χρονο και αποδοτικά εργαλεία λογισμικού στους υπολογιστες Cray.

Στους γονεις μου Νικολαο και Μαρια στη Θεσσαλονικη της Ελλαδος οφειλω τα περισσοτερα. Η αγαπη τους, η πιστη τους, το διαρκες ενδιαφερον και η συνεχης φροντιδα ησαν εντονα και διαρκως αισθητα παρα την αποσταση. Τους ευχαριστω εκ βαθους καρδιας. Ειδικες ευχαριστιες απευθυνονται στη Valérie στο Παρισι της Γαλλιας για την τρυφεροτητα και την αφοσιωση της.

Επισης ευχαριστω τους θειους μου Ντινο και Μπιλλυ στο Μοντρεαλ του Καναδα για την βοηθεια τους και τις ενθαρρυνσεις τους κατα την διαρκεια των μακρων ετων της ερευνης μου στο πανεπιστημιο McGill, και τα τωρινα και παλαιοτερα μελη του εργαστηριου CAD για την συνεργασια και φιλια τους.

Τελος αναγνωρίζεται με ευγνωμοσύνη η οικονομική υποστηρίξη από το Συμβουλίο Ερευνής Φυσικών Επιστήμων και Μηχανολογίας (NSERC) του Κανάδα και το Κεντρο Ερευνής και Πληροφορικής του Μοντρεάλ (CRIM).

# Table of Contents

Abstract	ii
Résumé	iii
Περιληψη	iv
Contributions to Original Knowledge	v
Acknowledgments	vi
Ευχαριστιες	vii
Table of Contents	viii
CHAPTER 1 Introduction	1
1.1 Problem definition	3
1.2 Earlier work on open boundary problems	5
1.2.1 High-frequency methods	5
1.2.2 Integral methods	6
1.2.3 Differential methods	6
1.3 Thesis outline	10
CHAPTER 2 3D Finite Element Analysis of Time-Harmonic Proble	ms 12
2.1 Maxwell's equations	12
2.1.1 Interface conditions	13
2.1.2 Boundary conditions - Surfaces of symmetry	13
2.1.3 The curl-curl equation	
2.2 Variational formulation - Functional	14
2.3 Curvilinear coordinate system - Covariant projections	
2.4 Finite Element discretization	
CHAPTER 3 The Absorbing Boundary Condition Concept	23
3.1 Conditions of the fields on a surface S at infinity	24

3.2 The vector radiation function and the expansion theorem	25
3.3 The differential operators $B_N$ and the absorbing boundary condition	26
3.4.1 The first order ABC	28 29 29
CHAPTER 4 Implementation of the Absorbing Boundary Condition (ABC) in a Variational Formulation	31
4.1 Problems without symmetries where the ABC spherical surface S is closed	31
4.2 Problems with symmetries where the ABC spherical surface S is open	34
CHAPTER 5 Programming Considerations	38
5.1 The subroutines and a brief description	39
5.2 Working with the covariant components	42
5.2.1 The surface divergence in covariant projections	42
5.2.1 The surface divergence in covariant projections: a simpler way	44
CHAPTER 6 Results	48
6.1 Spherical TE wave functions	49
6.1.1 The $(m, n) = (0,1)$ case	51
6.1.2 The $(m, n) = (0,2)$ case	53
6.1.3 The $(m, n) = (1,1)$ case	54
6.1.4 The $(m, n) = (1,2)$ case	
6.2 Scattering from a metallic sphere	62
6.3 Computational considerations	72
CHAPTER 7 Conclusions	75
7.1 Suggestions for further work	77
APPENDIX A An alternative form for the Homogeneous Neumann	90

APPENDIX B Local Geometric and Field node resolution	81
B.1 Local geometric node numbering  B.2 Local field node numbering	82 83
APPENDIX C Supplementary Vector Identities in Spherical Coordinates	84
APPENDIX D	86
<b>D.1</b> The $L_N(\nabla_i H_{nr})$ operator	86
D.2 The B <sub>2</sub> (H) operator	88
APPENDIX E	93
E.1 The functional for the second order ABC	93
E.2 The Absorbing Boundary Condition as a natural condition to the variational formulation	95
APPENDIX F Description of the Input Data Structure	97
F.1 The file "input.dat" for a two-element problem	99
F.2 The file "mesphe.dat" for the mesh generator	101
DEEDENCES	100

#### CHAPTER 1

#### Introduction

Since the evolution of computers in early 60's, the numerical solution of equations that describe physical phenomena opened new horizons in our ability to better understand the behaviour of nature. This ignited a tremendous effort among scientists and engineers in developing computer-aided methods that would predict the behaviour of such physical phenomena. The new era of computer simulation was born.

In the world of electromagnetics, computer simulation techniques have proven to be powerful tools in predicting and giving a better understanding of the behaviour of electromagnetic fields and the performance of various devices. For scattering problems in the frequency domain, where the operating frequency is known, integral equation techniques, such as the Method of Moments (MoM), were the first to be exploited and for years they dominated the research, as well as the commercial market [Richmond-65]. Such techniques were, and still are, successfully used in antenna design, and in scattering by conducting and dielectric objects. More on the available computer programs based on integral formulations and moment method solutions may be found in [Balanis-89], chapter 12.

The implementation of numerical techniques generally leads to a system of equations, which in matrix notation is:

$$[A] \cdot [x] = [b]$$
 (1.1)

[A] is the final square matrix, [b] is the known right hand side, and the solution is the unknown column vector [x].

CHAPTER 1

Integral equation techniques produce a non-symmetric and dense final matrix. By the word dense, it is meant that all the entries of the matrix are assumed to be non-zero. The inversion of such a matrix is a process with a computational cost proportional to  $N^3$  where N is the number of equations in the problem, and its memory storage requirements are proportional to  $N^2$ . Integral methods are effective when the scatterers' geometrical dimensions are large compared to the wavelength, but when many dielectric materials of complicated geometries are present, they require far more storage and computational effort because all the dielectric interfaces have to be modelled.

For the latter type of problems, differential equation techniques, such as Finite Differences (FD) or Finite Elements (FE), are superior to integral equations. They are based on a partial differential equation and the final matrix they produce is sparse. After a standard procedure the matrix can be banded. In addition, if the variational formulation is employed, the final matrix is symmetric. Problems with many dielectric materials are handled without extra computational cost. FD are more suitable for problems with more regular geometries, while FE can easily handle any kind of arbitrary geometries and give better accuracy when highly complex inhomogeneities are present. A typical figure for sparsity is 0.1%, i.e. 99.9% of the entries in the matrix are known to be zero, and therefore do not have to be stored. Symmetric sparse matrices are highly efficient in memory storage requirements and computational cost. Depending on the method used, N<sup>1.5</sup> or N<sup>2</sup> are typical costs for solving such matrices.

Both techniques, FD and FE, have been exploited in the past and they provide excellent results when the problem's geometric domain is finite. That means the geometric space is enclosed by surfaces where known boundary conditions or symmetries are imposed, e.g. the microwave resonator, where the volume of interest is enclosed by conductors. For open boundary problems though, where the geometric domain is not

2

CHAPTER 1

bounded by any surface with known boundary conditions and extends to infinity, FD or FE suffer because an artificial boundary has to be used in order to truncate the infinite domain.

Integral equation techniques have the advantage that they solve unbounded problems, without any extra complications. Such methods though suffer from huge memory requirements and high computational cost, due to the dense matrices they produce. However, for a small class of problems with a few electrically-large regions, in each of which the material is homogeneous, integral techniques are to be preferred. Although the produced matrices are dense, their size is smaller than those of the Finite Element Method, and are in general preferable in computational cost. Nevertheless, a comparison in accuracy and computational cost done by Peterson [Peterson-89a, Peterson-89b] showed that for highly inhomogeneous and complex scatterers of relatively small electrical dimensions, the differential equation techniques are to be preferred from integral equations.

Therefore, one should think, a numerical technique based on a partial differential equation, capable of handling open boundaries would be attractive. This is the approach of the current work.

#### 1.1 Problem definition

This treatise deals with the implementation of the Finite Element Method (FEM) in solving open boundary vector wave problems. A new type of boundary condition is introduced. It is based on a local symmetric differential operator, in other words it does not destroy the sparsity and symmetry of the FE matrices. This boundary condition is applied on the surface of a closed sphere. The mathematical sphere truncates the infinite domain of the problem to a finite one and should completely enclose the volume of

CHAPTER 1

. .

interest. The volume of interest is defined as the three-dimensional region that contains all the metallic and dielectric scatterers, which may be of any shape and complexity. The FEM can be applied in the finite region.

The role of this new type of boundary condition is to absorb all outgoing electromagnetic waves causing almost no reflection on the surface of the sphere. Due to its absorbing character, the boundary condition is called an Absorbing Boundary Condition (ABC), and the sphere an Absorbing Boundary Sphere or Absorbing Boundary Surface (ABS).

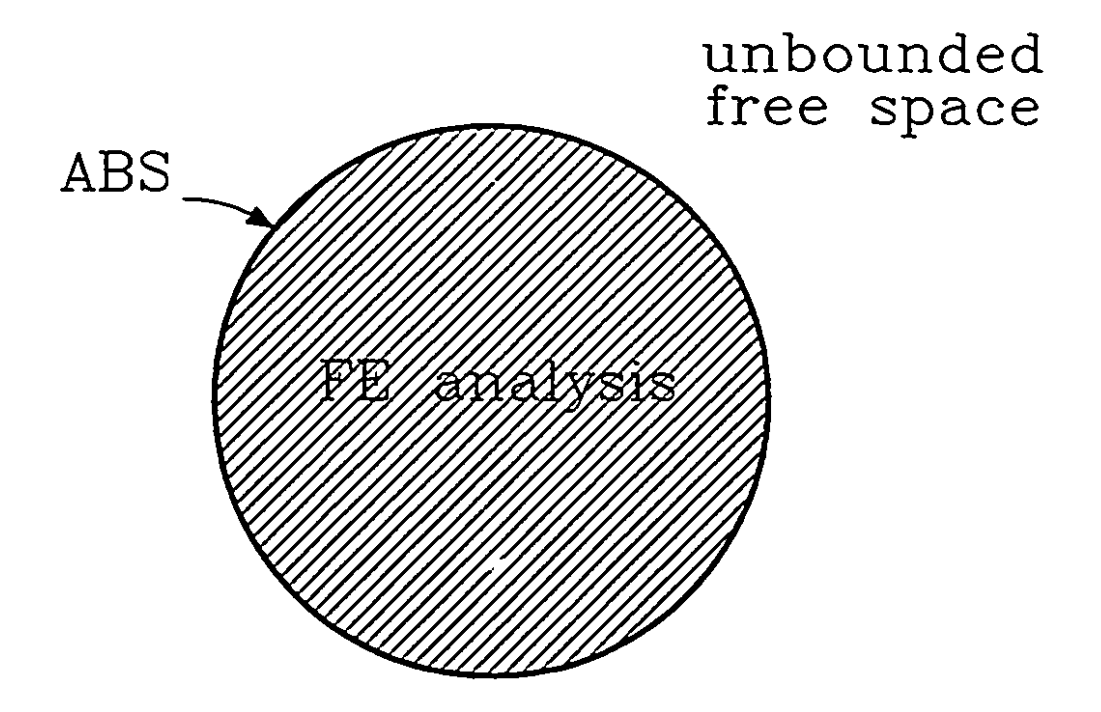


Figure 1.1 A cross section of a typical 3D open boundary problem. The gray area represents the finite volume where the FEM is applied. The ABC is applied on the ABS and absorbs all outgoing waves.

It should be noted, however, that for static problems, a zero boundary condition is often placed on an artificial boundary that is far away from the sources, where the fields

CHAPTER 1

are in any case almost zero [Emson-88]. Such a boundary condition however, cannot be applied in wave problems because it would cause reflections on the artificial boundary and it would lead to erroneous results no matter how far the artificial boundary may be placed.

#### 1.2 Earlier work on open boundary problems

The techniques used in high frequency open boundary vector problems can be classified as follows:

high-frequency i.e. Geometrical Theory of Diffraction (GTD) and its variants. methods

integral i.e. Electric (or Magnetic) Field Integral Equation, Extended Boundary Condition Method, Volume Integral Equation.

differential

i.e. Finite Differences Time Domain (FDTD), Time Domain Finite

Volume (TDFV), Finite Elements Time Domain (FETD), Finite

Elements (in frequency domain), Hybrid (a combination of Finite

Elements for a finite region coupled to an integral technique for the

infinite exterior), Infinite Elements, Ballooning.

#### 1.2.1 High-frequency methods

The GTD, an extension of geometrical optics, is an efficient tool for problems with regular geometries and electrically large scatterers. It is, however, less efficient and accurate when metallic and dielectric scatterers of irregular shape are present [Hansen-81].

#### 1.2.2 Integral methods

Integral methods start by posing the physical problem as an integral equation. There are two kinds of integral equations: surface and volume. The surface techniques formulate the problem in terms of equivalent surface currents that flow over closed 3D surfaces that contain homogeneous material [Iskander-83]. The volume techniques formulate the problem in terms of equivalent volume currents flowing inside the dielectric scatterer [Schaubert-84, Hagmann-86]. The mathematical formulations are usually transformed to a matrix equation by the Method of Moments [Harrington-68]. Integral methods are computationally expensive relative to differential methods when complicated dielectrics are present - see the discussion in introduction. Also, they suffer from singular terms in certain cases and an increase in discretization or in frequency may lead to a divergence of the numerical solution.

#### 1.2.3 Differential methods

Differential methods start by posing the physical problem as a differential equation. For a well-posed problem proper boundary conditions are required. Special boundary conditions have to be imposed on the outer surface that terminates the discretized volume of interest.

In the FDTD technique the lattice truncation plane and the lattice truncation conditions gave acceptable accuracy in absorbing the outgoing radiation [Umanshankar-82]. All FDTD methods however, suffer from the stepped edge approximation of curved objects not fitting directly into the finite difference grid. In addition, because FDTD requires a topologically regular grid, it is difficult or inefficient to get a grid of varying density which is needed for problems of complicated geometries. The contour FDTD is an alternative that can model curved objects [Katz-91]. A more promising approach was proposed by Fusco et al. [Fusco-91] using curvilinear coordinates

CHAPTER 1 6

and contravariant field components. However, the topological inefficiency of the finite difference grid still remains. The FETD method was proposed by Cangellaris et al. [Cangellaris-87] to combine the simplicity of the explicit integration scheme of the FDTD method with the versatility of the finite element spatial discretization procedures. It uses an irregular grid, but for stability reasons and for the CFL criterion to be satisfied the grid has to be structured. The TDFV method (a Lax-Wendroff explicit scheme) has also been successfully used in canonical antennas and array problems using the body fitted coordinates for modelling complex structures [Mohammadian-91]. The difference with the other methods is that this doesn't require an interlaced mesh for the electric and magnetic fields.

All Time Domain methods are efficient for electrically large scatterers due to their explicit integration schemes. However, since a structured grid is required, they are not efficient for problems requiring grids of highly localized different densities. Such problems may include many arbitrarily shaped dielectrics of high permittivity. However, frequency domain results over a range of frequencies can be obtained from time domain results using the Fast Fourier Transform. The related cost using frequency domain techniques would be quite high since the problem has to be solved separately for each frequency. Thus, the TD techniques are to be preferred. If a single frequency is needed, frequency domain techniques are computationally cheaper.

Finite Elements are differential methods that use unstructured, irregular meshes. They fall into two categories according the final matrix they produce: a) partially dense, and b) sparse. Partially dense techniques, i.e. ballooning, series methods, hybrid, result in a complete coupling of the degrees-of-freedom on the outer boundary; therefore, the piece of the final matrix corresponding to the outer boundary is dense. The loss of sparsity makes them more computationally expensive. Sparse techniques include infinite elements and ABCs.

7

CHAPTER 1

The Boundary-matching method (Ballooning), a finite element technique initially proposed by Silvester et al. [Silvester-77], and later modified by Dasgupta [Dasgupta-84], solves the Laplacian problem of open type. It relies on treating the exterior region as a single super element. Ballooning has not been used in free-space scattering problems [Emson-88]. The Transfinite Element Method introduced by Lee et al. [Lee-87], is a series solution technique similar to the unimoment method proposed earlier by Mei [Mei-74]. In both techniques the interior region is solved by finite elements (or finite differences) and on the outer circular boundary a series of analytic basis functions are applied.

A hybrid technique, called the picture-frame method, uses finite elements in separate regions of the problem where inhomogeneous materials are present and links these regions or "frames" with an integral equation [McDonald-80]. Variations and improvements of this approach applied to two-dimensional Laplacian or wave problems may be found in [Marin-82, Orikasa-83, Collins-90, Ramahi-91a]. An extension to 3D scalar potential problems was presented by Meunier et al. [Meunier-86]. A 3D vector hybrid approach with application in hyperthermia, a medical cancer therapy, was presented by Lynch et al. [Lynch-86]. The inhomogeneous patient is modelled with finite elements and boundary elements are used for the unbounded fields external to the patient. A vector finite element-boundary integral formulation for scattering by 3D cavities in an infinite ground plane was later presented by Jin et al. [Jin-91]. The technique employs finite elements for the interior region and appropriate radiation integrals for the exterior. The resulting equations are solved by demanding tangential continuity on the exterior boundary surface. Hybrid methods may suffer from uniqueness problems for electrically large scatterers [Peterson-89b].

Infinite elements have been applied successfully in open regions. A set of local shape functions including a decay factor is used in the exterior elements that extend to

CHAPTER 1 8

infinity [Rahman-84, McDougall-89]. The accuracy of the method depends on the proper choice of the decay factors. They have not been used for electromagnetic scattering in free space.

Engquist et al. proposed absorbing boundary conditions using Padé approximations for the scalar 2D wave equation [Engquist-77]. They are local and they keep the sparsity pattern of the system of differential equations. First and second approximations that lead to well-posed symmetric matrices were given. They are more suitable when the truncation contour is a rectangle. Bayliss et al. introduced new absorbing boundary conditions based on the Sommerfeld radiation condition [Bayliss-82]. They are applied on a spherical truncation surface. Symmetric first and second order conditions and their implementation for the finite element method are given. Preliminary 3D examples with axial symmetry are given using linear elements, clearly showing the superiority of the second order compared to the first. D'Angelo et al. compared Engquist-Majda and Bayliss-Turkel second order absorbing boundary conditions for the scalar wave equation [D'Angelo-89, D'Angelo-90]. It was shown that the Bayliss-Turkel ABC is more accurate than the Engquist-Majda even when it is brought closer to the scatterers and therefore it is more efficiently computationaly. More applications using 2D scalar ABCs can be found in [Ramahi-89, Pearson-89, Webb-90, Sumbar-91]. Finally Mittra et al. and later Ramahi et al. proposed new 2D ABCs that can be applied on an outer boundary of any shape [Mittra-89, Ramahi-91b].

Peterson was the first to develop first and second order ABCs of the Bayliss-Turkel type for the vector 3D wave equation [Peterson-88]. His second-order expression however does not lead to symmetric matrices. D'Angelo et al. derived a second order 3D vector Engquist-Majda ABC [D'Angelo-90]. In 3D their derivations for a vector Engquist-Majda ABC produced a non-symmetric operator and for acceptable results the outer boundary had to be placed 0.8 wavelengths away from the scatterer.

CHAPTER 1 9

In this thesis, a symmetric, second-order ABC for the vector 3D wave equation is developed [Webb-89, Kanellopoulos-91].

#### 1.3 Thesis outline

This thesis is organized as follows:

Chapter 2 gives a brief description of Maxwell's equations and the variational formulation of the problem. It follows a summary of the curvilinear coordinate system and the definition of the covariant components of a three dimensional vector. Then the Finite Element discretization using curvilinear covariant projection elements is presented.

The Absorbing Boundary Condition concept and the derivations of the new 3D vector n th order ABC are found in Chapter 3. Explicit expressions for first and second order ABCs are given. The implementation of symmetric first and second order ABCs in a variational formulation is described in Chapter 4. The special treatment required for the Absorbing Boundary Sphere is discussed in detail in the end of Chapter 4.

Chapter 5 describes the main subroutines of the computer program written to implement the new theory. The non-trivial treatment of the surface divergence term in covariant components is given at the end of the chapter.

The results of a series of test and of realistic problems are given in Chapter 6. All problems were carefully chosen so that a comparison with analytical solutions be available. The convergence and the efficiency of both first and second order ABCs are demonstrated in each of the problems analyzed.

Chapter 7 summarizes the new contributions presented in this dissertation. It stresses the efficiency of the second order ABCs and indicates the weakness of the method. Probing further, new ideas are proposed for the generalization and the improvement of the new technique.

The text and the equations in this thesis were written with the Lotus Manuscript word processing software [Lotus Manuscript-89]. The Autocad drafting package was used for the drawings [AutoCAD-88], and the Grapher data visualization package for the diagrams [GRAPHER-88].

#### **CHAPTER 2**

# 3D Finite Element Analysis of Time-Harmonic Problems

#### 2.1 Maxwell's equations

The physical laws that govern the behaviour of electromagnetic fields are expressed by Maxwell's equations. In a three dimensional space with no volume currents or charges and for time harmonic fields, this behaviour is described by:

$$\nabla \times \mathbf{E} = -j\omega \mu_a \mu_c \mathbf{H} \tag{2.1}$$

$$\nabla \times \mathbf{H} = j \omega \epsilon_0 \epsilon_r \mathbf{E} \tag{2.2}$$

$$\nabla \cdot \epsilon_{0} \epsilon_{r} \mathbf{E} = 0 \tag{2.3}$$

$$\nabla \cdot \mu_o \mu_c H = 0 \tag{2.4}$$

where f is the square root of minus one,  $\omega$  is the angular frequency,  $\varepsilon_0$  and  $\mu_0$  are the permittivity and permeability of free space respectively,  $\varepsilon_r$  and  $\mu_r$  are the relative permittivity and permeability of medium. The last two quantities are functions of position and may be complex. The vectors E for the electric field and H for the magnetic field are assumed to be finite and at all ordinary points to be continuous functions of position and time, with continuous derivatives [Stratton-41]. Should an abrupt change occur in the physical properties of the medium, the fields and their derivatives may be discontinuous. In such case the field behaviour is determined by the interface conditions. A unique solution to a given problem may not be obtained unless proper boundary conditions are specified.

#### 2.1.1 Interface conditions

Should a change occur in the physical properties of the medium, the following quantities remain continuous across the surface of discontinuity, also called interface:

$$H \times \hat{n}$$
  $\mu_{\star} H \cdot \hat{n}$   $E \times \hat{n}$   $\epsilon_{\star} E \cdot \hat{n}$ 

where n is the unit normal to the interface. The interface conditions are necessary for a well posed problem.

#### 2.1.2 Boundary conditions - Surfaces of symmetry

Boundary conditions prescribe to given values the tangential field components on a surface. A unique solution may only be obtained if the proper boundary conditions are imposed. Let a surface be S and  $\bar{\mathbf{n}}$  being the unit vector normal to the surface. The following boundary conditions may apply:

- Homogeneous Dirichlet, where the tangential component of the magnetic field is zero:  $\mathbf{H} \times \mathbf{\hat{n}} = 0$ . Such a surface is often called a perfect magnetic wall and it is usually a plane of symmetry.
- Inhomogeneous Dirichlet, where the tangential component of the magnetic field is assigned a nonzero value:  $H \times \hat{n} = H_0$  where  $H_0$  is the given value. Such a surface is often called an excitation surface or port, since it drives the problem.
- Homogeneous Neumann, where the tangential component of the electric field is zero:  $E \times \hat{n} = 0$  or  $(\nabla \times H) \times \hat{n} = 0$ . Such a surface is often called perfect electric wall and it is usually either a perfect conductor or a plane of symmetry. Using equation (2.2) this boundary condition may be rewritten as:  $H \cdot \hat{n} = 0$  (see Appendix A). Therefore, on a perfect electric conductor the normal component of the magnetic field is zero.

#### 2.1.3 The curl-curl equation

Taking the curl of (2.2) and substituting in that the curl of E from (2.1), we get a second order differential equation, the vector Helmholtz or curl-curl equation:

$$\nabla \times \frac{1}{\epsilon_r} \times \nabla \times \mathbf{H} - k_0^2 \mu_r \mathbf{H} = 0$$
 (2.5)

where the normalized frequency is given by:  $k_0 = \omega \sqrt{\epsilon_0 \mu_0}$ . Throughout this work various expressions are given for the magnetic field H. Similar expressions hold for the electric field E and will not be given explicitly.

The vector Helmholtz equation has a unique solution given the boundary conditions of the problem.

#### 2.2 Variational formulation - Functional

As an alternative to solving a differential equation that describes the physical problem (strong form) one can solve a weak form, such as a variational principle. The variational formulation looks for the stationary point of a symmetric bilinear form, the functional, subject to certain boundary conditions. Electromagnetic problems defined by the two curl Maxwell equations (2.1),(2.2) or the curl-curl equation (2.5), may be formulated variationally. Such vector variational formulations can be found in [Morse-53, Berk-56, Webb-83]. For a driven problem and for linear, isotropic, lossy materials and for time-harmonic fields the suggested functional is given by:

$$F(H) = \int_{V} \left\langle \frac{1}{\epsilon_{r}} (\nabla \times H) \cdot (\nabla \times H) - k_{0}^{2} \mu_{r} H \cdot H \right\rangle dV$$
 (2.6)

where V is the volume of interest and it is assumed to be dividable into a finite number of non-overlapping sub-volumes (Section 2.4). In such a case the material properties  $\epsilon$ , and  $\mu$ , are assumed constant inside the sub-volumes but can be discontinuous

throughout the volume V. In addition, the magnetic field H is assumed to be  $C_1$  continuous in each of the sub-volumes and tangentially continuous across sub-volume interfaces, see equation (2.11).

The stationary point of the functional (2.6), subject to the boundary conditions of the problem, is the unique solution. Note that, although the original differential equation is second-order, only first derivatives appear in (2.6).

The interface conditions (Sec. 2.1.1) should be satisfied everywhere in volume V, and on all sub-volume interfaces, see equation (2.11). However, not all four interface conditions have to be enforced explicitly. It has been shown [Webb-81, Crowley-88b] that the enforcement of only tangential field continuity is necessary. The other interface conditions, as well as the homogeneous Neumann boundary condition are satisfied naturally at the stationary point of the functional. For this reason these conditions are called **natural** conditions to the variational formulation.

The enforcement of just tangential field continuity between two adjacent sub-volumes can be beautifully implemented by covariant projection elements [Crowley-88a]. An outline of this approach is presented in the following section.

#### 2.3 Curvilinear coordinate system - Covariant projections

In the general or curvilinear coordinate system, a three dimensional vector H can be written as:

$$H = H_{\epsilon}a^{\epsilon} + H_{\eta}a^{\eta} + H_{\nu}a^{\nu}$$
 (2.7)

or as:

$$H = H^{\xi} a_{\xi} + H^{\eta} a_{\eta} + H^{\nu} a_{\nu}$$
 (2.8)

The  $H_{\xi}, H_{\eta}, H_{\tau}$  are the covariant components or covariant projections of the field, the vectors  $\mathbf{a}^{\xi}, \mathbf{a}^{\eta}, \mathbf{a}^{\tau}$  are the reciprocal unitary vectors, the  $H^{\xi}, H^{\eta}, H^{\tau}$  are the contravariant components or contravariant projections of the field and the vectors  $\mathbf{a}_{\xi}, \mathbf{a}_{\eta}, \mathbf{a}_{\tau}$  are the unitary vectors. The reciprocal unitary vectors, as well as the unitary vectors are not necessarily of unit length and they are used as basis vectors in the curvilinear coordinate system. The unitary and the reciprocal unitary vectors satisfy the following conditions:

$$a_{\xi} \cdot a^{\xi} = 1$$
,  $a_{\xi} \cdot a^{\eta} = a_{\xi} \cdot a^{v} = 0$   
 $a_{\eta} \cdot a^{\eta} = 1$ ,  $a_{\eta} \cdot a^{\xi} = a_{\eta} \cdot a^{v} = 0$  (2.9)  
 $a_{\eta} \cdot a^{v} = 1$ ,  $a_{\eta} \cdot a^{\xi} = a_{\eta} \cdot a^{\eta} = 0$ 

A six-faced curvilinear structure and the curvilinear coordinate system are illustrated in Figure 2.1. An excellent description of the unitary and reciprocal basis vectors and their properties may be found in [Stratton-41], page 38.

Multiplying equation (2.7) by one of the unitary vectors, say  $a_{\xi}$  we get:

$$H \cdot a_{\xi} = H_{\xi} \tag{2.10}$$

Thus, the covariant projection  $H_{\xi}$  is nothing but the projection of the field H in the direction of the unitary vector  $\mathbf{a}_{\xi}$ . It should be noted, however, that the direction of the vector  $H_{\xi}\mathbf{a}^{\xi}$  is normal to the surface defined by the unitary vectors  $\mathbf{a}_{\eta}$ ,  $\mathbf{a}_{v}$  which is not parallel to the vector  $\mathbf{a}_{\xi}$ . In other words, the direction of each component of the field H defined in (2.7) is normal to one of the surfaces of constant  $\xi$ ,  $\eta$  or v. In addition, the projection of H along the direction  $\mathbf{a}^{\xi}$  is not just  $H_{\xi}\mathbf{a}^{\xi}$ . The other two components have in general non zero projections in that direction.

**CHAPTER 2** 

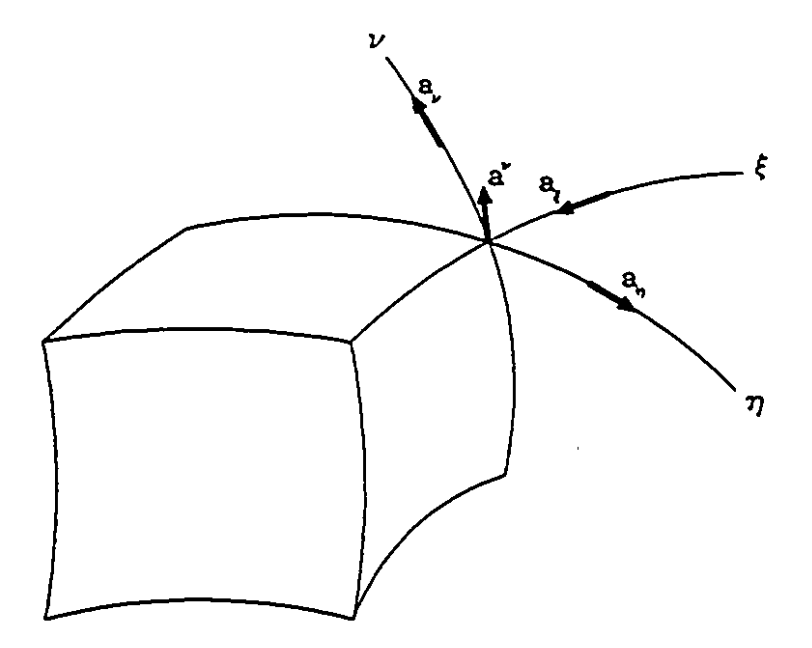


Figure 2.1 Curvilinear element in the general coordinate system. It has 6 faces which are surfaces of constant  $\xi, \eta$  or  $\vee$ . The unitary vectors  $\mathbf{a}_{\xi}, \mathbf{a}_{\eta}, \mathbf{a}_{\psi}$  are always tangent to the coordinate axes  $\xi, \eta, \vee$ . The reciprocal unitary vector  $\mathbf{a}^{\psi}$  is normal to the surface defined by  $\mathbf{a}_{\xi}, \mathbf{a}_{\eta}$ , which is a surface of constant  $\vee$ . Similarly, the reciprocal unitary vectors  $\mathbf{a}^{\xi}$  and  $\mathbf{a}^{\eta}$  are normal to the surfaces of constant  $\xi$  and  $\eta$  respectively.

Setting  $H_{\xi}$  and  $H_{\eta}$  to zero is equivalent to setting to zero the field tangent to a surface of constant  $\vee$ . The importance of using covariant projection curvilinear elements will become clear in the next section.

#### 2.4 Finite Element discretization

In order to solve a problem numerically, its infinite degrees of freedom have to be made finite. In the finite element method, the volume of interest is divided into a finite number of non overlapping sub-volumes, called finite elements. They are defined in space by the shape functions. Similarly, trial functions describe the field (scalar or vector) dis-

tribution inside them [Zienkiewicz-77, Silvester-90]. The discretized functional is given by:

$$F(H) = \sum_{i=1}^{M} \int_{V_i} \left\langle \frac{1}{\epsilon_r} (\nabla \times H) \cdot (\nabla \times H) - k_0^2 \mu_r H \cdot H \right\rangle dV$$
 (2.11)

where M is the number of sub-volumes in the problem.

In this work, each finite element is a curvilinear brick as shown in Figure 2.1. It has a local curvilinear coordinate system  $(\xi, \eta, v)$  and it is bounded by 6 faces. These faces are surfaces of constant  $\xi, \eta$  or v. The origin of the local curvilinear coordinate system lies in the centre of the element. The element occupies the region:

$$-1 \le \xi \le 1$$
  
 $-1 \le \eta \le 1$  (2.12)  
 $-1 \le \nu \le 1$ 

A set of scalar shape functions defines the geometry of the element in the local coordinate system. There are 27 geometric nodes in the element, arranged in a  $3 \times 3 \times 3$  grid (see Appendix B). Each geometric node has a corresponding shape function. In this work this function is a second order polynomial in each of  $\xi$ ,  $\eta$  and v. It has a value of one at its own geometric node, and zero at the other 26. Thus, any point  $p(x_p, y_p, z_p)$  inside the element can be given in cartesian coordinates by:

$$x_{p} = \sum_{i=1}^{27} x_{i} g_{i}(\xi_{p}, \eta_{p}, v_{p})$$

$$y_{p} = \sum_{i=1}^{27} y_{i} g_{i}(\xi_{p}, \eta_{p}, v_{p})$$

$$z_{p} = \sum_{i=1}^{27} z_{i} g_{i}(\xi_{p}, \eta_{p}, v_{p})$$
(2.13)

where  $g_i(\xi_p, \eta_p, v_p)$  is the second-order shape function corresponding to the  $\ell$ th geometric point, evaluated at the point  $p(\xi_p, \eta_p, v_p)$ . The functions  $g_i$ 's are explicitly known a priori, [Crowley-88b]. The parameters  $(x_i, y_i, z_i)$  are the cartesian

coordinates of the geometric point i. There is a one to one correspondence between the local curvilinear and the global (eg. cartesian) coordinate system [Crowley-88b]. The local geometric node numbering is illustrated in Appendix B.

A set of vector trial functions has to be used in order to model the field distribution inside the element. The vector trial functions are similar to the scalar shape functions, but now there are directions assigned to each of them. The directions are that of the reciprocal basis vectors, eqn.(2.7). It is not necessary to use the same order polynomials as trial functions for the field components. In fact, it has been shown that the choice of mixed order vector trial functions, first and second, is crucial in avoiding spurious corruptions [Crowley-88a].

The nodes for the vector trial functions are called field nodes, to distinguish them from the earlier geometric nodes. There are 54 field nodes in each element, 18 in each of the three directions in the local coordinate system, Figure 2.2. Two adjacent elements have a total of 96 field nodes (54+54-12) after field continuity is imposed. The degrees of freedom (DOF) of a problem is the total number of field nodes that do not have prescribed values.

Expressions similar to (2.13) hold for the covariant field components. The field at any given point p inside the element is given by:

$$H|_{p} = H_{\xi}a^{\xi}|_{p} + H_{\eta}a^{\eta}|_{p} + H_{\nu}a^{\nu}|_{p}$$
 (2.14)

 $= \sum_{i=1}^{n} \frac{1}{i} = \sum_{i=1}^{n} \frac{1}{i$ 

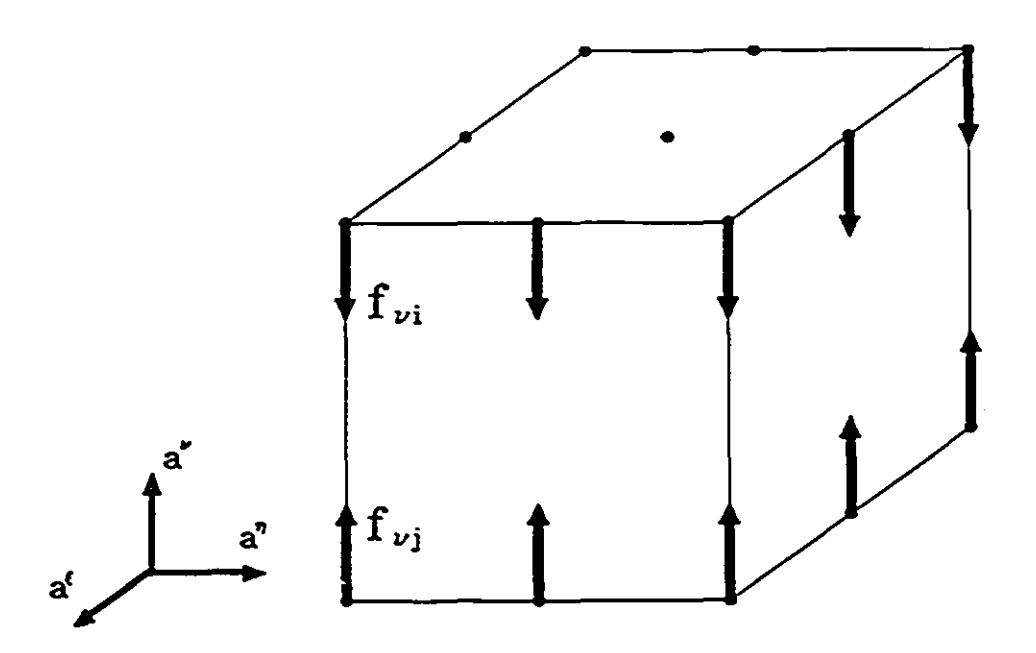


Figure 2.2 The 18 vector trial functions for the covariant field component H<sub>v</sub>. They vary quadratically on surfaces of constant  $\vee$  and linearly along the  $\vee$  local coordinate direction.

$$H_{\xi} a^{\xi} |_{p} = \sum_{i=1}^{18} H_{\xi i} f_{\xi i}(\xi_{p}, \eta_{p}, v_{p})$$

$$H_{\eta} a^{\eta} |_{p} = \sum_{i=1}^{18} H_{\eta i} f_{\eta i}(\xi_{p}, \eta_{p}, v_{p})$$

$$H_{v} a^{v} |_{p} = \sum_{i=1}^{18} H_{v i} f_{v i}(\xi_{p}, \eta_{p}, v_{p})$$
(2.15)

where  $f_{\xi_i}(\xi_p, \eta_p, v_p) = f_{\xi_i}(\xi_p, \eta_p, v_p) a^{\xi}$  is the vector trial function that corresponds to the  $\xi$ th  $\xi$  field node, evaluated at the point  $p(\xi_p, \eta_p, v_p)$ . It is of mixed order and varies linearly with  $\xi$  and quadratically with  $\eta$  and v. Similarly for the vector trial functions  $f_{\eta_i}$  and  $f_{v_i}$ . They vary linearly with  $\eta$  and v respectively and quadratically with the other coordinates. All vector trial functions point inwards for the proper and

consistent imposition of tangential field continuity. Each of the parameters  $H_{\xi_i}$  is the covariant component at node *i*. Similarly for  $H_{\eta_i}$  and  $H_{\nu_i}$ . The local field node distribution may be found in Appendix B.

Expression (2.15), for each finite element, is substituted into the functional (2.11) and the integrations carried out. In this work Gauss-Quadrature was used for the integrations. This results in a quadratic for the unknowns  $H_{\xi i}$ ,  $H_{\eta i}$ ,  $H_{\nu i}$ : differentiating to find the stationary point gives a set of linear equations.

Once the parameters  $H_{\xi i}$ ,  $H_{\eta i}$ ,  $H_{\psi i}$  have been found, the field can be evaluated everywhere in the element using (2.14). The cartesian field components may be found as follows:

Each of the reciprocal unitary vectors  $\mathbf{a}^{\mathfrak{t}}$ ,  $\mathbf{a}^{\eta}$ ,  $\mathbf{a}^{\star}$  can be expressed as a linear combination of the cartesian unit basis vector set - see equations (6) and (9), page 39, in [Stratton-41]. Thus, the magnetic field H in (2.7) can be expressed in its cartesian components in the cartesian coordinate system as:

$$H = (H_{\xi} a_{x}^{\xi} + H_{\eta} a_{x}^{\eta} + H_{\nu} a_{x}^{\nu}) \hat{a}_{x} +$$

$$(H_{\xi} a_{y}^{\xi} + H_{\eta} a_{y}^{\eta} + H_{\nu} a_{y}^{\nu}) \hat{a}_{y} +$$

$$(H_{\xi} a_{z}^{\xi} + H_{\eta} a_{z}^{\eta} + H_{\nu} a_{z}^{\nu}) \hat{a}_{z}$$

$$(2.16)$$

where  $a_x^{\xi}$  is the x component of the reciprocal unitary vector  $a^{\xi}$  and so forth. The  $a_x, a_y, a_z$  are the cartesian unit basis vectors.

There are some important advantages in using curvilinear covariant projection elements:

- 1) Their curvilinear shape allows a better modelling of curved objects.
- 2) The imposition of vector boundary conditions becomes as simple as the imposition of scalar boundary conditions.
- Only tangential field continuity is imposed across elements, which is consistent with the variational principle. This leaves the normal components free, so they can be discontinuous when abrupt changes in material properties or sharp metallic edges are present.
- The use of mixed order trial functions for the field distribution frees the problem from any spurious corruptions that may appear even in deterministic problems [Crowley-88b, Pinchuk-88].

#### CHAPTER 3

# The Absorbing Boundary Condition Concept

Consider the following open boundary problem, shown in Figure 3.1. The volume of interest V contains the electromagnetic source eI, the metallic scatterers mI, m2 and the dielectric scatterers dI, d2, d3. The closed surface S truncates the infinite domain of the problem and renders the volume of interest V finite dimensions.

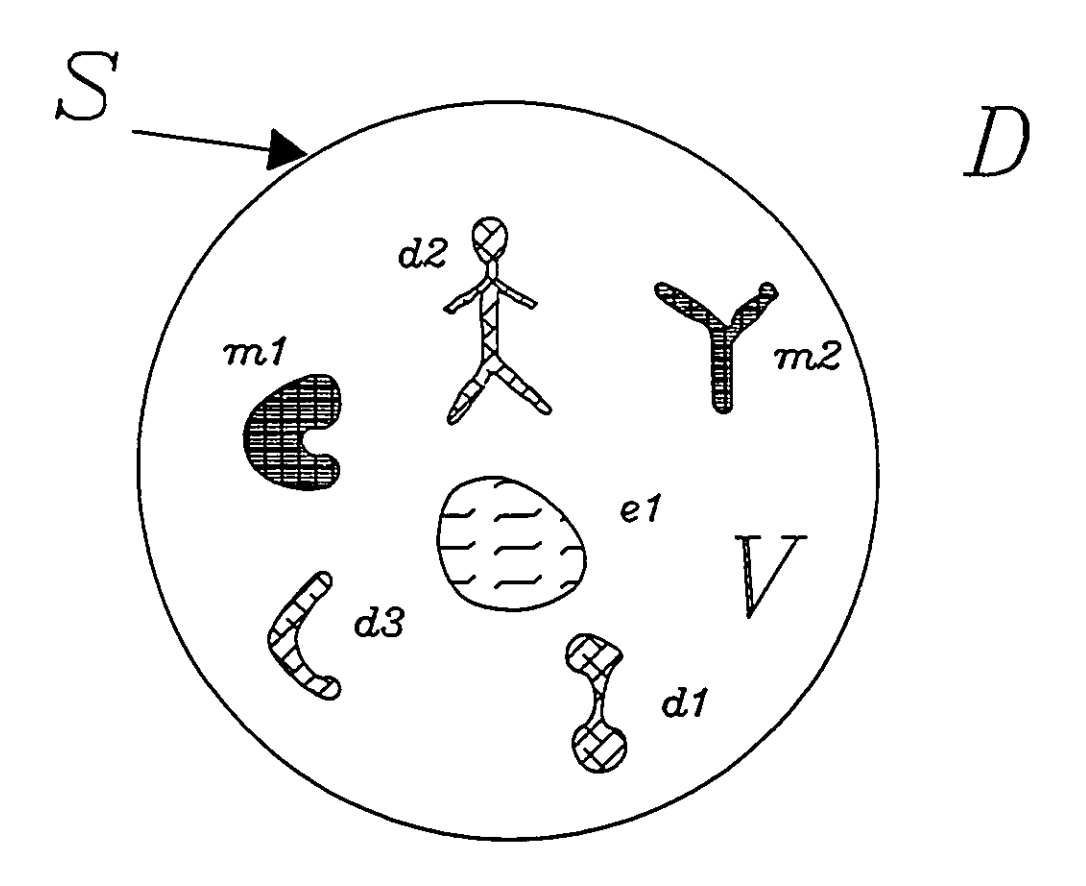


Figure 3.1 A typical open boundary problem. The surface S encloses the volume V where electromagnetic sources, metallic and dielectric scatterers are present.

The above three-dimensional problem can be solved with finite elements if a known boundary condition is imposed on the surface S. Such a boundary condition should simulate the behaviour of the infinite space outside the closed surface S. This can be done by absorbing all the outward propagating waves from the volume V, incident on the surface S from within. Thus, the artificial surface S should be invisible to the outgoing waves and no reflections would occur on S.

The search for such an absorbing boundary condition is the focal point of this work.

## 3.1 Conditions of the fields on a surface S at infinity

In open boundary problems, infinity can be regarded as a separate boundary. A condition at infinity is necessary for the problem to be well posed. For scalar fields, the Sommerfeld radiation condition determines the behaviour of the fields at infinity [Wilcox-56a], and it is given by:

$$\lim_{R \to \infty} R \left( \frac{\partial \mathbf{u}}{\partial R} - j k_0 \mathbf{u} \right) = 0 \tag{3.1}$$

where u is a scalar wave function with a time variation of the form  $e^{j\omega t}$ , and  $k_0$  is the normalized frequency given in Section 2.1.3.

For vector fields, the Silver-Müller radiation condition gives the behaviour of the field on a closed surface at infinity [Wilcox-56b]:

$$\lim_{R \to \infty} \int_{r=R} |\hat{\mathbf{a}}_r \times (\nabla \times \mathbf{H}) - jk_0 \mathbf{H}|^2 dS = 0$$
 (3.2)

where H is a vector wave function,  $dS = R^2 \sin \theta d\theta d\phi$  is the surface element of a sphere of radius R and  $\tilde{a}_r$  is the unit vector normal to the surface S.

Essentialy, the Silver-Müller radiation condition is an Absorbing Boundary Condition (ABC) on a sphere of infinity radius. It insures that there is no reflection on

that sphere of outward-propagating waves. More precisely, it guarantees that there are no incoming waves from infinity. This ABC is the vector form of the Sommerfeld radiation condition.

## 3.2 The vector radiation function and the expansion theorem

Consider the exterior domain D which consists of all points lying outside a closed boundary surface S, see Figure 3.1. A complex-valued vector field H defined in the domain D is a vector radiation function if it satisfies both the curl-curl equation (2.5) and the Silver-Müller radiation condition (3.2).

According to the expansion theorem [Wilcox-56b], for an exterior domain D[r > c]. a vector radiation function can be written as:

$$H = H(r,\theta,\phi) = g \sum_{n=0}^{\infty} \frac{h_n(\theta,\phi)}{r^{n+1}}$$
 (3.3)

where r,  $\theta$ ,  $\phi$  are the spherical coordinates and  $g = e^{-jk_0 r}$ .

The first term of this series varies as  $\frac{1}{r}$  and satisfies the vector absorbing boundary condition introduced in the previous section. To put it in another way, the first term of the series is annihilated by the absorbing operator:

$$\mathbf{a}_r \times \nabla \times - j k_0$$

However, on the sphere r = R all the terms of the series are present: a perfect absorbing operator would annihilate them all. In general, local differential operators cannot do this. However, operators can be constructed which annihilate more terms, and which are therefore more accurate.

## 3.3 The differential operators $B_N$ and the absorbing boundary condition

A scalar expression similar to (3.3) exists for scalar wave functions. In [Bayliss-82] an expansion has been derived for a general N th-order differential operator that exactly annihilates the first N terms of the scalar expansion. In this section analogous operators  $B_N$  are defined that annihilate the first N terms of any vector radiation function H.

From (3.3) and (C1.c) the  $(\theta, \phi)$  part and the radial part of the vector H can be written as:

$$H_{t} = H_{t}(r, \theta, \phi) = \sum_{n=0}^{\infty} g \frac{\mathbf{h}_{nt}(\theta, \phi)}{r^{n-1}}, \qquad H_{r} = H_{r}(r, \theta, \phi) = \sum_{n=0}^{\infty} g \frac{\mathbf{h}_{nr}(\theta, \phi)}{r^{n-1}}$$
(3.4)

Using the following relation:

$$\frac{\partial}{\partial r} \left( \frac{g}{r^{n-\alpha}} \right) = -\frac{g}{r^{n-\alpha}} \left( j k_0 + \frac{n+\alpha}{r} \right) \tag{3.5}$$

and the vector identity (C.6) we get:

$$\hat{\mathbf{a}}_r \times \nabla \times \mathbf{H}_{nt} = \left( j k_0 + \frac{n}{r} \right) \mathbf{H}_{nt}$$
 (3.6)

where g is defined in section 3.2,  $\bar{a}_r$  is the unit vector in the radial direction and

$$H_{nt} = H_{nt}(r, \theta, \phi) = g \frac{h_{nt}(\theta, \phi)}{r^{n+1}}$$
(3.7)

We now define the differential operator

$$L_N(\mathbf{u}) = \hat{\mathbf{a}}_r \times \nabla \times \mathbf{u} - \left(jk_0 + \frac{N}{r}\right)\mathbf{u}$$
 (3.8)

From (3.8), using (3.6) and for  $N \ge 0$  and  $n \ge 0$ , we have:

$$L_N(\mathbf{H}_{nt}) = L_N\left(g\frac{\mathbf{h}_{nt}(\theta,\phi)}{r^{n+1}}\right) = (n-N)g\frac{\mathbf{h}_{nt}(\theta,\phi)}{r^{n+2}}$$
(3.9)

and for N = n = K, (3.9) gives:

$$L_K(\mathbf{H}_{Kt}) = 0 \tag{3.10}$$

Similarly, using (3.8), (C.7) and for  $N \ge 0$  and  $n \ge 0$ , it is shown in Appendix D.1 that:

$$L_{N}(\nabla_{t}\hat{\mathbf{a}}_{r}\cdot\mathbf{H}_{nr}) = L_{N}(\nabla_{t}\mathbf{H}_{nr}) =$$

$$= L_{N}\left(\nabla_{t}\left\{g\frac{\mathbf{h}_{nr}(\theta,\phi)}{r^{n+1}}\right\}\right) = (n+1-N)\nabla_{t}\left\{g\frac{\mathbf{h}_{nr}(\theta,\phi)}{r^{n+2}}\right\} \quad (3.11)$$

where:

$$H_{nr} = H_{nr} \cdot \hat{a}_r$$
 ,  $h_{nr} = h_{nr} \cdot \hat{a}_r$  and 
$$H_{nr} = g \frac{h_{nr}(\theta, \phi)}{r^{n+1}}$$
 (3.12)

For N = n + 1 = K + 1 (3.11) gives:

$$L_{K+1}(\nabla_t H_{Kr}) = 0 (3.13)$$

In (3.10), the operator  $L_K$  annihilates the  $\frac{1}{r^{K-1}}$  term of the vector  $H_t$  defined in (3.4) and so  $L_{K-1}$  annihilates the  $\frac{1}{r^{K}}$  term. In (3.13), the operator  $L_{K+1}(\nabla_t)$  annihilates the  $\frac{1}{r^{K-1}}$  term of the vector  $H_r$ , and so  $L_K(\nabla_t)$  annihilates the  $\frac{1}{r^{K}}$  term. Thus, an operator of the form  $L_{K-1}(H_t) + L_K(\nabla_t H_r)$  annihilates the  $\frac{1}{r^{K}}$  term of the vector radiation function  $H_r$  (3.3). In both cases  $L_K$  and  $L_{K-1}$  have the effect of multiplying by  $\frac{1}{r}$ , but leaving the  $\theta$ ,  $\phi$  dependance unchanged.

The operators  $B_N$ , N = 1.2,... are now defined as:

$$B_N(\mathbf{u}) = (L_{N-1})^N(\mathbf{u}_t) + s(L_N)^{N-1}(\nabla_t \mathbf{u}_r)$$
 (3.14)

where s is an arbitrary number. The superscript N denotes that the operator  $L_{N-1}$  is applied N times; similarly for the superscript N-1.

Applying the operator  $B_N$  to  $H_n$  we have that:

**CHAPTER 3** 

$$B_{N}(\mathbf{H}_{n}) = B_{N}\left(g\frac{\mathbf{h}_{n}(\theta,\phi)}{r^{n+1}}\right) =$$

$$= (n+1-N)(n+2-N)\cdots(n-1)(n)g\frac{\mathbf{h}_{nt}(\theta,\phi)}{r^{n+1-N}} +$$

$$s(n+1-N)(n+2-N)\cdots(n-1)\nabla_{t}\left\langle g\frac{\mathbf{h}_{nr}(\theta,\phi)}{r^{n+N}}\right\rangle$$
(3.15)

In the expressions (3.3), (3.12) for the vector radiation function it is true that  $h_{1,r}(\theta,\phi)=0$ , or  $H_1=H_{1,r}$ . This is because H, since it satisfies the curl-curl equation (2.5) has also to satisfy  $\nabla \cdot H=0$  [Wilcox-56b]. Then from (3.15), it is obvious that the right-hand side vanishes for  $n=0,1,\ldots,N-1$ , i.e. the operator  $B_N$  annihilates the first N terms of the vector radiation function H. Further, for n>N-1 each of the terms on the right-hand side in (3.15) is proportional to  $\frac{1}{r^{n-N-1}}$  (considering the  $\frac{1}{r}$  term included in the  $\nabla_r$  operator). Thus,

$$B_N(H) = O\left(\frac{1}{r^{2N+1}}\right)$$
 (3.16)

The above is an approximate absorbing boundary condition on the spherical surface S of radius r. The approximation gets better as r increases. For N=1, it improves at the rate  $1/r^3$ , and for N=2 at the rate  $1/r^5$  [Webb-89].

## 3.4 The first and second order Absorbing Boundary Conditions

In general, an absorbing boundary condition takes the form:

$$\hat{\mathbf{a}}_r \times \nabla \times \mathbf{u} = P(\mathbf{u}) \tag{3.17}$$

where P is a linear operator on u. Note that in both operators  $P_1$  and  $P_2$  (3.19) and (3.21) no radial derivatives are present.

**CHAPTER 3** 

#### 3.4.1 The first order ABC

For N = 1, (3.14) gives:

$$B_{1}(H) = L_{0}(H_{t}) + s\nabla_{t}H_{r}$$

$$= \hat{a}_{r} \times \nabla \times H_{t} - jk_{0}H_{t} + s\nabla_{t}H_{r} \quad \text{using (3.8)}$$

$$= \hat{a}_{r} \times \nabla \times H - jk_{0}H_{t} + (s-1)\nabla_{t}H_{r} \quad \text{using (C.5)}$$
or

$$B_1(\mathbf{H}) = \bar{\mathbf{a}}_r \times \nabla \times \mathbf{H} - \alpha(r)\mathbf{H}_r + (s-1)\nabla_r \mathbf{H}_r \qquad (3.18)$$

where  $\alpha(r) = jk_0$ .

The first order absorbing boundary condition  $B_1(H) = 0$  can be rewritten as  $\hat{a}_r \times \nabla \times H = P_1(H)$ , where  $P_1$  is defined by

$$P_1(\mathbf{u}) = \alpha(r)\mathbf{u}_r + (1-s)\nabla_r \mathbf{u}_r$$
 (3.19)

#### 3.4.2 The second order ABC

For N = 2, (3.14) gives:

$$B_2(H) = (L_1)^2(H_t) + sL_2(\nabla_t H_r)$$

and after some algebra we get (see Appendix D.2):

$$B_{2}(H) = -\frac{1}{\beta(r)}\hat{\mathbf{a}}_{r} \times \nabla \times \mathbf{H} + \frac{\alpha(r)}{\beta(r)}\mathbf{H}_{t}$$
$$+\nabla \times \hat{\mathbf{a}}_{r}[\hat{\mathbf{a}}_{r} \cdot (\nabla \times \mathbf{H})] + (s-1)\nabla_{t}(\nabla \cdot \mathbf{H}_{t})$$
$$+(2-s)\alpha(r)\nabla_{t}\mathbf{H}_{r} \qquad (3.20)$$

where  $\alpha(r) = jk_0$  and  $\beta(r) = 1/(2jk_0 + 2/r)$ .

The second order absorbing boundary condition  $B_2(H) = 0$  can be rewritten as  $\mathbf{a}_r \times \nabla \times \mathbf{H} = P_2(\mathbf{H})$ , where  $P_2$  is defined by

$$P_{2}(\mathbf{u}) = \alpha(r)\mathbf{u}_{t} + \beta(r)\nabla \times \tilde{\mathbf{a}}_{r}[\tilde{\mathbf{a}}_{r} \cdot (\nabla \times \mathbf{u})]$$

$$+ (s-1)\beta(r)\nabla_{t}(\nabla \cdot \mathbf{u}_{t})$$

$$+ (2-s)\alpha(r)\beta(r)\nabla_{t}\mathbf{u}_{r}$$
(3.21)

#### **CHAPTER 4**

# Implementation of the Absorbing Boundary Condition (ABC) in a Variational Formulation

This chapter deals with the variational formulation of the problem. A functional F is derived for the first and second order ABC. The stationary point of F is the solution to the curl-curl equation in volume V:

$$\nabla \times \frac{1}{\epsilon_r} \nabla \times \mathbf{H} - k_0^2 \mu_r \mathbf{H} = 0$$

(see eqn. (2.5) in Section 2.1.3) with the ABC (first and second order) applied on a spherical surface S which encloses the volume V:

$$\hat{\mathbf{a}}_r \times \nabla \times \mathbf{H} = P_{1,2}(\mathbf{H})$$

see eqns. (3.17), (3.19) and (3.21) in Section 3.4.

# 4.1 Problems without symmetries where the ABC spherical surface S is closed

The following functional can be derived from eqn. (2.5) using a standard method [Linz-79, Chapter 7]:

$$F(H) = \int_{V} \left\langle H \cdot \nabla \times \frac{1}{\epsilon_{r}} \nabla \times H - k_{0}^{2} \mu_{r} H \cdot H \right\rangle dV$$
 (4.1)

where all the parameters have been explained in Section 2.2 and the vector field H may be complex. Applying the vector identity

$$A \cdot \nabla \times \nabla \times B = (\nabla \times A) \cdot (\nabla \times B) - \nabla \cdot (A \times \nabla \times B)$$

and using the divergence theorem on (4.1) we get:

$$F(H) = \int_{V} \left\{ \frac{1}{\epsilon_{r}} (\nabla \times H) \cdot (\nabla \times H) - k_{0}^{2} \mu_{r} H \cdot H \right\} dV - \int_{S} \frac{1}{\epsilon_{r}} H \times \nabla \times H \cdot dS$$
 (4.2)

where the closed surface S completely surrounds the volume V. The above expression for the functional F is the generalized form of (2.6). The difference between (2.6) and (4.2) is the extra surface term  $\int_{S} \frac{1}{\epsilon_r} H \times \nabla \times H \cdot dS$ . The absence of this term in (2.6) causes the homogeneous Neumann boundary condition (Section 2.1.2) to be naturally satisfied at the stationary point of F, see Section 3.4 in [Silvester-90]. If the surface S is a sphere, then by using the vector identity  $B \times C \cdot A = C \times A \cdot B = -A \times C \cdot B$  we can rewrite the surface integral in (4.2) as:

$$\int_{S} \frac{1}{\epsilon_r} H \times \nabla \times H \cdot dS = -\int_{\epsilon_r} \frac{1}{\epsilon_r} \hat{a}_r \times \nabla \times H \cdot H dS$$

and (4.2) becomes:

$$F(H) = \int_{V} \left\{ \frac{1}{\epsilon_{r}} (\nabla \times H) \cdot (\nabla \times H) - k_{0}^{2} \mu_{r} H \cdot H \right\} dV + \int_{S} \frac{1}{\epsilon_{r}} \tilde{a}_{r} \times \nabla \times H \cdot H dS (4.3)$$

In Section 3.4, two approximate expressions  $P_1(H)$  and  $P_2(H)$  have been derived for the integrand quantity  $\bar{a}_r \times \nabla \times H$ , which correspond to the first and second order ABC. We want the stationary point of F in (4.3) to satisfy the Absorbing Boundary Conditions  $B_n(H) = 0$  naturally, (n = 1 or 2). It has been shown in the Appendix E.2, that this will be the case if  $\bar{a}_r \times \nabla \times H$  is simply replaced by  $P_n(H)$  in equation (4.3). Thus, the functional F is now given by:

$$F(H) = \int_{V} \left\langle \frac{1}{\epsilon_{r}} (\nabla \times H) \cdot (\nabla \times H) - k_{0}^{2} \mu_{r} H \cdot H \right\rangle dV + \int_{S} \frac{1}{\epsilon_{r}} P_{n}(H) \cdot H dS \quad (4.4)$$

The operator  $P_n(H)$  is the absorbing boundary operator associated with the energy flow through the surface S, and n = 1, 2 for the first or second order ABC respectively. The variational formulation requires that the linear operator  $P_n$  is symmetric:

$$\int_{S} P_{n}(\mathbf{u}) \cdot \mathbf{v} dS = \int_{S} P_{n}(\mathbf{v}) \cdot \mathbf{u} dS$$
 (4.5)

where u and v are complex vector functions.

For the first order ABC, the choice s=1 only gives a symmetric operator, see eqn. (3.19):

$$P_1(H) = \alpha(r)H_t \tag{4.6}$$

Assuming that all dielectric materials are inside the volume V and the region close to and outside the surface S is air, the corresponding functional is:

$$F(H) = \int_{V} \left\langle \frac{1}{\epsilon_{r}} (\nabla \times H)^{2} - k_{0}^{2} \mu_{r} H^{2} \right\rangle dV + \int_{S} \alpha(r) H_{i}^{2} dS \qquad (4.7)$$

For the second order ABC, the choice s = 2 only gives the symmetric operator, see eqn. (3.21):

$$P_{2}(H) = \alpha(r)H_{t} + \beta(r)\nabla \times \hat{\mathbf{a}}_{r}[\hat{\mathbf{a}}_{r} \cdot (\nabla \times H)] + \beta(r)\nabla_{t}(\nabla \cdot H_{t})$$

$$(4.8)$$

Again, assuming that all dielectric materials are inside the volume V and the region close to and outside the surface S is air, the corresponding functional is given by (Appendix E.1):

$$F(H) = \int_{V} \left\langle \frac{1}{\epsilon_{r}} (\nabla \times H)^{2} - k_{0}^{2} \mu_{r} H^{2} \right\rangle dV +$$

$$\int_{S} \left\{ \alpha(r) H_{t}^{2} + \beta(r) [\tilde{a}_{r} \cdot (\nabla \times H)]^{2} - \beta(r) (\nabla \cdot H_{t})^{2} \right\} dS \qquad (4.9)$$

Requiring that F be stationary leads to a symmetric matrix equation. Peterson's expression however, for the second order ABC corresponds to the choice s = 1, which gives a non-symmetric operator [Peterson-88]. His ABC can be implemented by a weighted-residual formulation, but this does not lead to a symmetric matrix equation.

## 4.2 Problems with symmetries where the ABC spherical surface S is open

This section deals with problems with symmetries where the spherical surface S is just part of a sphere, i.e. half, quarter or eighth. In this case the first variation of the functional F gives:

$$\frac{1}{2}\delta(F(H)) = \int_{V} \left\{ \frac{1}{\epsilon_{r}} \nabla \times (\delta H) \cdot \nabla \times H - k_{0}^{2}(\delta H) \cdot H \right\} dV 
+ \int_{S} \left\{ \alpha(\delta H_{t}) \cdot H_{t} + \beta(r) \left[ \hat{a}_{r} \cdot (\nabla \times \delta H) \right] \left[ \hat{a}_{r} \cdot (\nabla \times H) \right] \right] 
- \beta(r) (\nabla \cdot \delta H_{t}) (\nabla \cdot H_{t}) dS$$
(4.10)

After some algebra and using #19 p.501 and #42 p.503 in [Van Bladel-64], we get:

$$\frac{1}{2}\delta(F(H)) = \int_{V} \delta H \cdot \left(\nabla \times \frac{1}{\epsilon_{r}} \nabla \times H - k_{0}^{2} H\right) dV$$

$$+ \int_{S} \delta H \cdot \left\{\alpha(r) H_{t} + \nabla \times H \times \hat{a}_{r} + \beta(r) \nabla_{t} (\nabla \cdot H_{t}) + \beta(r) \nabla \times \hat{a}_{r} [\hat{a}_{r} \cdot (\nabla \times H)] \right\} dS$$

$$+ \int_{C} \hat{a}_{m} \cdot \left\{\delta H_{t} \nabla \cdot H_{t} + \delta H \times \hat{a}_{r} [\hat{a}_{r} \cdot (\nabla \times H)] \right\} dC \quad (4.11)$$

where S is a surface that is part of a sphere, C is the boundary of S and  $\bar{a}_m$  is the unit vector in the plane tangent to the spherical surface and perpendicular to C, see Figure 4.1. Each integral in (4.11) must vanish for any  $\delta H$  at the stationary point of F, so:

$$\nabla \times \frac{1}{\epsilon_r} \nabla \times H - k_0^2 H = 0 \tag{4.12}$$

$$\alpha(r)H_t + \nabla \times H \times \hat{\mathbf{a}}_r + \beta(r)\{\nabla_t(\nabla \cdot H_t) + \nabla \times \hat{\mathbf{a}}_r[\hat{\mathbf{a}}_r \cdot (\nabla \times H)]\} = 0 \quad (4.13)$$

$$\hat{\mathbf{a}}_{m} \cdot (\delta \mathbf{H}_{t} \nabla \cdot \mathbf{H}_{t} + (\delta \mathbf{H}) \times \hat{\mathbf{a}}_{r} [\hat{\mathbf{a}}_{r} \cdot (\nabla \times \mathbf{H})]) = 0 \qquad (4.14)$$

(4.12) is the governing curl-curl equation in volume V, and (4.13) is the second order Absorbing Boundary Condition applied on the spherical surface S. Equation (4.14) can

be rewritten as:

$$\hat{\mathbf{a}}_{m} \cdot \delta \mathbf{H}_{t} \nabla \cdot \mathbf{H}_{t} + \hat{\mathbf{a}}_{c} \cdot \delta \mathbf{H}_{t} [\hat{\mathbf{a}}_{c} \cdot (\nabla \times \mathbf{H})] = 0 \tag{4.15}$$

where  $\hat{a}_c$  is the unit vector on the plane tangent to the spherical surface, and tangential to C, see Figure 4.1. Note that  $H_t$  denotes the magnetic field tangent to the spherical surface S, rather than the magnetic field tangent to the contour C.

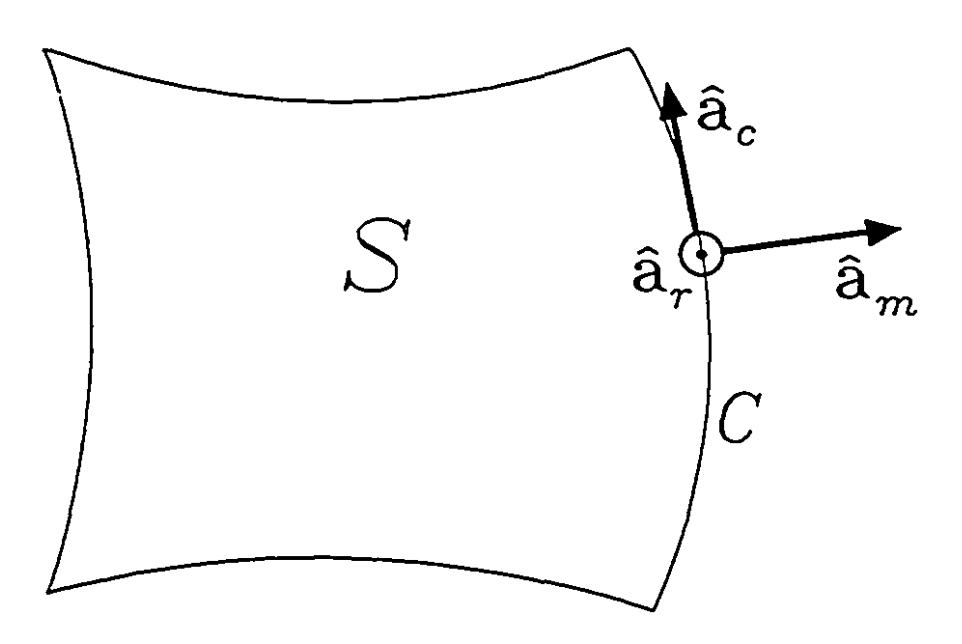


Figure 4.1 A surface S that is part of a sphere, its boundary C and the unit vectors  $\mathbf{a}_{r}$ .  $\mathbf{a}_{m}$  and  $\mathbf{a}_{c}$ .

Suppose now that C lies on a magnetic wall, i.e. it is the intersection of the spherical surface S and a magnetic wall. Then,  $\frac{1}{2} \cdot \delta H_t = 0$  is imposed explicitly because of the magnetic wall. Then (4.15) implies  $\nabla \cdot H_t = 0$ . Since  $H_r$  and  $\frac{\partial H_r}{\partial r}$  are set to zero on the magnetic wall,

$$\nabla \cdot \mathbf{H}_{t} = 0 \implies \nabla \cdot \mathbf{H}_{t} + \frac{1}{r^{2}} \frac{\partial}{\partial r} (r^{2} \mathbf{H}_{r}) = 0$$
 (4.16)

i.e.  $\nabla \cdot \mathbf{H} = 0$ . So, the correct divergence condition arises naturally.

Suppose now that C lies on an electric wall, i.e. it is the intersection of the spherical surface S and an electric wall. Then, in order for (4.15) to be satisfied, it is necessary that  $\nabla \cdot \mathbf{H}_t = 0$  and  $\mathbf{\hat{a}}_r \cdot (\nabla \times \mathbf{H}) = 0$  on C. The latter condition is equivalent to  $\mathbf{E}_r = 0$  on C which is correct due to the electric wall. The first condition, however, imposes something which is untrue. Thus, in order to have the right boundary conditions, we need to explicitly impose  $\mathbf{\hat{a}}_m \cdot \delta \mathbf{H}_t = 0$  on C on electric walls.

If the surface integral of the second order absorbing boundary condition in (4.9) is divided into integrals over quadrilaterals before the first variation of the functional is taken, see (2.11), then the first variation includes a line integral similar to that in (4.11) around the boundary of each quadrilateral  $C_i$ :

$$\int_{C_{i}} \{\hat{\mathbf{a}}_{m} \cdot \delta \mathbf{H}_{i} \nabla \cdot \mathbf{H}_{i} + \hat{\mathbf{a}}_{c} \cdot \delta \mathbf{H}_{i} [\hat{\mathbf{a}}_{r} \cdot (\nabla \times \mathbf{H})]\} dC \qquad (4.17)$$

Now, two such integrals will contribute to each line separating two quadrilaterals, one from each quadrilateral. The first variation of the functional will vanish if and only if the sum of these two contributions is zero, for each such line on the absorbing boundary surface. Since the tangential field continuity is imposed, (see Section 2.2),  $|\hat{\mathbf{a}}_c \cdot \delta \mathbf{H}_t|$  will be the same on both sides of the line, and the vanishing of the first variation just enforces the continuity of  $\hat{\mathbf{a}}_c \cdot (\nabla \times \mathbf{H})$  which is correct. However,  $\hat{\mathbf{a}}_m \cdot \delta \mathbf{H}_t$ , is not continuous, and requiring that the first variation of the functional vanishes forces that  $\nabla \cdot \mathbf{H}_t = 0$  on both sides of the lines, a restriction which is in general wrong, as discussed above. To correct this, continuity of  $\hat{\mathbf{a}}_m \cdot \delta \mathbf{H}_t$  has to be enforced over the absorbing boundary surface.

In conclusion, for the proper imposition of the second order Absorbing Boundary Condition, extra conditions have to be explicitly enforced:

36

CHAPTER 4

- a) on the ABC spherical surface, normal continuity has to be imposed on the magnetic field components tangent to the sphere, between the quadrilaterals the ABC surface is divided into.
- b)  $a_m \cdot \delta H_t = 0$  has to be imposed on those parts of C which lie on electric walls.

## CHAPTER 5

## **Programming Considerations**

A computer program has been written in standard Fortran 77 [Balfour-79] to implement the numerical method presented in this dissertation. The program is in modular form and well documented. It solves the problem in the deterministic sense, i.e. for a given excitation frequency it gives one field solution. The code was successfully tried on the following computers:

- a) an 80386 IBM compatible with 25Mhz clock speed, 80387 co-processor, 16Mb RAM 80Mb (18ms) hard disk and the NDP Fortran-386 compiler [NDP Fortran-90] under DOS 3.3.
- b) a SUN 4/110 (first generation of SPARC machines) with 8Mb RAM, 0.9 MFLOPS and the SUN Fortran compiler under the SunOS Release 4.1.1.
- c) a CRAY Y-MP super-computer with the CFT-77 Fortran compiler and the BCS library [BCSLIB-EXT-89] under UNICOS 6.0.12.

The program solves for the stationary point of the functional (4.4) in volume V where metallic and lossy dielectric materials can be present. It uses curvilinear finite elements, (see Sections 2.3, 2.4). After the input data are read, it automatically imposes tangential field continuity between elements having common faces. Since the final matrix is expected to be very sparse, the problem's sparsity pattern is found and stored to be used later by the solver. The entries of the sparse matrix are calculated for each element in turn during the local element assembly, and placed in the right position in the global matrix. All the computations involve the contributions of the field components. There are two kinds of interpolation functions:

- a) these for the spatial resolution and are used to define the geometrical shape of every curvilinear element, and
- b) these for the field resolution and are used to define the field distribution inside every curvilinear element.

The interpolation functions for the spatial resolution are 2nd order polynomials, but the ones for the field resolution are mixed order polynomials (1st and 2nd), so that no spurious modes are present. All interpolation functions are calculated and stored. Two sets of interpolation functions are used: one for the volume integral and one for the surface integral. For the integrations, Gauss quadrature is used. After the boundary conditions are imposed, the normal continuity is imposed on the covariant projections on the ABC spherical surface. The matrix equation is solved and the solution is stored. This solution contains the covariant projections field components. Finally, the solution is transformed back to the cartesian or spherical components and the result is written out to an ASCII file. The following Section gives a brief description of the subroutines used. The subroutines are listed with the same order as they are called by the main program.

## 5.1 The subroutines and a brief description

READIN: Reads from file "input.dat" the geometrical information of the

finite elements, material properties and field excitation. All

input data are in cartesian coordinates. More details on the

input data structure can be found in Appendix F.

HITRI: From the 27 geometric nodes of each curvilinear element, it

constructs the 54 field nodes for that element (for the

geometric and field node definition see Section 2.4 and

Appendix B) and imposes tangential field continuity between

elements with common faces. Each field component is con-

sidered as a field node. Also, it finds the pairs of the covariant projections that have to be made continuous on the ABC surface, (normal field continuity). At present it is necessary that the edges of the faces lying on the ABC spherical surface be colinear with lines of constant  $\theta$  or  $\phi$ .

SPAT:

Builds the sparsity pattern of the final matrix.

PRECAL:

Prepares the interpolation functions for the local volume integrations at Gauss points which lie inside each element. They will be used later by ASSEMB. Note that the interpolation functions for the spatial resolution are different from those for the field resolution.

PCAL2D:

Prepares the interpolation functions for the local surface integrations at Gauss points which lie on the quadrilaterals that form the ABC spherical surface. These points however, do not lie on the boundaries of these quadrilaterals. The same distinction between spatial and field resolutions applies here too.

CAL2D1:

Prepares the interpolation functions for the local surface integrations for the spatial resolution at the geometric nodes but for degenerate quadrilaterals: that is quadrilaterals that have one edge of zero length. It is only used for the assembling of the surface divergence term.

ASSEMB:

It is called once for each finite element in turn. It builds the local matrices for the volume integral and the surface integral of (4.4) and then puts it in the appropriate positions in the

sparse global matrix. Both first and second order ABCs can be assembled. More on assembling the final matrix can be found in Section 5.2.

COMPUT:

Prepares the interpolation functions at the geometric nodes (as opposed to the Gauss points) of each element. These values will be used later by SETBV, MODIFY and CARTES.

SETBV:

Sets the boundary values at the appropriate positions. These values are in terms of the covariant projection field components. For the case of a magnetic wall, the tangential components are set to zero. For an excitation surface, the covariant projections are set to known non zero values after being converted from the cartesian input values.

CONMOD:

Modifies the matrix [A] and creates a non zero right-hand side [b], so the new equation is now:  $[A] \cdot [x] = [b]$  where [x] is the unknown vector, instead of  $[A] \cdot [x] = 0$ , where some of the elements in [x] have prescribed values.

MODIFY:

Imposes normal continuity on the field components that lie on the ABC surface.

SOLVER:

Solves the matrix equation  $[A] \cdot [x] = [b]$ , where [A] is a complex, symmetric indefinite matrix. A frontal solver was used written by J.P. Webb and based on [Irons-80]. It is very efficient in using as little RAM as possible, however, it creates two scratch files which are of considerable size. This solver (subroutines 'cldltd' and 'cldlti') ran successfully on the 80386 IBM compatible and the Sun 4/110 computers. The Boeing

Computer Services library [BCSLIB-EXT-89] was used on the Cray Y-MP super-computer. The whole process is done in RAM and no scratch files are created.

CARTES:

It converts the solution from covariant projections to cartesian or spherical components and prints the result to the ASCII file "field.out". For each finite element this file contains: the coordinates for the geometric nodes and the three field components on every geometric node.

#### 5.2 Working with covariant components

Assembling the global matrix of the discretized form of the first variation of (4.4), requires that all the calculations are in covariant components. For the volume part, Crowley's implementation was used to build the volume terms, [Crowley-88b]. The surface part of the functional includes a dot product for the first order ABC, eqn. (4.7), and a dot, a curl and a divergence term, eqn. (4.9).

The dot term in covariant projections is straight forward using trial functions defined on the surface of the quadrilateral. The radial component of curl in covariant projections is given in Chapter 1, p.47. eqn. (61) [Stratton-41]. However, there is no expression given in covariant projections for the surface divergence term. The procedure used to express this term in covariant projections is explained below.

## 5.2.1 The surface divergence in covariant projections

Stratton gives the following expression for the divergence of a 3-component field, p.45, eqn.(55), [Stratton-41]:

$$\nabla \cdot \mathbf{H} = \frac{1}{\sqrt{g}} \sum_{i=1}^{3} \frac{\partial}{\partial \mathbf{u}^{i}} (\mathbf{H}^{i} \sqrt{g})$$
 (5.1)

Using the above expression, the surface divergence is given by:

$$\nabla_{s} \cdot \mathbf{H} = \frac{1}{\sqrt{g}} \sum_{i=1}^{2} \frac{\partial}{\partial \mathbf{u}^{i}} (\mathbf{H}^{i} \sqrt{g})$$
 (5.2)

where H' are the contravariant components on the surface,  $\sqrt{g} = |a_1 \times a_2|$ , and  $a_1$  and  $a_2$  are the unitary vectors, see Figure 5.1.

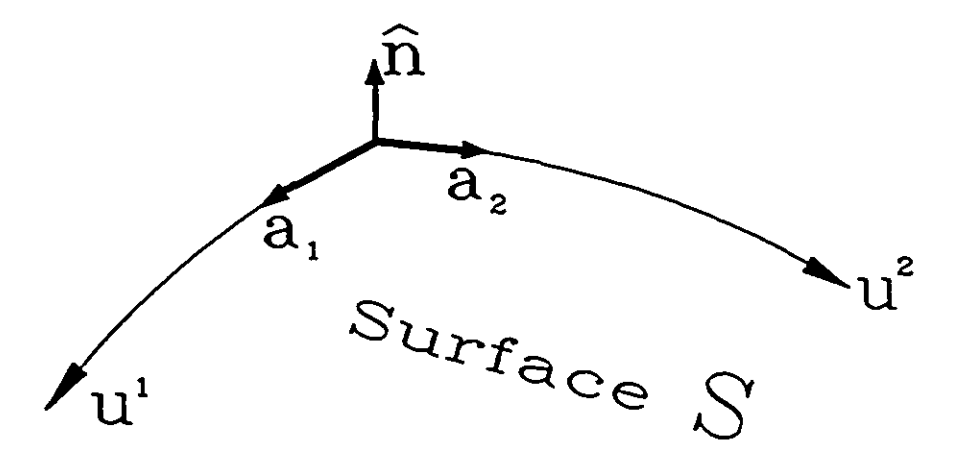


Figure 5.1 The unitary vectors  $a_1$  and  $a_2$  of a two-dimensional surface in 3-D space.

Let the vector  $\bar{\mathbf{n}}$  be the unit normal to the surface, see Figure 5.1:

$$\hat{\mathbf{n}} = \frac{\mathbf{a}_1 \times \mathbf{a}_2}{\sqrt{q}} \tag{5.3}$$

Then, the reciprocal unitary vector a 1 is given by:

$$\mathbf{a}^1 = \frac{1}{\sqrt{\sigma}} \mathbf{a}_2 \times \mathbf{\tilde{n}} \tag{5.4}$$

and therefore:

$$\mathbf{a}^{1} \cdot \mathbf{a}_{1} = (\mathbf{a}_{2} \times \mathbf{\hat{n}}) \cdot \mathbf{a}_{1}$$
$$= \frac{(\mathbf{a}_{1} \times \mathbf{a}_{2}) \cdot (\mathbf{a}_{1} \times \mathbf{a}_{2})}{g} = 1$$

which is correct, see eqn. (2.9). Similarly:

$$\mathbf{a}^2 - \frac{1}{\sqrt{g}} \mathbf{a}_1 \times \mathbf{\hat{n}} \tag{5.5}$$

and it is also true that  $a^2 \cdot a_2 = 1$ . So, the contravariant component  $H^1$  is given by:

$$H^1 = H \cdot a^1$$

and using (5.3) and (5.4) this becomes:

$$H^{1} = H_{1} \frac{1}{q} |a_{2}|^{2} - H_{2} \frac{(a_{1} \cdot a_{2})}{q}$$
 (5.6)

Similarly, for the contravariant component H2 we have:

$$H^2 = H \cdot a^2$$
  
=  $H_2 \frac{1}{a} |a_1|^2 - H_1 \frac{(a_1 \cdot a_2)}{a}$ 

and finally the surface divergence in (5.2) can be rewritten in covariant components as:

$$\nabla_{S} \cdot H = \frac{1}{\sqrt{g}} \{ \frac{\partial}{\partial u^{1}} \frac{1}{\sqrt{g}} (|a_{2}|^{2} H_{1} - (a_{1} \cdot a_{2}) H_{2}) + \frac{\partial}{\partial u^{2}} \frac{1}{\sqrt{g}} (|a_{1}|^{2} H_{2} - (a_{1} \cdot a_{2}) H_{2}) \}$$

$$(5.7)$$

## 5.2.2 The surface divergence in covariant projections: a simpler way

Expression (5.7) is very complicated to code. An easier approach for the computer implementation is given below.

Assuming that the surface S is a sphere, the tangential field in spherical coordinates is given by:

$$H_{t} = H_{\theta} \tilde{a}_{\theta} + H_{\bullet} \tilde{a}_{\bullet} \tag{5.8}$$

where  $\hat{\mathbf{a}}_{\bullet}$  and  $\hat{\mathbf{a}}_{\bullet}$  are two of the three spherical unit basis vectors. The surface divergence on S is given by:

$$\nabla_{t} \cdot \mathbf{H}_{t} = \frac{1}{r} \frac{\partial \mathbf{H}_{\theta}}{\partial \theta} + \frac{\mathbf{H}_{\theta}}{r \tan(\theta)} + \frac{1}{r \sin(\theta)} \frac{\partial \mathbf{H}_{\bullet}}{\partial \phi}$$
 (5.9)

The H<sub>0</sub> and H<sub>0</sub> components of the field can be expressed as (see also Section 2.4):

$$H_{\theta} = \sum_{i=1}^{9} H_{\theta i} g_{i}(u^{1}, u^{2})$$
 (5.10)

$$H_{\bullet} = \sum_{i=1}^{9} H_{\bullet i} g_{i}(u^{1}, u^{2})$$
 (5.11)

where  $g_i(u^1, u^2)$  are second-order trial functions in two dimensions similar to those described in eqn. (2.13). The surface divergence term of the functional (4.9) over the area of a quadrilateral is given by [Stratton-41]:

$$\int (\nabla_t \cdot H_t)^2 dS = \int_{u^1-1}^1 \int_{u^2-1}^1 (\nabla_t \cdot H_t)^2 \sqrt{g} du^1 du^2$$
 (5.12)

where g has been defined in Section 5.2. Using (5.10) and (5.11), the above may be rewritten as:

$$\int (\nabla_{t} \cdot \mathbf{H}_{t})^{2} dS = \sum_{i=1}^{9} \sum_{j=1}^{9} \mathbf{H}_{\theta i} \mathbf{H}_{\theta j} Q_{ij}^{\theta \theta} + \sum_{i=1}^{9} \sum_{j=1}^{9} \mathbf{H}_{\phi i} \mathbf{H}_{\phi j} Q_{ij}^{\phi \phi} + \sum_{i=1}^{9} \sum_{j=1}^{9} \mathbf{H}_{\phi i} \mathbf{H}_{\theta j} Q_{ij}^{\phi \theta} + \sum_{i=1}^{9} \sum_{j=1}^{9} \mathbf{H}_{\phi i} \mathbf{H}_{\theta j} Q_{ij}^{\phi \theta}$$
(5.13)

or in matrix form:

$$\int (\nabla_t \cdot \mathbf{H}_t)^2 dS = \mathbf{H}_{\theta \bullet}^{\mathsf{T}} Q \mathbf{H}_{\theta \bullet}$$
 (5.14)

Indices i, j refer to the interpolation points, and  $H_{\theta \bullet}$  is a column vector of the  $\theta$  and  $\phi$  values of the field. The square matrix Q has entries of the form:

$$Q_{ij}^{\theta \phi} = \sum_{ig=1}^{3} \sum_{jg=1}^{3} wg(ig) wg(jg) \sqrt{|u^{1}|^{2} |u^{2}|^{2} - (u^{1} \cdot u^{2})^{2}} q_{ij}^{\theta \phi}|_{ig,jg}$$

where the indices ig, jg refer to the integration Gauss points which lie on the spherical surface but not on the contour of the quadrilaterals the spherical is divided into, and wg's are the Gauss weights. The quantities  $q_{ij}^{\theta \phi}$  are functions of r,  $\theta$ ,  $\phi$ ,  $u^1$  and  $u^2$ , and they are evaluated at every Gauss point ig, jg. Similar expressions exist for  $Q_{ij}^{\theta \theta}$ ,  $Q_{ij}^{\phi \theta}$  and  $Q_{ij}^{\phi \theta}$ .

Equation (5.13) gives the surface divergence term of the functional in spherical field components. The field in covariant projections is given by:

$$H = H_1 a^1 + H_2 a^2$$

Then, the H<sub>e</sub> and H<sub>e</sub> field components are given by:

$$H_{\theta} = H \cdot \hat{a}_{\theta} = H_{1} a^{1} \cdot \hat{a}_{\theta} + H_{2} a^{2} \cdot \hat{a}_{\theta} \qquad (5.15)$$

$$H_{\bullet} = H \cdot \hat{a}_{\bullet} = H_{1} a^{1} \cdot \hat{a}_{\bullet} + H_{2} a^{2} \cdot \hat{a}_{\bullet}$$
 (5.16)

The covariant projections H<sub>1</sub> and H<sub>2</sub> can be expressed as:

$$H_1 = \sum_{i=1}^{6} H_{1i} f_{1i}(u^1, u^2)$$
 (5.17a)

$$H_2 = \sum_{i=1}^{6} H_{2i} f_{2i}(u^1, u^2)$$
 (5.17b)

where  $f_{1i}(u^1, u^2)$ ,  $f_{2i}(u^1, u^2)$  are mixed order trial functions in two dimensions similar to those described in eqn. (2.15). Using (5.15) and (5.17) the  $H_0$  component at the geometric node  $\ell$  is given by:

$$H_{\theta i} = \left( \sum_{j=1}^{6} H_{1j} f_{1j}(u^{1}, u^{2}) \right) a^{1} \cdot \hat{a}_{\theta} \Big|_{i} + \left( \sum_{j=1}^{6} H_{2j} f_{2j}(u^{1}, u^{2}) \right) a^{2} \cdot \hat{a}_{\theta} \Big|_{i} (5.18)$$

Similar expression holds for  $H_{\bullet i}$ . Thus, the relation between spherical and covariant field components is given by:

$$H_{ee} - M H_{12}$$

where M is a non-square matrix. Then eqn. (5.14) becomes:

$$\int (\nabla_t \cdot H_t)^2 dS = H_{\theta \bullet}^T Q H_{\theta \bullet}$$

$$= (M H_{12})^T Q M H_{12}$$

$$= H_{12}^T U H_{12}$$
 (5.19)

where  $U = M^{T}QM$ .

Expression (5.19) gives the surface divergence term in the covariant projection field components and it was used in the computer program implementation.

## **CHAPTER 6**

#### Results

The computer program described in the previous chapter was tested on a range of problems in order to check the validity and the performance of the proposed Absorbing Boundary Conditions. The purpose was to demonstrate the following:

- a) the efficiency and accuracy of the ABCs;
- b) convergence;
- c) difference in performance between first and second order ABCs; and
- d) the behaviour of degenerate elements, i.e. elements having a face of zero area.

Two sets of numerical experiments were performed. The first set modelled individual spherical wave functions. The second numerical experiment solved the realistic problem of scattering of an incident plane wave by a metallic sphere.

Since there was no previous experience, a large number of FE meshes were tried with different element densities. The results presented in this chapter are from meshes that gave accurate results with the minimum number of elements.

In all cases analytic solutions were available and they were compared with the computed FE results. The object here is to provide a detailed check on field values rather than comparison with macroscopic parameters, so that a thorough understanding of the behaviour of the ABCs is obtained.

## 6.1 Spherical TE wave functions

Analytical expressions for spherical TE wave functions may be found in Chapter 6 of [Harrington-61]. In a source-free homogeneous region of space, and for spherical waves, the analytical expressions for the magnetic field components are given by:

$$H_r = \frac{1}{j\omega\mu_r\mu_0} \left( \frac{\partial^2}{\partial r^2} + k_0^2 \right) F_r \qquad (6.1)$$

$$H_{\theta} = \frac{1}{r \sin(\theta)} \frac{\partial A_r}{\partial \phi} + \frac{1}{j \omega \mu_r \mu_0} \frac{1}{r} \frac{\partial^2 F_r}{\partial r \partial \theta}$$
 (6.2)

$$H_{\bullet} = -\frac{1}{r} \frac{\partial A_{r}}{\partial \theta} + \frac{1}{j \omega \mu_{r} \mu_{\theta}} \frac{1}{r \sin(\theta)} \frac{\partial^{2} F_{r}}{\partial r \partial \phi}$$
 (6.3)

For an outgoing TE spherical wave, the wave potentials F, and A, are given by:

$$F_r = \sum_{m=0}^{\infty} C_{m,n} \sqrt{\frac{\pi k_0 r}{2}} \quad H_{n+\frac{1}{2}}^{(2)}(k_0 r) \quad P_n^m(\cos(\theta)) \quad e^{jm\phi}$$
 (6.4)

$$A_r = 0 \tag{6.5}$$

where m, n are integers,  $C_{m,n}$  are constants,  $H_{n-\frac{1}{2}}^{(2)}$  are the Hankel functions of the

second kind, p.138, #24.30 in [Spiegel-68], and P<sub>n</sub> are the associated Legendre functions of the first kind, p.149, #26.2 in [Spiegel-68].

For every set of integers (m, n), equations (6.1) - (6.4) give a magnetic field which is an exact solution to Maxwell's equations in spherical coordinates. Any true field can be represented as a linear superposition of these spherical harmonics.

We now consider the boundary value problem where the magnetic field components He and He are constrained on the surface of a sphere. Their constrained values are given by (6.2) and (6.3). Outside this sphere is free space. The solution to this problem is an outgoing spherical wave, characterized by the set of integers (m, n).

49

This boundary value problem was solved using finite elements and ABCs. The results were compared with the analytical ones. Four (m,n) cases are considered here. Essentially, the volume modelled with finite elements is the space between two concentric spheres. The inner sphere is the excitation surface, where both  $H_{\theta}$  and  $H_{\phi}$  are constrained, and the outer sphere is the absorbing boundary surface, where the ABC is imposed, see Figure 6.1.

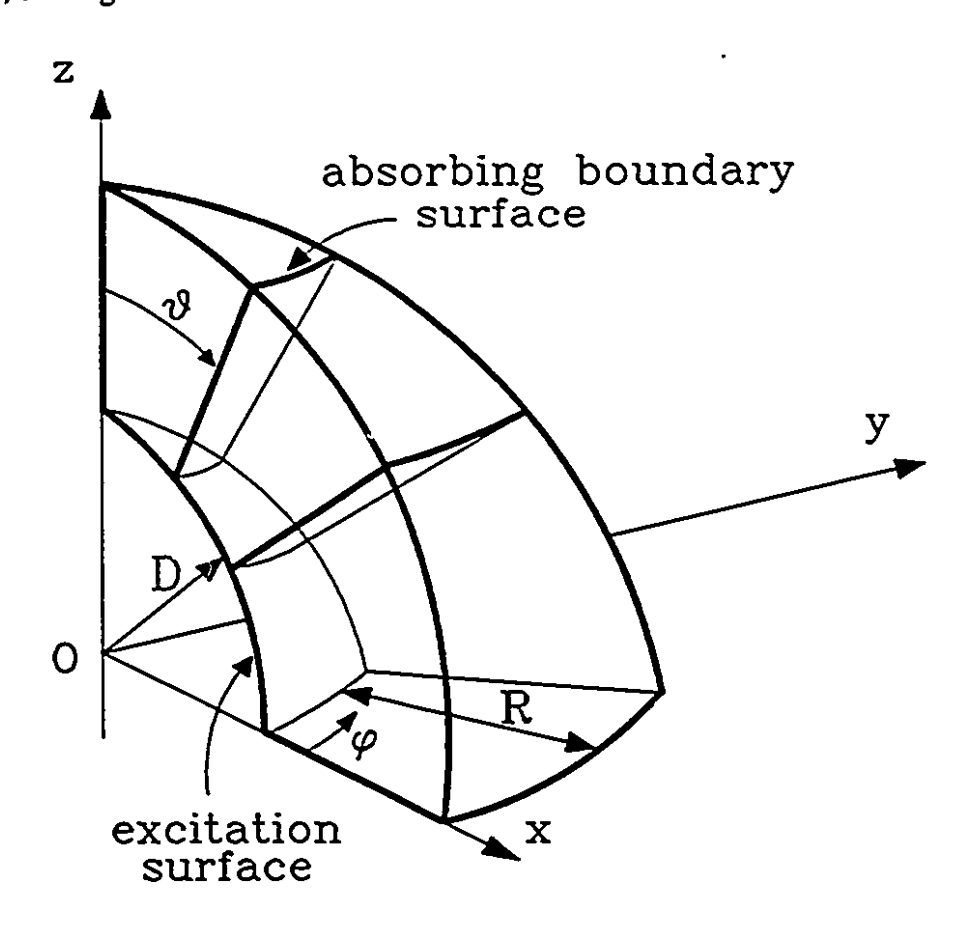


Figure 6.1 Modelling a sector of a sphere with curvilinear elements. In this mesh there are three elements in the  $\Theta$  direction, and one in r and  $\phi$  directions respectively.

Because of symmetries, only sections of the problem were modelled in each case. The curvilinear nature of the elements made them easy to fit to the spherical inner and outer boundaries. In the first two cases degenerate curvilinear elements were successfully used.

Such elements, because they are simple to use, are very promising in finite element meshes that model complicated structures, where otherwise more than one type of conventional elements would have to be used.

A simple 3D mesh generator was written to facilitate the generation of input data. It reads the file "mesphe.dat" and such a file is illustrated in Appendix F.2. It produces the output file "mesphe.out" which is used as input data by the finite element code.

## 6.1.1 The (m, n) = (0,1) case

In this case the field varies only in the r and  $\theta$  directions and  $H_{\bullet} = 0$ . Therefore, only one element was used in the  $\phi$  direction. There were four elements in the  $\theta$  direction and one element every  $0.03 \lambda$  in the r direction, where  $\lambda$  is the wavelength. The size of each curvilinear element was  $(r, \theta, \phi) = (0.03 \lambda, 22.5^{\circ}, 10^{\circ})$ . Note the degenerate elements touching the z axis, see Figure 6.1. Due to symmetries, the modelled volume was confined by boundary surfaces holding the following boundary conditions:

Boundary surface			Boundary Condition
r	=	0.3 λ	excitation surface (prescribed H <sub>9</sub> and H <sub>4</sub> )
r	=	R	Absorbing Boundary Condition
θ	=	0°	electric wall
θ	=	90°	magnetic wall
ф	=	0°	electric wall
ф	=	10°	electric wall

Figure 6.2 shows how the error changes as the absorbing boundary surface is moved outwards. In the smallest problem (R=0.06 wavelengths) there were 8 elements and 318 field nodes, and in the largest (R=0.3 wavelengths) 40 elements and 1422 field nodes.

(For field node definition see Section 2.4.) Results for first and second order Absorbing Boundary Conditions are included. The error shown is the largest value of

$$e = |H_{\text{FEM}} - H_{\text{exact}}|$$

over the volume modelled, expressed as a percentage of  $|H_{exact}|$  at the point where the largest value of e occurs.

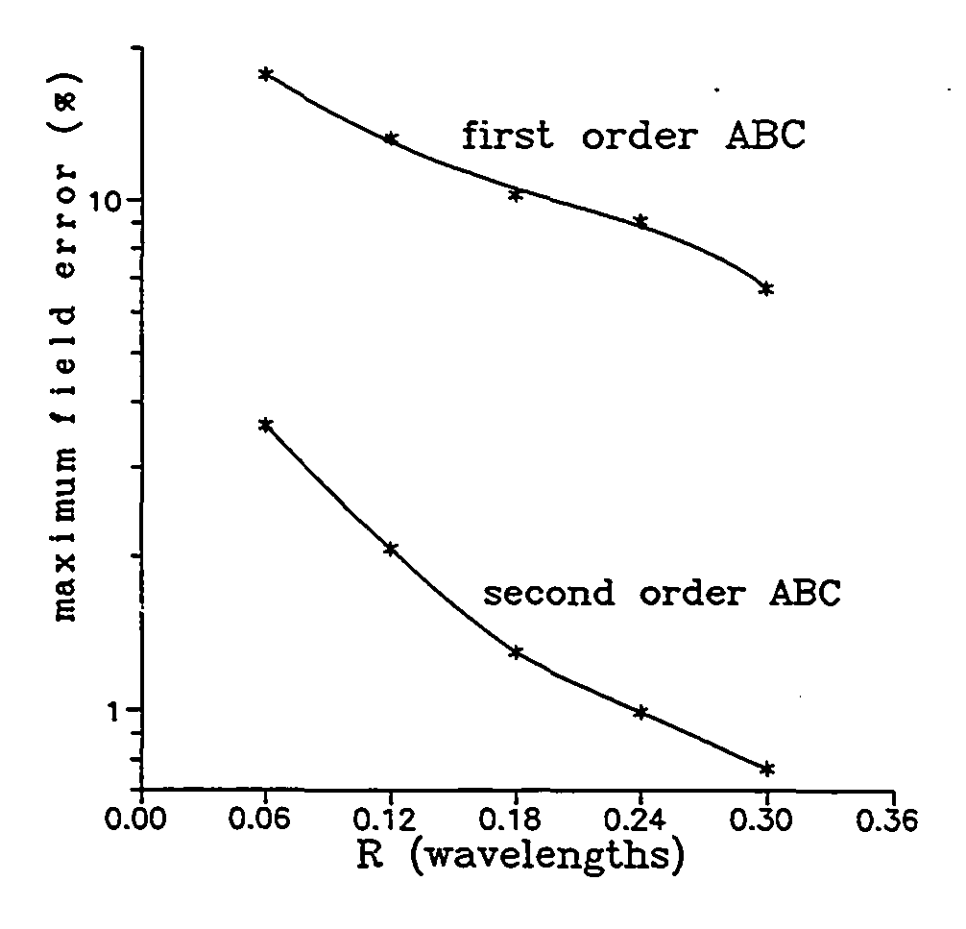


Figure 6.2 Solution error versus R, which is the distance between the excitation surface and the absorbing boundary surface, for the case (m,n) = (0,1).

#### 6.1.2 The (m, n) = (0,2) case

In this case the field varies only in the r and  $\theta$  directions and  $H_{\bullet} = 0$ . Therefore, only one element was used in the  $\phi$  direction. There were six elements in the  $\theta$  direction and one element every  $0.03 \lambda$  in the r direction, where  $\lambda$  is the wavelength. The size of each curvilinear element was  $(r, \theta, \phi) = (0.03 \lambda, 9.12^{\circ}, 10^{\circ})$ . Note the degenerate elements touching the z axis, see Figure 6.1. Due to symmetries, the modelled volume was confined by boundary surfaces holding the following boundary conditions:

Boundary surface			Boundary Condition
r	=	0.3 λ	excitation surface (prescribed H <sub>0</sub> and H <sub>0</sub> )
r	=	R	Absorbing Boundary Condition
θ	=	0°	electric wall
Э	=	54.7356°	magnetic wall
ф	=	0°	electric wall
ф	=	10°	electric wall

Figure 6.3 shows how the error changes as the absorbing boundary surface is moved outwards. In the smallest problem (R=0.12 wavelengths) there were 24 elements and 870 field nodes, and in the largest (R=0.48 wavelengths) 96 elements and 3294 field nodes. Results for first and second order Absorbing Boundary Conditions are included. The error e has been defined in Section 6.1.1.

The second order ABC absorbs any outward-propagating wave with a  $\frac{1}{r}$  and  $\frac{1}{r^2}$  variation; it absorbs less completely waves with  $\frac{1}{r^3}$  variation and even less completely waves with  $\frac{1}{r^4}$  variation. The variable n in (m,n) determines the variation of the field along the r direction. For the (0,2) case the field varies as  $\frac{1}{r^4}$  while in (0,1) it varies as

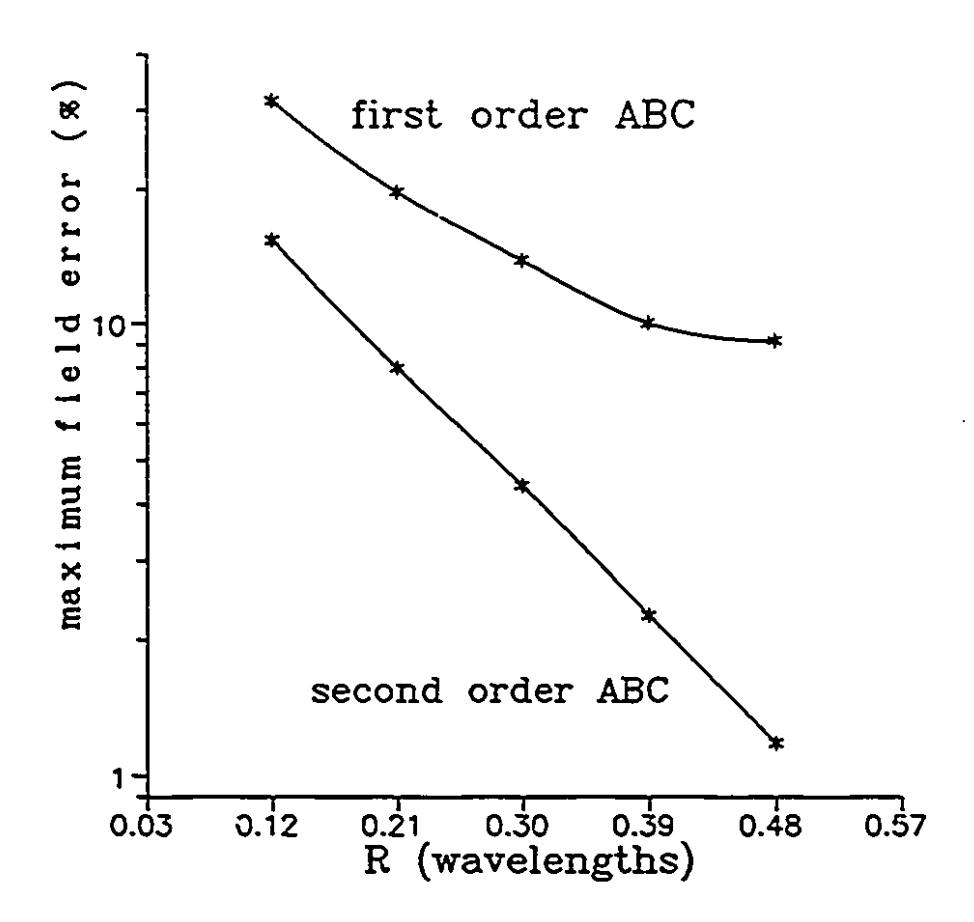


Figure 6.3 Solution error versus R, which is the distance between the excitation surface and the absorbing boundary surface, for the case (m, n) = (0,2).

 $\frac{1}{r^3}$ , see eqns. (6.1) - (6.4). In both cases the ABC is an incomplete absorber. For the (0,2) case the absorbing boundary surface has to be placed further away in order to absorb the outward-propagating wave as efficiently as in the (0,1) case. Larger values of n would require that the absorbing boundary surface is placed even further for good absorption.

#### 6.1.3 The (m, n) = (1,1) case

In this case the field varies in all three coordinate directions r,  $\theta$  and  $\phi$ . There were four elements in the  $\theta$  and  $\phi$  directions and one element every  $0.03 \lambda$  in the r

direction, where  $\lambda$  is the wavelength. The size of each curvilinear element was  $(r, \theta, \phi)$  =  $(0.03 \, \lambda, 21.75^{\circ}, 22.5^{\circ})$ . However,  $H_{\theta}$  and  $H_{\phi}$  are undefined on the z axis, so the previous meshes touching the z axis cannot be used because no boundary condition can be imposed on the degenerate surface  $\theta = 0^{\circ}$ . To overcome this problem, the z axis was not modelled. Instead a new excitation surface  $\theta = 3^{\circ}$  was introduced, so, no degenerate elements were present, see Figure 6.4. Due to symmetries, the modelled volume was confined by boundary surfaces holding the following boundary conditions:

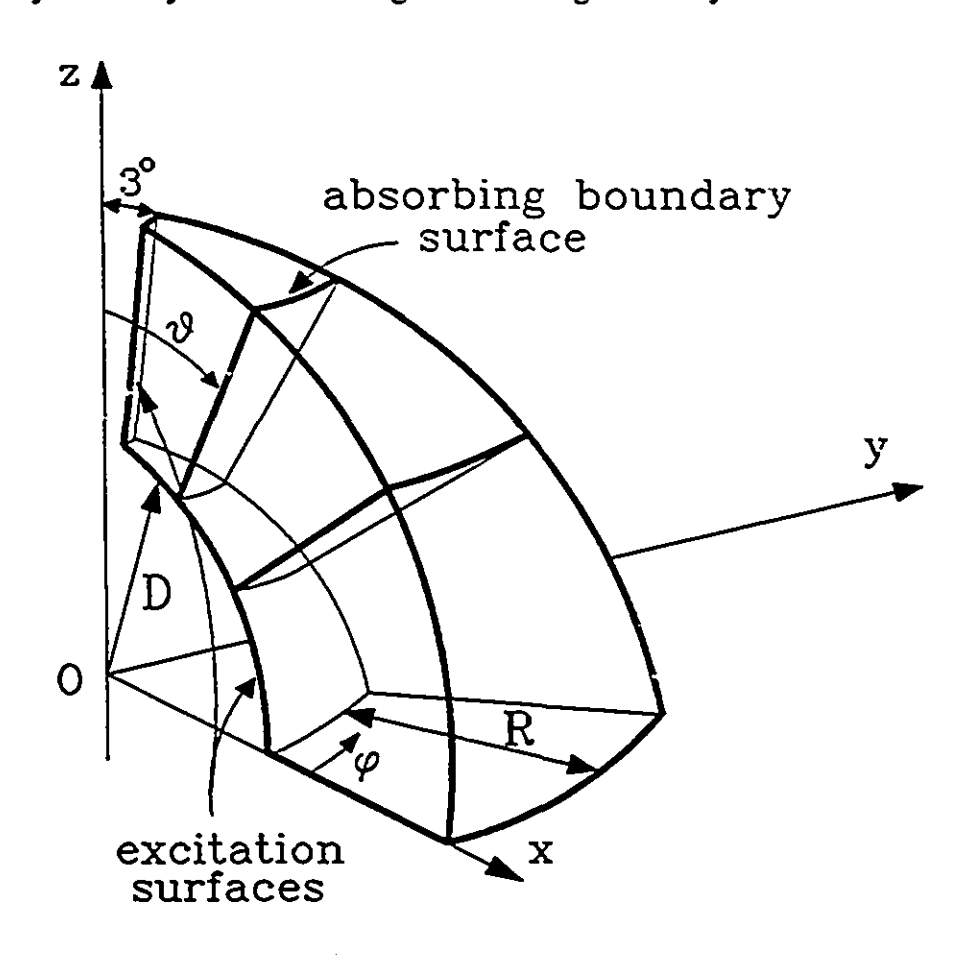


Figure 6.4 Modelling a sector of a sphere with curvilinear elements. There are no elements touching the z axis.

Boundary surface	Boundary Condition
------------------	--------------------

r	=	0.3 λ	excitation surface (prescribed He and He)	)
r	=	R	Absorbing Boundary Condition	
θ	=	3°	excitation surface (prescribed H, and H.	)
θ	=	90°	electric wall	
ф	=	0°	electric wall	
ф	=	90°	magnetic wall	

Figure 6.5 shows how the error changes as the absorbing boundary surface is moved outwards. In the smallest problem (R=0.06 wavelengths) there were 32 elements and 1044 field nodes, and in the largest problem (R=0.3 wavelengths) there were 160 elements and 4644 field nodes. Results for first and second order Absorbing Boundary Conditions are included. The error e was defined in Section 6.1.1.

For this spherical harmonic (1,1) the absorbing boundary surface absorbs as efficiently as in the (0,1) case. This is because in both cases the field varies as  $\frac{1}{r^3}$ .

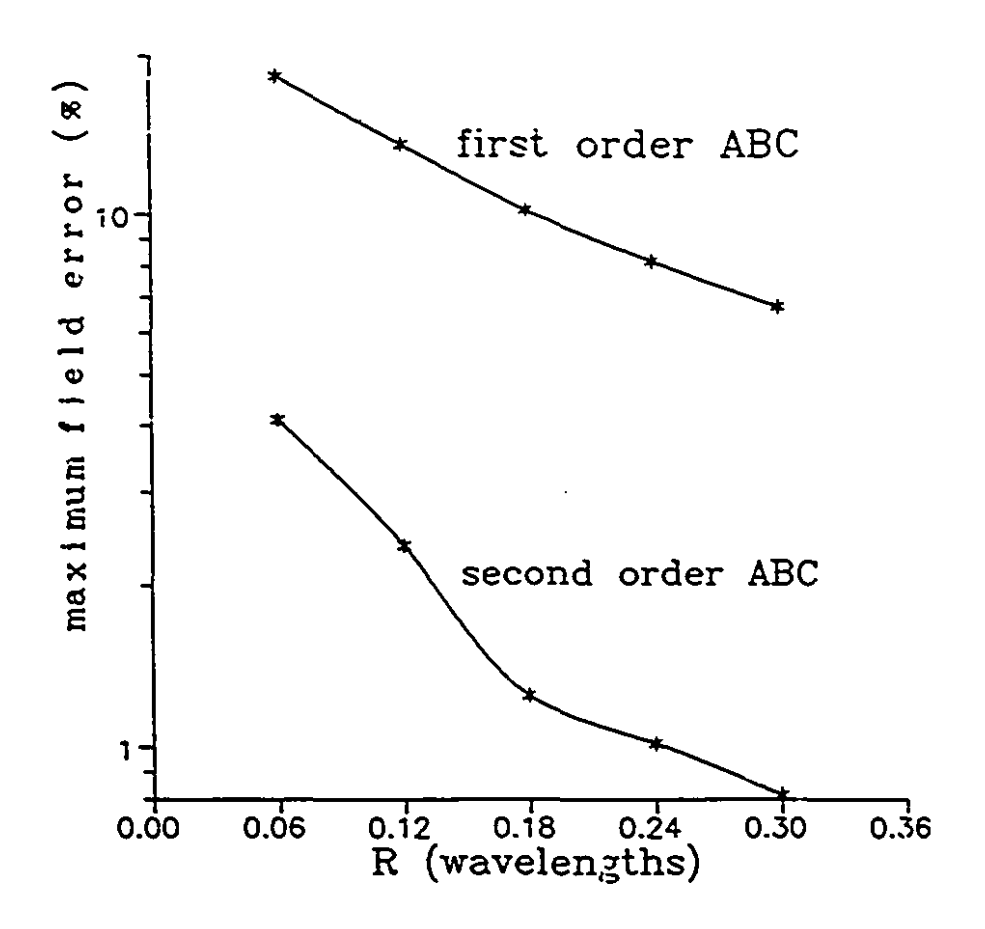


Figure 6.5 Solution error versus R, which is the distance between the excitation surface and the absorbing boundary surface, for the case (m, n) = (1,1).

Figure 6.6 shows how the error changes as the mesh density changes. The absorbing boundary surface is at a constant distance of  $r = R = 0.3 \,\lambda$  from the excitation surface. In the smallest problem there was one element in the  $\theta$  and  $\phi$  directions and two elements in the r direction. The next mesh had two elements in the  $\theta$  and  $\phi$  directions and four elements in the r direction. For three elements in  $\theta$  and  $\phi$  there were six elements in the r direction and so forth. All elements have the same size within the same mesh. However, they are different from one mesh to the other. In the smallest problem there were 2 elements and 96 field nodes, and in the largest problem there were 250 elements and 7040 field nodes. Results for first and second order Absorbing Boundary

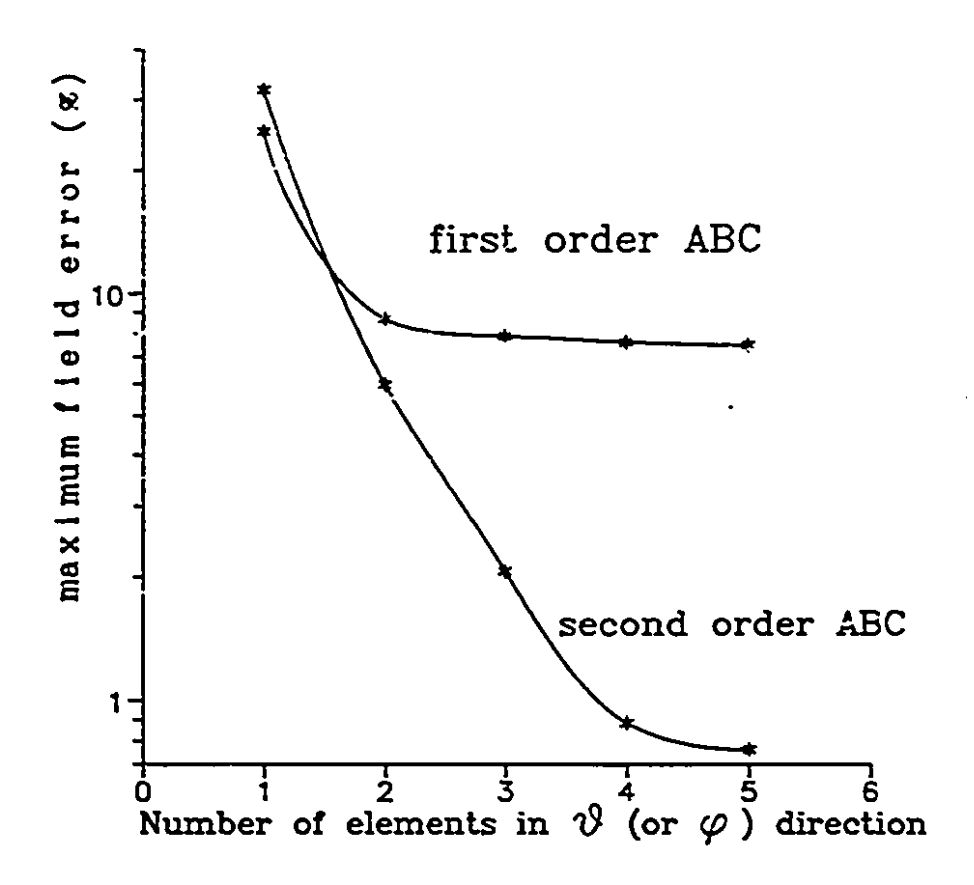


Figure 6.6 Convergence results as the mesh density increases for the case  $(m \cdot n) = (1,1)$ . The absorbing boundary surface has been kept at a constant distance  $R = 0.3 \lambda$ . The number of elements in the r direction are twice as many as in  $\Theta$  (or  $\Phi$ ) direction.

Conditions are included. Note that when further discretization of the mesh does not improve the performance of the ABCs, the error from the second order ABC is about one order of magnitude smaller than that from the first order.

#### 6.1.4 The (m, n) = (1,2) case

In this case the field varies in all three coordinate directions r,  $\theta$  and  $\phi$ . There were three elements in the  $\theta$  direction, five in  $\phi$  and one element every  $0.03 \lambda$  in the r direction, where  $\lambda$  is the wavelength. The size of each curvilinear element was  $(r, \theta, \phi)$ 

=  $(0.03 \lambda, 15^{\circ}, 18^{\circ})$ . No degenerate elements were present. Due to symmetries, the modelled volume was confined by boundary surfaces holding the following boundary conditions:

Boundary surface			Boundary Condition
r	=	0.3 λ	excitation surface (prescribed $H_{\bullet}$ and $H_{\bullet}$ )
r	=	R	Absorbing Boundary Condition
θ	=	45°	electric wall
θ	=	90°	magnetic wall
ф	=	0°	electric wall
ф	=	90°	magnetic wall

Figure 6.7 shows how the error changes as the absorbing boundary surface is moved outwards. In the smallest problem (R=0.06 wavelengths) there were 30 elements and 988 field nodes, and in the largest problem (R=0.48 wavelengths) there were 240 elements and 6952 field nodes. Results for first and second order Absorbing Boundary Conditions are included. The error e has been defined in Section 6.1.1.

For this spherical harmonic (1,2) the absorbing boundary surface absorbs as efficiently as in the (0,2) case. This is because in both cases the field varies as  $\frac{1}{r^4}$ .

Figures 6.8 and 6.9 show the amplitude and phase of the magnetic field component  $H_r$  for the (1,2) case, at the geometric point  $(r,\theta,\phi) = (0.36 \lambda, 60^{\circ}, 72^{\circ})$ , versus the distance R between the excitation surface and the absorbing boundary surface. The computed component  $H_r$  generally had a larger error than the other two components since it is the least prescribed by the boundary conditions. The results from the second order ABC converge better to the theoretical values than those from the first order.

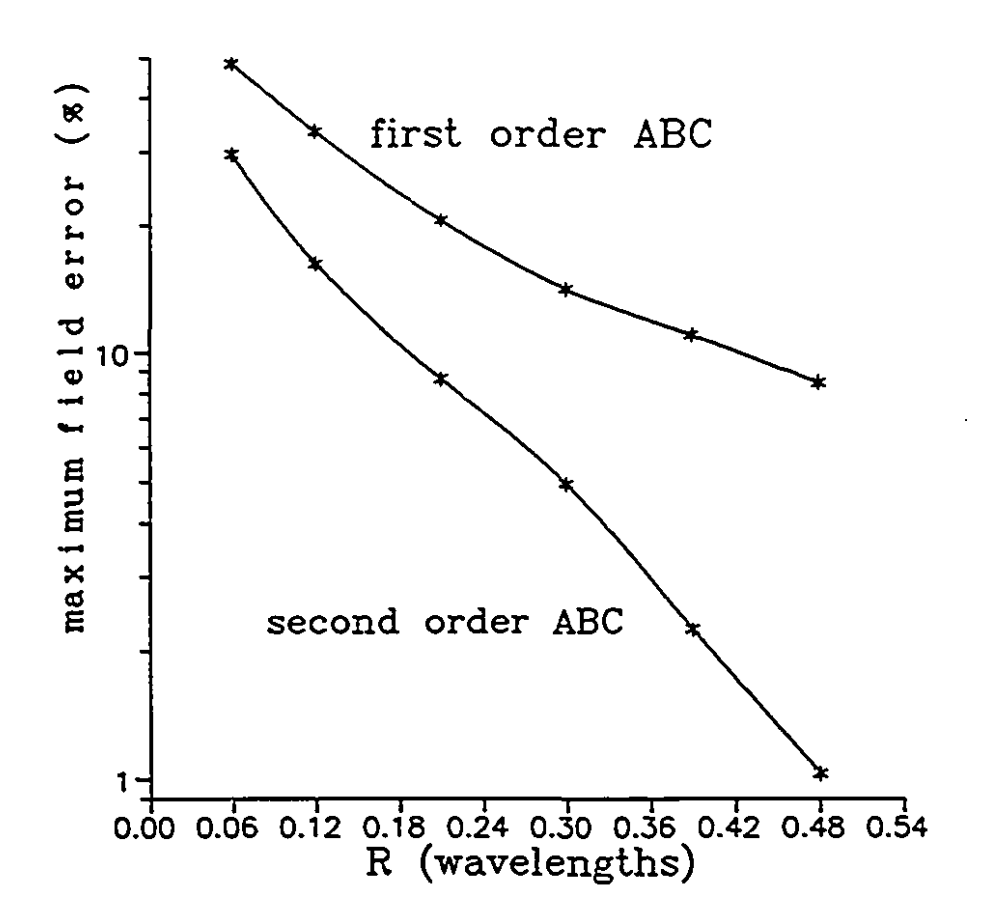


Figure 6.7 Solution error versus R, which is the distance between the excitation surface and the absorbing boundary surface, for the case  $(m \cdot n) = (1,2)$ .

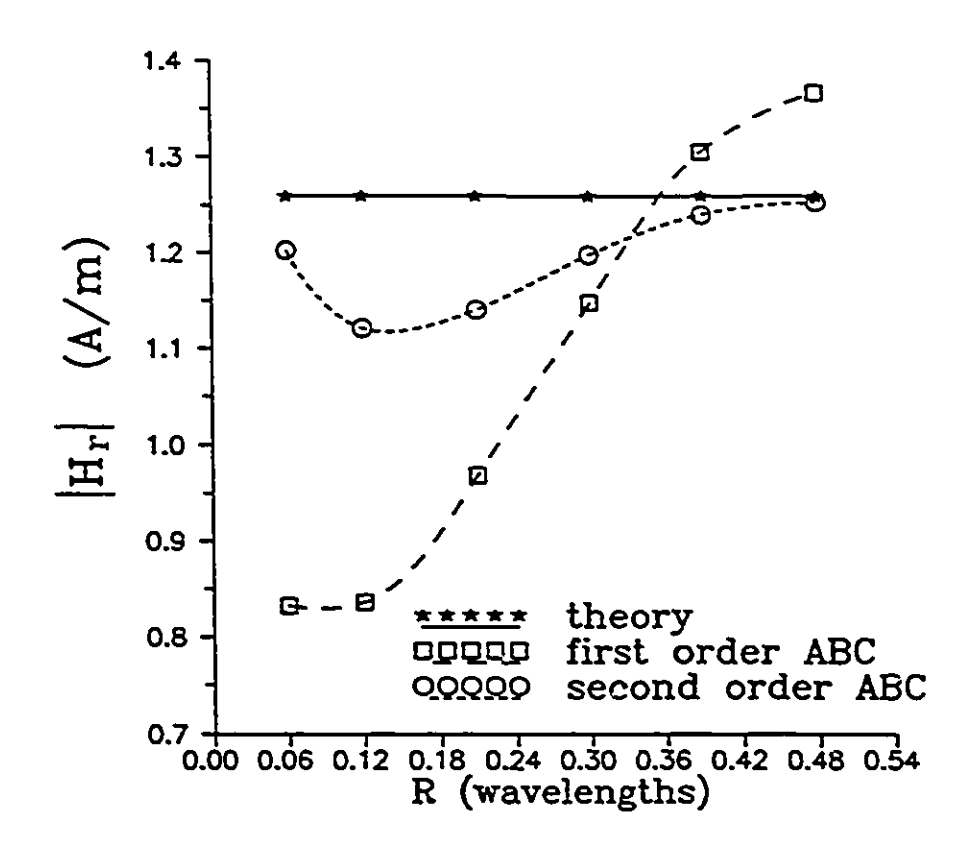


Figure 6.8 Amplitude of the magnetic field component  $H_r$  versus  $R_r$ , which is the distance between the excitation surface and the absorbing boundary surface, for the case  $(m \cdot n) = (1,2)$ .

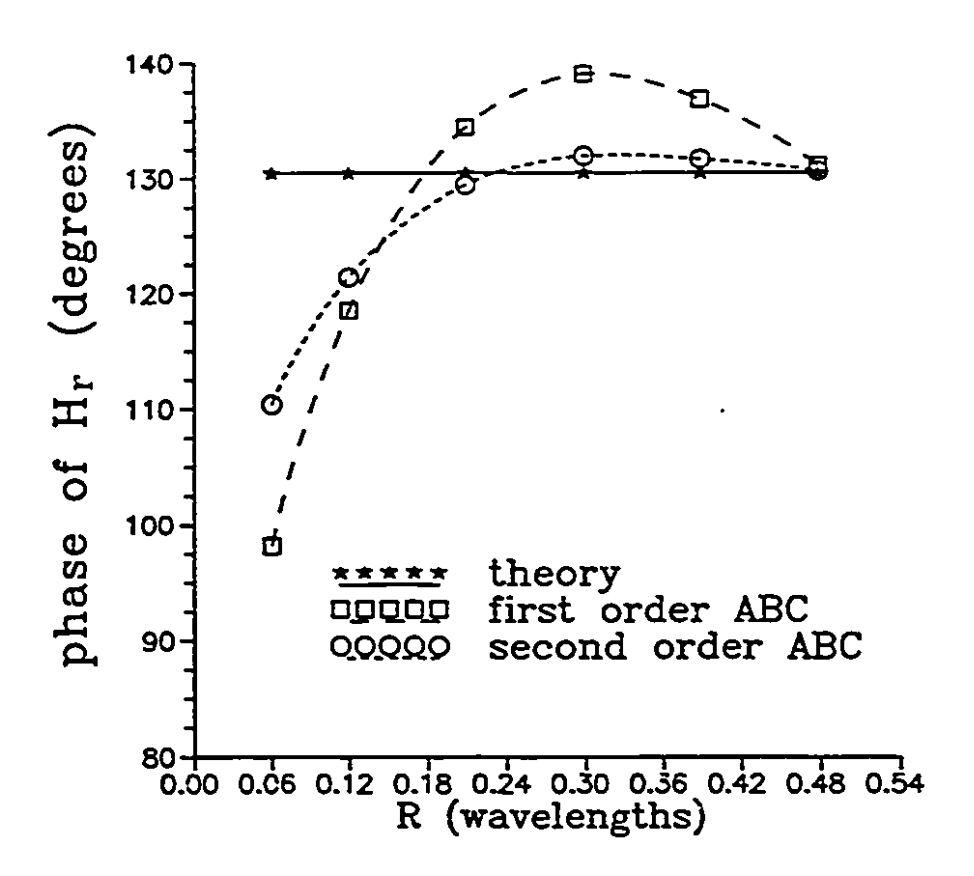


Figure 6.9 Phase of the magnetic field component  $H_r$  at one point versus R, which is the distance between the excitation surface and the absorbing boundary surface, for the case (m, n) = (1,2).

## 6.2 Scattering from a metallic sphere

Consider the boundary value problem of scattering of an incident plane wave by a metallic sphere, see Figure 6.12. For an x-polarized and z-traveling plane wave incident on a metallic sphere of centre (0,0,0), the magnetic field is given by:

$$H_y^i = \frac{E_0}{\eta_0} e^{-jk_0 r \cos(\theta)}$$

where  $E_0$  is a constant, and  $\eta_0$  is the intrinsic impedance of free space:  $\eta_0 = 376.73$  Ohms. The wave potentials for the scattered field are given by:

$$A_r^s = \frac{E_0}{\eta_0 k_0 \mu_r} \cos(\phi) \sum_{n=1}^{\infty} b_n \sqrt{\frac{\pi k_0 r}{2}} H_{n-\frac{1}{2}}^{(2)}(k_0 r) P_n^1(\cos(\theta))$$
 (6.6)

$$F_r^s = \frac{E_0}{k_0} \sin(\phi) \sum_{n=1}^{\infty} c_n \sqrt{\frac{\pi k_0 r}{2}} H_{n-\frac{1}{2}}^{(2)}(k_0 r) P_n^1(\cos(\theta))$$
 (6.7)

The constants  $b_n$  and  $c_n$  are defined in eqn. (6-102), page 294, [Harrington-61]. The magnetic field H is given by eqns. (6.1) - (6.3). The total field is, of course, the sum of the incident and scattered fields.

This boundary value problem was solved using finite elements and ABCs. The results were compared with the analytical ones. The volume modelled with finite elements was the space between two concentric spheres. The inner sphere is the metallic sphere, and it is the excitation surface, where both H<sub>0</sub> and H<sub>0</sub> are constrained to known values of the scattered field given by eqns. (6.2), (6.3), (6.6) and (6.7). The outer sphere is the absorbing boundary surface, where the ABC is imposed. Since H<sub>0</sub> and H<sub>0</sub> are undefined on the z axis, the z axis was not modelled, see Figure 6.4. Due to symmetries, the modelled volume was also confined by boundary surfaces holding the following boundary conditions:

r	=	0.3 λ	excitation surface (prescribed $H_{\theta}$ and $H_{\bullet}$ )		
r	=	, <b>R</b>	Absorbing Boundary Condition		
θ	=	3°	excitation surface (prescribed $H_r$ and $H_{\bullet}$ )		

**Poundary Condition** 

 $\theta = 177^{\circ}$  excitation surface (prescribed H, and H<sub>•</sub>)

 $\phi = 0^{\circ}$  magnetic wall  $\phi = 90^{\circ}$  electric wall

Note that in this case a quarter of the sphere was modelled and not just an eighth as in (m, n) = (1,1) case. There were twelve and six elements in the  $\theta$  and  $\phi$  directions

Boundary surface

respectively, and one element every  $0.03 \lambda$  in the r direction, where  $\lambda$  is the wavelength. The size of each curvilinear element was  $(r.\theta.\phi) = (0.03 \lambda. 14.5^{\circ}. 15^{\circ})$ . The values of the Hankel and the associated Legendre functions required for the excitation field values were double checked using the Mathematica-386 software, see [Wolfram-88].

Figure 6.10 shows how the error changes as \* absorbing boundary surface is moved outwards. In the smallest problem (R=0.06 engths) there were 144 elements and 4360 field nodes, and in the largest problem (R=0.42 wavelengths) there were 1008 elements and 26848 field nodes. Results for first and second order Absorbing Boundary Conditions are included. The diagram clearly shows the superiority of the second order ABC.

Figure 6.11 shows how the error changes as the radius D of the metallic sphere is increased, while the absorbing boundary surface is kept at a constant  $R=0.36 \lambda$ . see Figure 6.10. This is equivalent to increasing the excitation frequency while keeping the ABC surface the same number of wavelengths away from the scatterer. It appears that there is almost no change for the second order results, while first order gives better values as D increases. For very big values of D the inner sphere would look rather like a plane scatterer and the first and second order results should give the same accuracy for an incident plane wave.

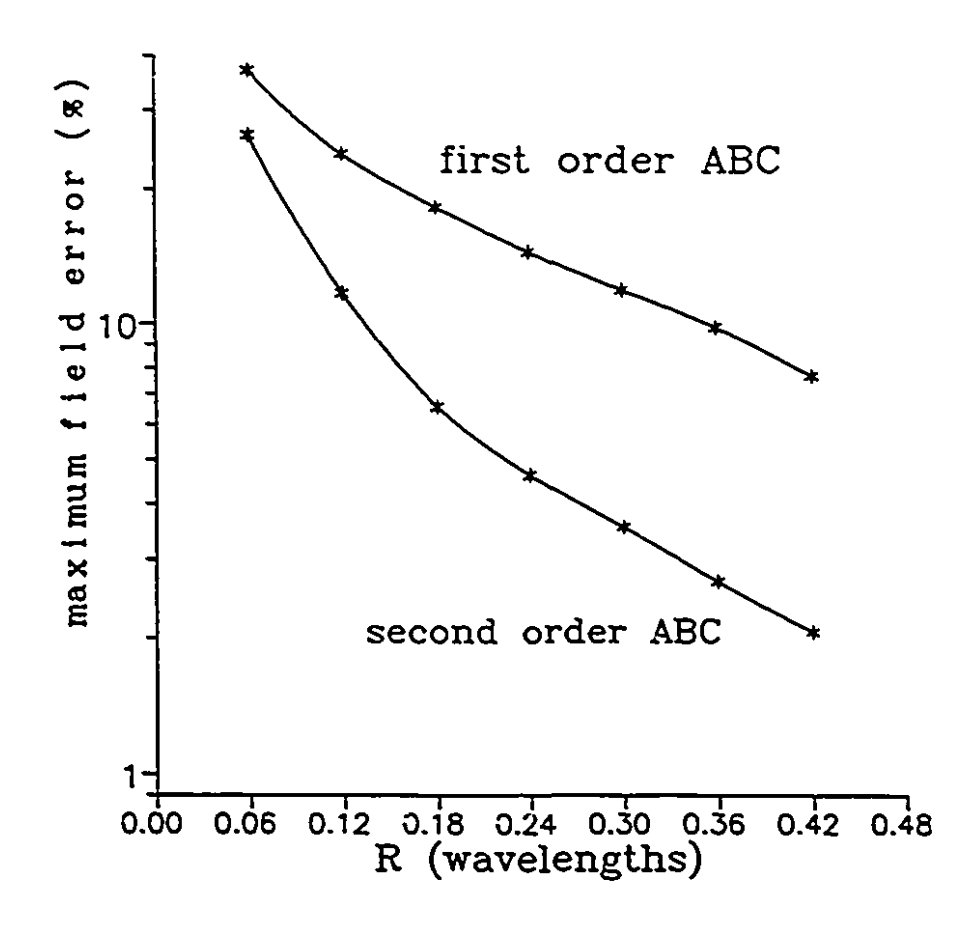


Figure 6.10 Scattering by a metallic sphere. Solution error versus R, which is the distance between the excitation surface and the absorbing boundary surface. The radius of the metallic sphere is D=0.3  $\lambda$ .

Figure 6.12 shows a y-z cross-section of the metallic sphere scatterer and the absorbing boundary surface in the presence of the incident plane wave  $E_x^i$ ,  $H_y^i$ . The line AB is along the radial direction at  $\theta = 24.75^\circ$  and  $\phi = 90^\circ$ . The next Figures compare calculated field values with the analytical ones on geometric points along AB. Accurate results were obtained (second order ABC) when the absorbing boundary surface was less than one half a wavelength away from the scatterer.

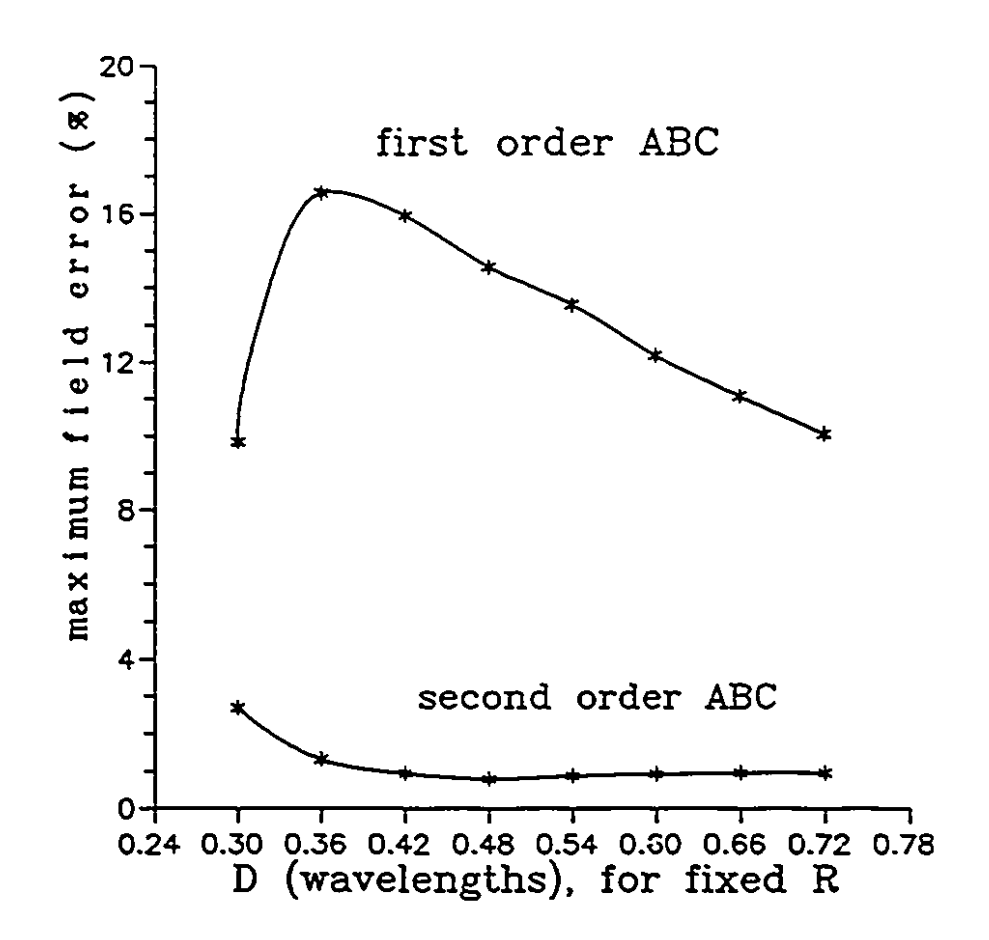


Figure 6.11 Scattering by a metallic sphere. Solution error versus D, for  $R = 0.36 \lambda$ . D is the radius of the metallic sphere, and R is the distance between the excitation surface and the absorbing boundary surface.

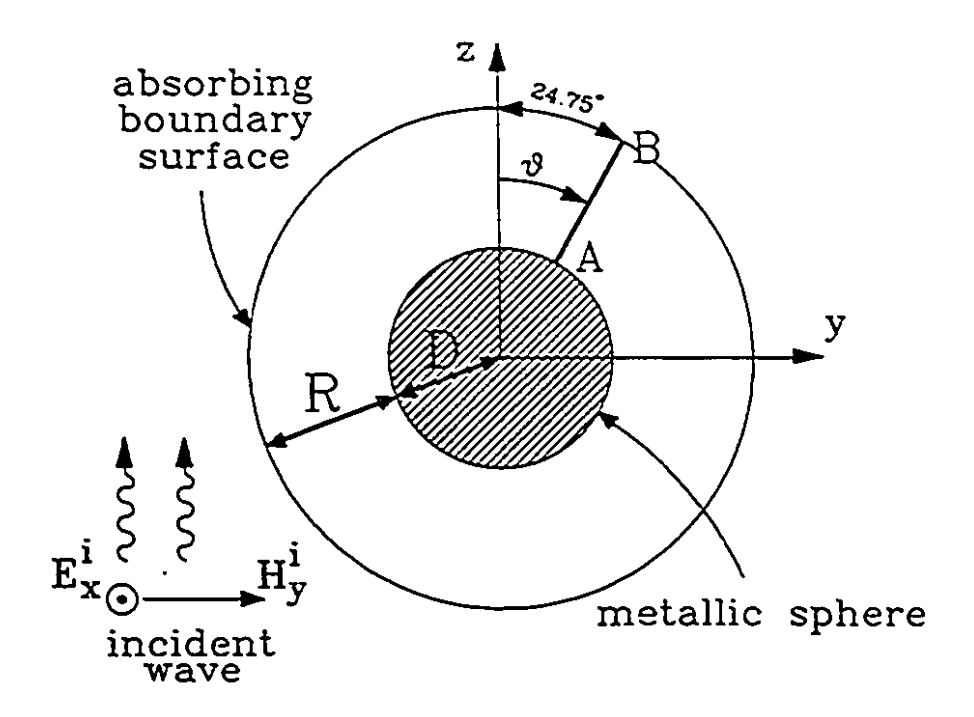


Figure 6.12 A y-z cross-section of the 3D geometry. The gray area is the metallic sphere of radius D which is completely enclosed by the concentric absorbing boundary surface of radius D+R. The incident plane wave is x-polarized and z-travelling. D =  $0.3 \lambda$  and R =  $0.36 \lambda$ , where  $\lambda$  is the wavelength.

Figure 6.13 shows values of the amplitude of the scattered field  $H^s$ , normalized to the incident field amplitude, versus r along AB, see Fig. 6.12. The percentage numbers are the errors e on the corresponding geometric points.  $e = |H_{\text{FEM}}^s - H_{\text{exact}}^s|$ , and they are expressed as a percentage of  $|H_{\text{exact}}^s|$ . The second order values are almost the same as the theoretical ones. The percentage error increases as we move away from the excitation surface. This is because on that surface the field components  $H_\theta$  and  $H_\phi$  have prescribed values.

Figures 6.14 and 6.16 show values of the amplitude of the scattered field components  $H_r^2$  and  $H_r^2$ , normalized to the incident field amplitude, versus r along

....

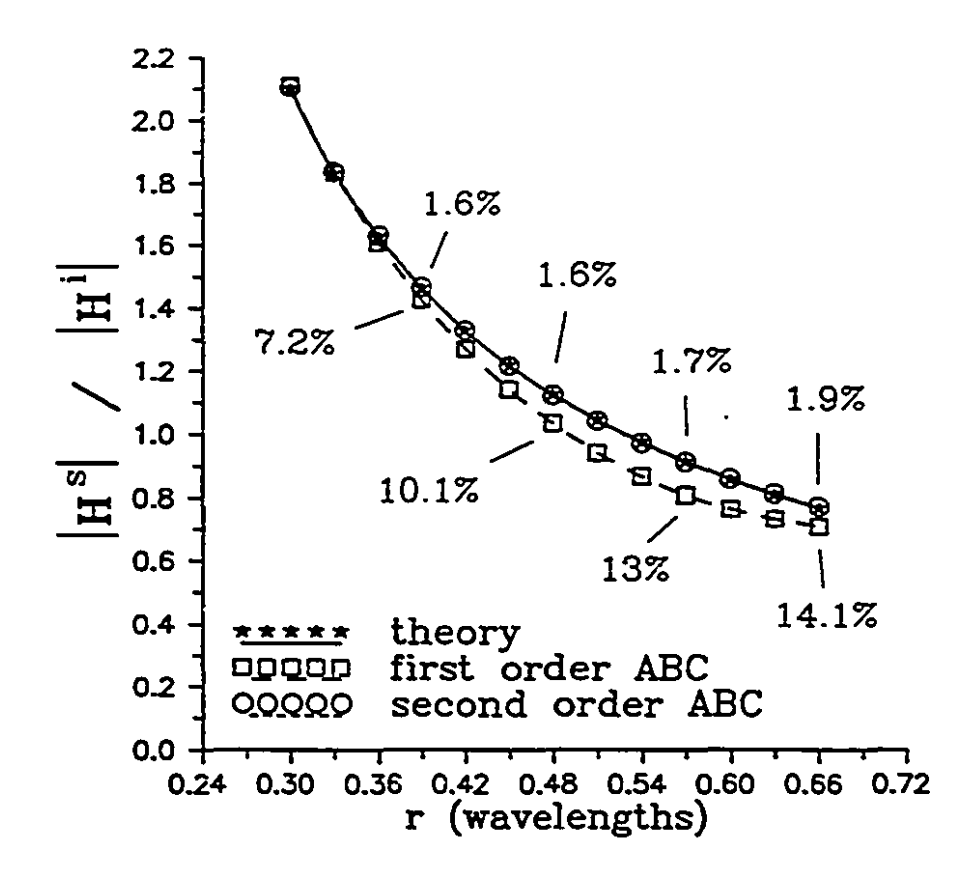


Figure 6.13 Scattering by a metallic sphere. Normalized amplitude of the scattered magnetic field H<sup>\*</sup> versus r along AB, see Fig. 6.12. The percentages are the errors at the corresponding points as a percentage of the theoretical values.

AB, see Fig. 6.12. Figures 6.15 and 6.17 show values of the phase of the scattered field components  $H_r^2$  and  $H_\theta^2$ , versus r along AB, see Fig. 6.12. On the  $\phi = 90^\circ$  plane  $H_\phi$  = 0. In all cases the superiority of the second order ABC is clear.

For scattering from an arbitrary metallic scatterer the electric field E formulation has to be used with the following boundary conditions on the surface of the scatterer:  $E^{z} = -E^{t}.$ 

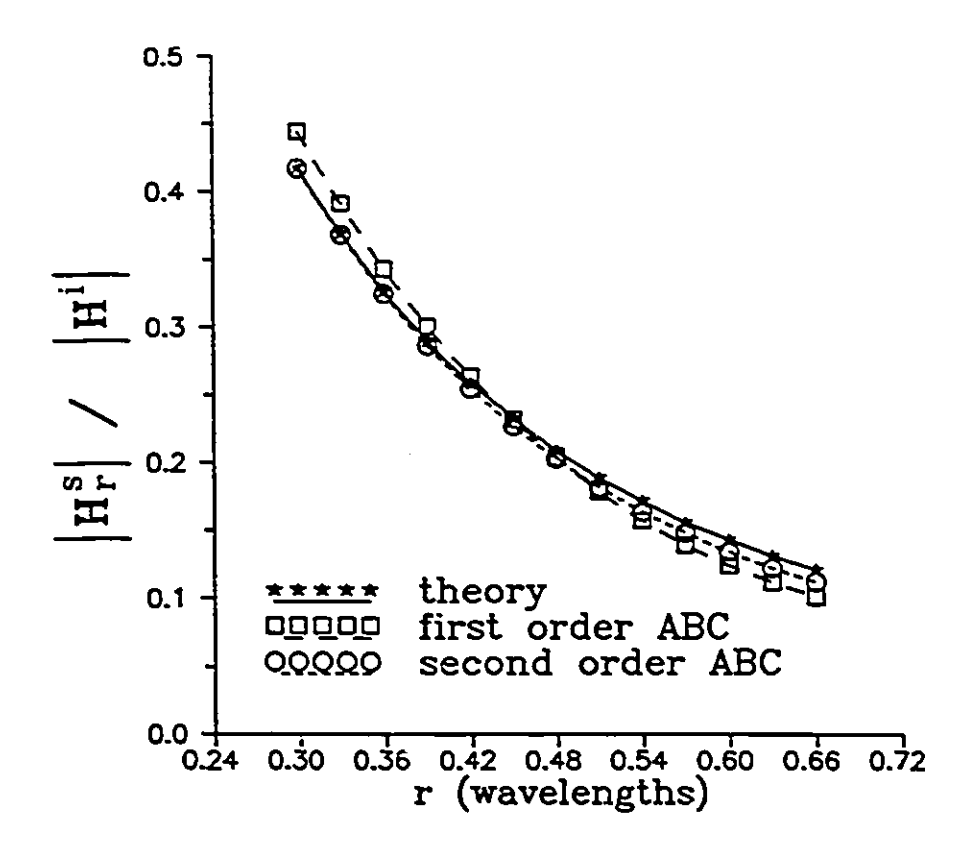


Figure 6.14 Scattering by a metallic sphere. Normalized amplitude of the scattered magnetic field component H<sup>\*</sup><sub>r</sub> versus r along AB, see Fig. 6.12.

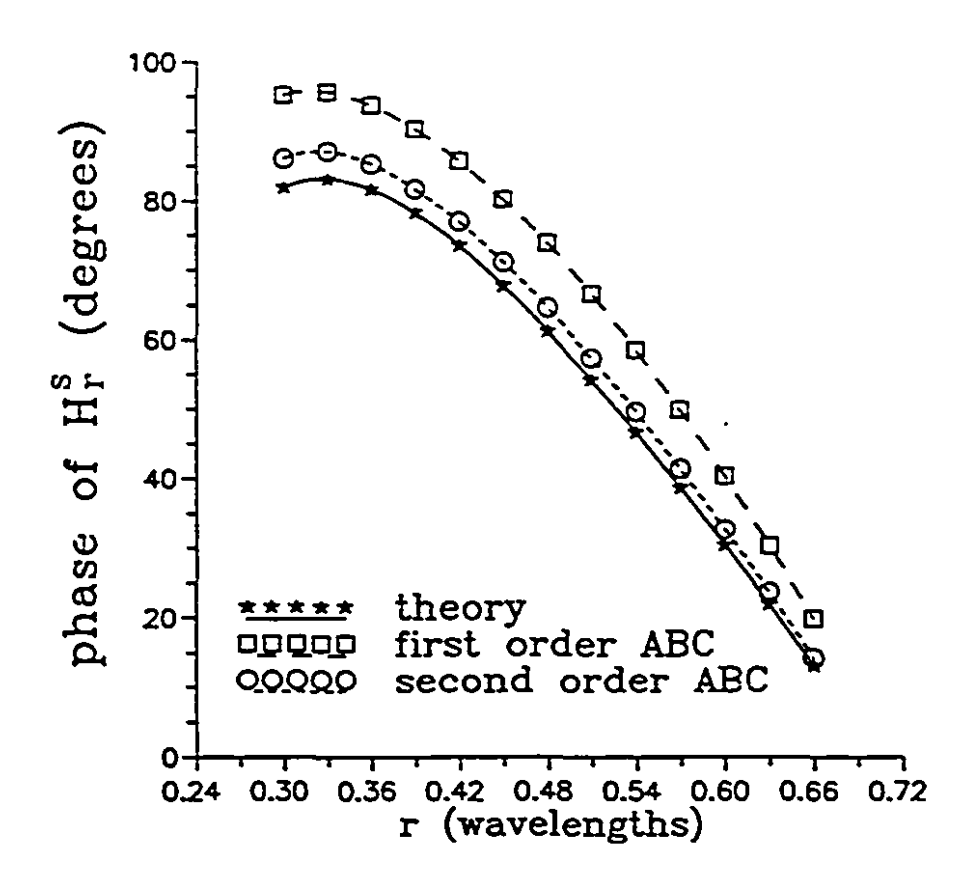


Figure 6.15 Scattering by a metallic sphere. Phase of the scattered magnetic field component H; versus r along AB, see Fig. 6.12.

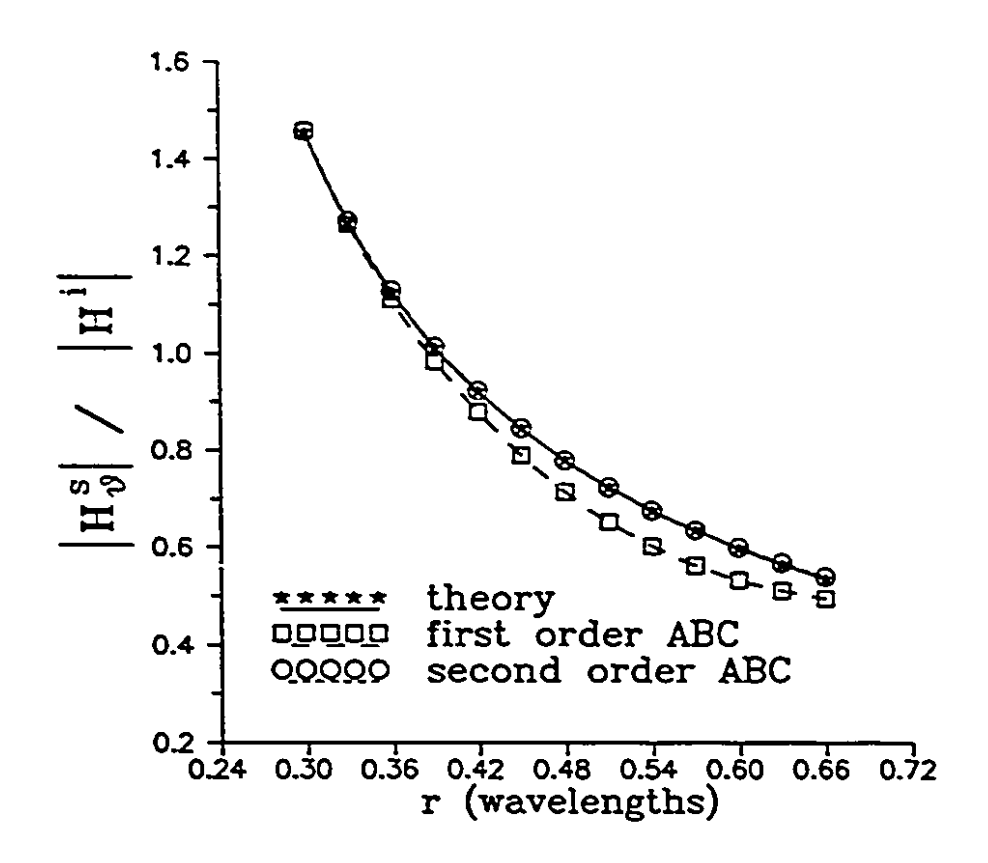


Figure 6.16 Scattering by a metallic sphere. Normalized amplitude of the scattered magnetic field component H<sub>0</sub><sup>\*</sup> versus r along AB, see Fig. 6.12.

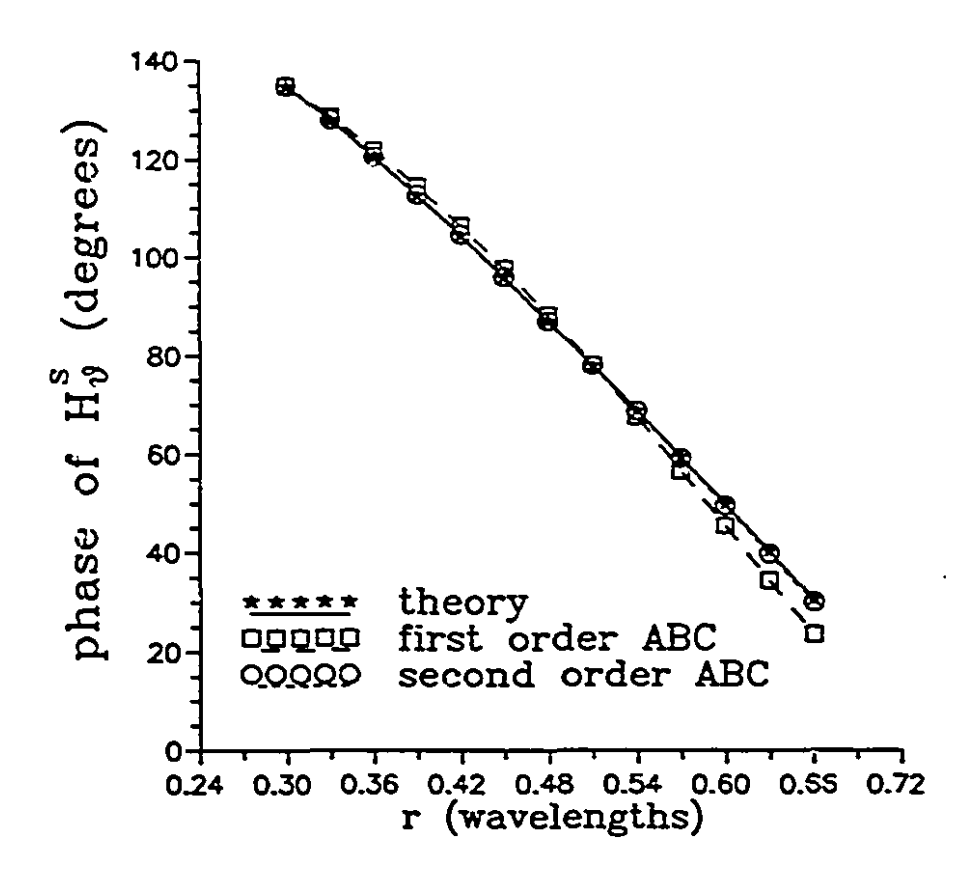


Figure 6.17 Scattering by a metallic sphere. Phase of the scattered magnetic field component H<sub>6</sub>\* versus r along AB, see Fig. 6.12.

### **6.3** Computational considerations

For a 30-element problem of 988 field nodes, the assembly of the global matrix took 7 minutes and 14 seconds and the solver 8 minutes and 40 seconds on an 80386-based computer, (see beginning of Chapter 5 for computer specifications). All times for the 80386-based computer refer to total time as opposed to CPU time only. The total disc space required by the solver for scratch files was 0.936 Mbytes. Similarly, for a 240-element problem of 6952 field nodes the assembly of the global matrix took 55

minutes and 49 seconds and the solver 9 hours and 1 minute and 65 seconds on the same computer. The disc space required in this case was 36.84 Mbytes. The next table gives more information regarding the computational cost on the 80386 computer.

80386							
Field nodes	Number of non- zeros in global matrix W	Computational cost in assembling the global matrix W	Computational cost in solving the simultaneous equations				
988	40062	7min 14s	8min 40s				
1840	79020	14min 10s	28min 14s				
3118	137457	24min 35s	1h 26min 1s				
4396	195894	34min 58s	3h 11min 1s				
5674	254331	45min 22s	5h 58min 6s				
6952	312768	55min 49s	9h 59min 1s				
7344	338766	58min 29s	15h 6min 37s				

For a 144-element problem of 4360 field nodes the assembly of the global matrix took 8 seconds and the solver 4 seconds of CPU time on the CRAY Y-MP super-computer. Similarly, for a 1008-element problem of 26848 field nodes the assembly of the global matrix took 53 seconds and the solver 152 seconds of CPU time on the same super-computer. The next table gives more information regarding the computational cost on the CRAY Y-MP computer. It should be noted here that the vectorized and parallelized BCS solver was used [BCSLIB-EXT-89], which is specifically written for the CRAY super-computers. No special instructions were implemented in the rest of the code

to take advantage of the architecture of vector parallel machines. Should such care had been taken for the rest of the code, the times for the matrix assembly would have been considerably smaller.

CRAY Y-MP							
Field nodes	Number of non- zeros in global matrix W	Computational cost in assembling the global matrix W	Computational cost in solving the simultaneous equations				
4360	219562	8s	4s				
8108	403600	15s	11s				
11856	587638	23s	34s				
19352	955714	38s	89s				
23100	1139752	45s	96s				
26848	1323790	<i>5</i> 3s	152s				
30596	1507828	60s	170s				
34344	1691866	68s	254s				

#### **CHAPTER 7**

#### **Conclusions**

In this treatise a new method has been proposed for the use of finite elements in three-dimensional open-boundary vector wave problems. It is based on new local differential boundary conditions, the Absorbing Boundary Conditions (ABCs), which are applied on a spherical surface that completely encloses the volume of interest. These boundary conditions preserve the *sparsity* and the *symmetry* of the finite element matrices providing a pure finite element technique as opposed to *hybrid* solutions, (FE combined with integral techniques), that alter the sparsity of the matrices. Existing vectorized sparse solvers take full advantage of such sparse matrices reducing drastically the computational cost.

General expressions for n th order ABCs have been derived. First and second order ABCs have been implemented into a symmetric bilinear form suitable for the finite element code.

Curvilinear covariant-projection elements of mixed order (first and second) have been used in all the analyzed problems. These elements enforce only tangential continuity on the magnetic field vector between the elements and they are free of spurious corruptions. Normal continuity is imposed naturally by the variational formulation. Their curvilinear nature makes them highly suitable for problems with curved surfaces. In addition, degenerate curvilinear elements have been successfully tested in this thesis. They are degenerate because at least one of their faces is shrunk to a line, i.e. a face of zero area. Such elements are very useful in problems where many and highly complicated dielectric materials have to be modelled. There is no need to use different types of finite elements in the same mesh, since curvilinear elements can model any geometry.

Several tests were tried to exploit the performance of the new method. They can be categorized into three groups:

- a) moving the absorbing boundary spherical surface away from the scatterer
- b) increasing the discretization of the finite element mesh
- c) increasing the excitation frequency

The numerical results obtained showed that the second order ABC is superior to that of the first order. For the realistic problem of scattering of a plane wave by a 3D metallic sphere, it was found that accurate results of an error smaller than 1% in field values were obtained, when the absorbing boundary sphere is placed less than half wavelength away from the scatterer, compared to at least one or two wavelengths, required by other type of boundary conditions [D'Angelo-90]. This minimizes the extra free space that has to be modelled, thus the number of the unknowns is not significantly increased and therefore neither is the computational cost. For the same geometry, the first order ABC absorbs less, giving a field solution with values having a 10% error, one order of magnitude higher than those of the second order. In both cases the error refers to comparisons of the numerical with the analytical field values on the same geometric points. The difference in computational cost in assembling the first from the second order ABC is negligible. Without a doubt, the second order ABC is to be preferred.

In all formulations throughout this dissertation the magnetic field H has been used. Identical expressions hold for the electric field E. Since no normal continuity is imposed by the curvilinear covariant-projection elements no special considerations have to be taken at dielectric interfaces when the electric field formulation is used. Similarly for the magnetic field and magnetic material interfaces. For the same reason, problems with sharp metallic edges can be modelled in a straight forward manner and without extra complications [Miniowitz-91], as well as problems where both magnetic and dielectric materials are present.

The work in this dissertation concludes that finite elements and Absorbing Boundary Conditions in open boundary electromagnetic problems can be as successful as they have been in closed boundary problems in the last two decades. The present technique opens a whole new area for potential applications in computer simulation with finite elements such as microwave junction radiation, microwave heating, and in particular hyperthermia, a technique used for cancer treatment, where many and highly inhomogeneous dielectrics (i.e. living tissues) are present. This is because the presence of dielectrics is easily treated by finite elements.

### 7.1 Suggestions for further work

FURTHER GENERALIZATION: Due to the presence of the surface divergence term in the formulation, normal continuity has to be imposed on the magnetic field components on the absorbing boundary spherical surface, see Section 4.2. This, however, does not amount to simply setting the covariant projections equal to each other, because the value of the normal field component does not in general equal to the value of the corresponding covariant projection at that point, see Section 2.3 and [Crowley-88b]. Thus, for the sake of simplicity for the computer code, by enforcing the edges of the elements lying on the absorbing boundary spherical surface to be colinear with the lines of constant  $\theta$  or  $\phi$ , makes the imposition of normal continuity a rather trivial task. This however, is by no means a restriction of the method. A modification of the code could easily allow the above mentioned edges to have any orientation possible.

HIGHER-ORDER ABSORBING BOUNDARY CONDITIONS: Symmetric bilinear forms for the finite element code with ABCs of order higher than two have not been implemented. Such ABCs require higher derivatives and the mixed order finite elements used in this work could no longer be used; therefore new higher-order mixed elements would have to be invented.

MULTI-SPHERICAL ABSORBING BOUNDARY SURFACE: As a disadvantage of the new method one could consider the analysis of problems with long and thin geometries, see Figure 7.1. In such cases the fact that the absorbing boundary surface has to be a sphere often leads to the inclusion of useless empty space which also has to be discretized, and the absorbing boundary sphere is at distances much greater than a half wavelength.

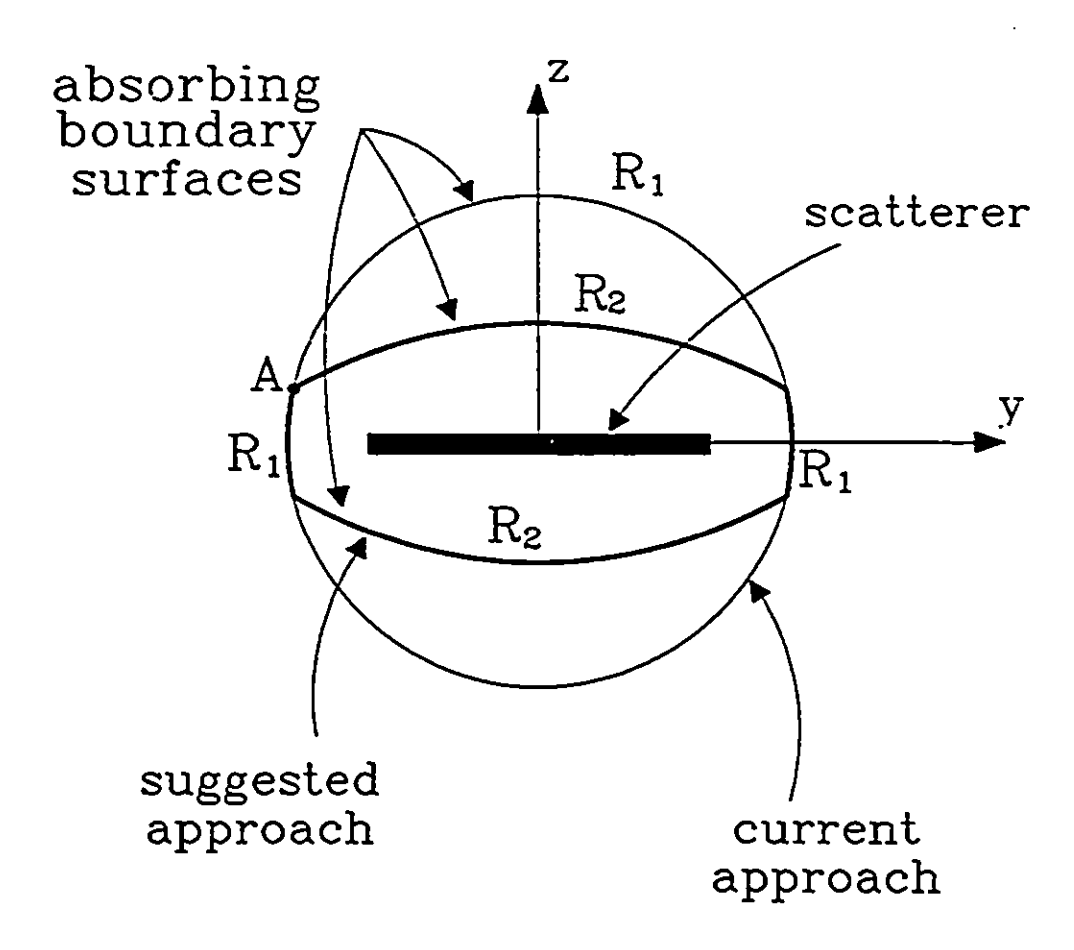


Figure 7.1 A y-z cross section of the 3D geometry of a typical open boundary problem. The approach followed in this thesis includes one spherical absorbing boundary surface of radius  $R_1$ . (thin line). The suggested approach could include a multi-spherical absorbing boundary surface of radii  $R_1$  and  $R_2$ . (thick line). Point A lies on the intersection line of the two spherical surfaces of radii  $R_1$  and  $R_2$ .

However, there is no restriction in the formulation to using only one absorbing boundary sphere. Thus, as an alternative many absorbing spherical surfaces of different radii could be introduced. Further investigation of this idea is needed. Figure 7.1 shows the current and the suggested method for a long and thin scatterer. In the current method the scatterer is enclosed by a sphere of radius  $R_1$ . In the suggested method the discretized volume would be enclosed by four different open spherical surfaces, two of radius  $R_1$  and two of radius  $R_2$ . Therefore the discretized region for the suggested method would be much smaller, resulting in smaller memory requirements and less computational cost.

AUTOMATIC MESH GENERATORS: Development of automatic mesh generators for spherical outer boundaries would facilitate a lot the method presented here. After the user specifies the geometry in the volume of interest, an automatic mesh generator could build the rest of the mesh for the remaining volume setting a spherical absorbing boundary surface at approximately half wavelength away from the closest scatterer.

VIRTUAL REALITY: Three-dimensional pre and post-processing could benefit greatly from the application of the concept of virtual reality [Rheingold-91]. "Moving" in a realistic 3D space would give the design engineer the ability to model more easily complex and highly inhomogeneous structures and would provide a better understanding of the field solution, resulting in more efficiently designed products. Medical techniques like hyperthermia are in great need of simulated experiments of electromagnetic energy deposition, and virtual reality suits perfectly these demands.

#### APPENDIX A

## An alternative form for the Homogeneous Neumann Boundary Condition

### (From Section 2.1.2)

Multiplying both sides of equation (2.5) by the unit vector  $\hat{\mathbf{n}}$  normal to the boundary surface, we get:

$$\mathbf{H} \cdot \hat{\mathbf{n}} = \frac{1}{k_0^2 \mu_r} \left( \nabla \times \frac{1}{\epsilon_r} \times \nabla \times \mathbf{H} \right) \cdot \hat{\mathbf{n}}$$
 (A.1)

The expression for the homogeneous Neumann boundary condition is given by:

$$\mathbf{E} \times \mathbf{\hat{n}} = 0$$

which can also be written as:

$$\frac{1}{\epsilon_{r}}(\nabla \times \mathbf{H}) \times \hat{\mathbf{n}} = 0 \tag{A.2}$$

From vector analysis it is true that:  $H \times \hbar = 0 \Rightarrow (\nabla \times H) \cdot \hbar = 0$ . Using this, equation A.2 gives:

$$\nabla \times \frac{1}{\epsilon_{r}} (\nabla \times \mathbf{H}) \cdot \hat{\mathbf{n}} = 0 \tag{A.3}$$

and because of (A.1) we get:

$$\mathbf{H} \cdot \mathbf{\hat{n}} = 0$$

**QED** 

### APPENDIX B

## Local Geometric and Field node resolution

## (From Section 2.4)

For better visualization and clarity, and without any loss of generality, let the current finite element be the cube shown in Figure B.1. The cube is analyzed in three planes: front, mid and back. In the following two sections the geometric as well as the field node resolution are shown on each plane.

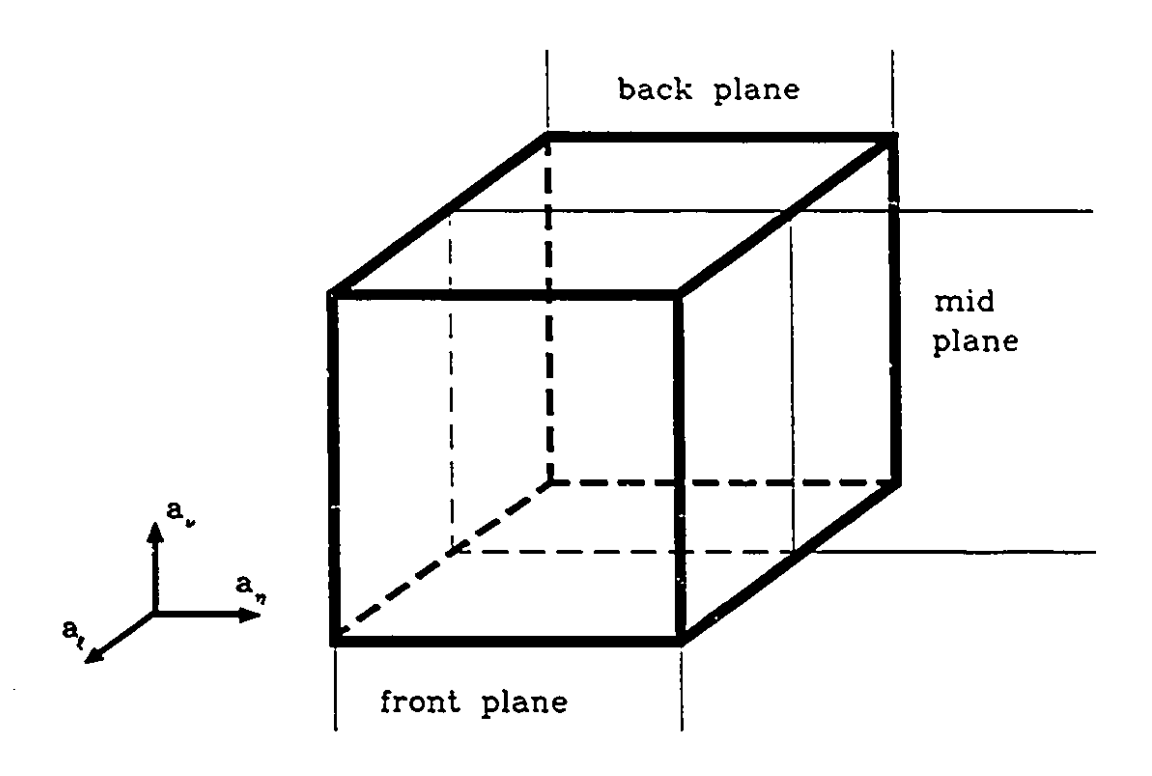


Figure B.1 A finite element and its three planes of analysis in the local curvilinear coordinate system.

## B.1 Local geometric node numbering

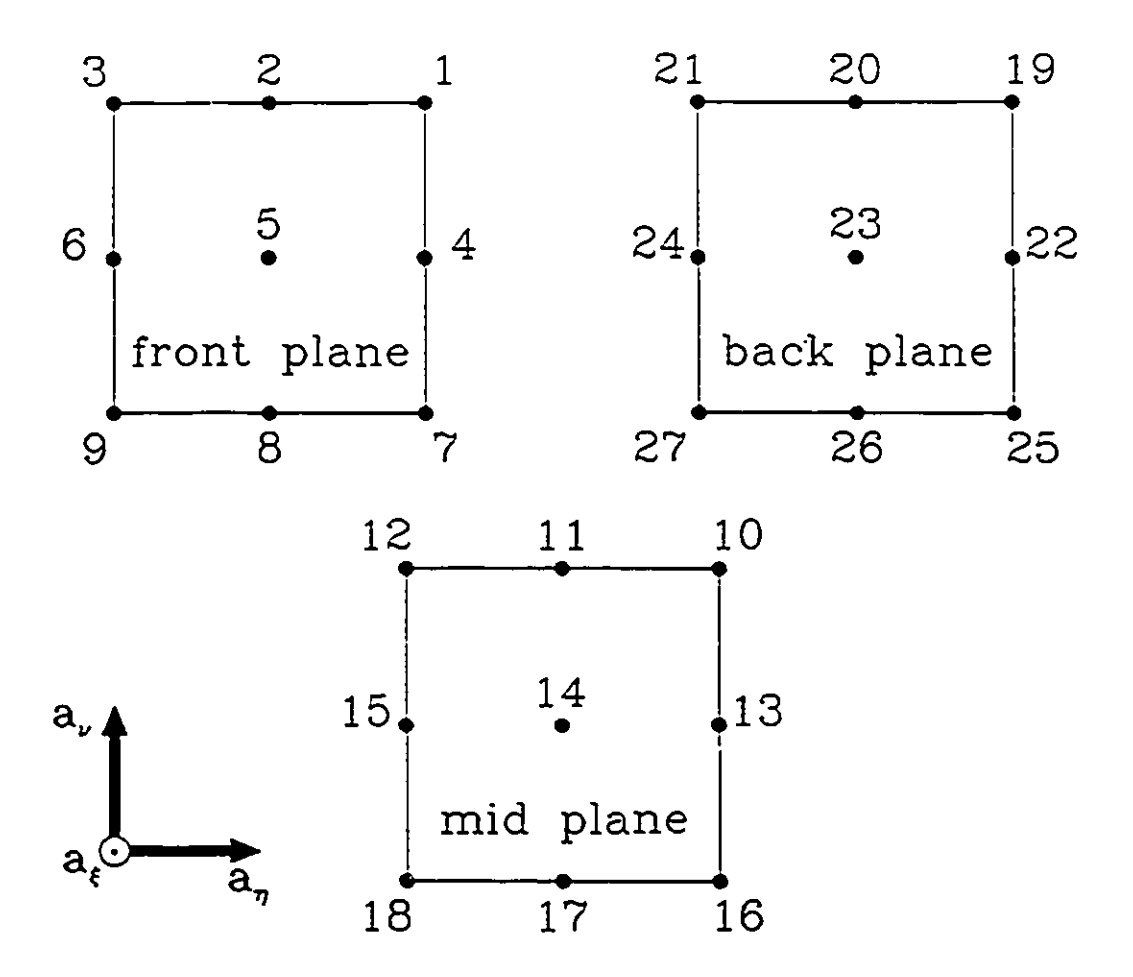


Figure B.2 The 27 geometric nodes of the finite element. For each geometric node there is a corresponding second order trial function with unit value on that node and zero on all the other nodes. The shape of the element in 3-D space is defined by the 27 geometric nodes interpolated by the trial functions.

## B.2 Local field node numbering

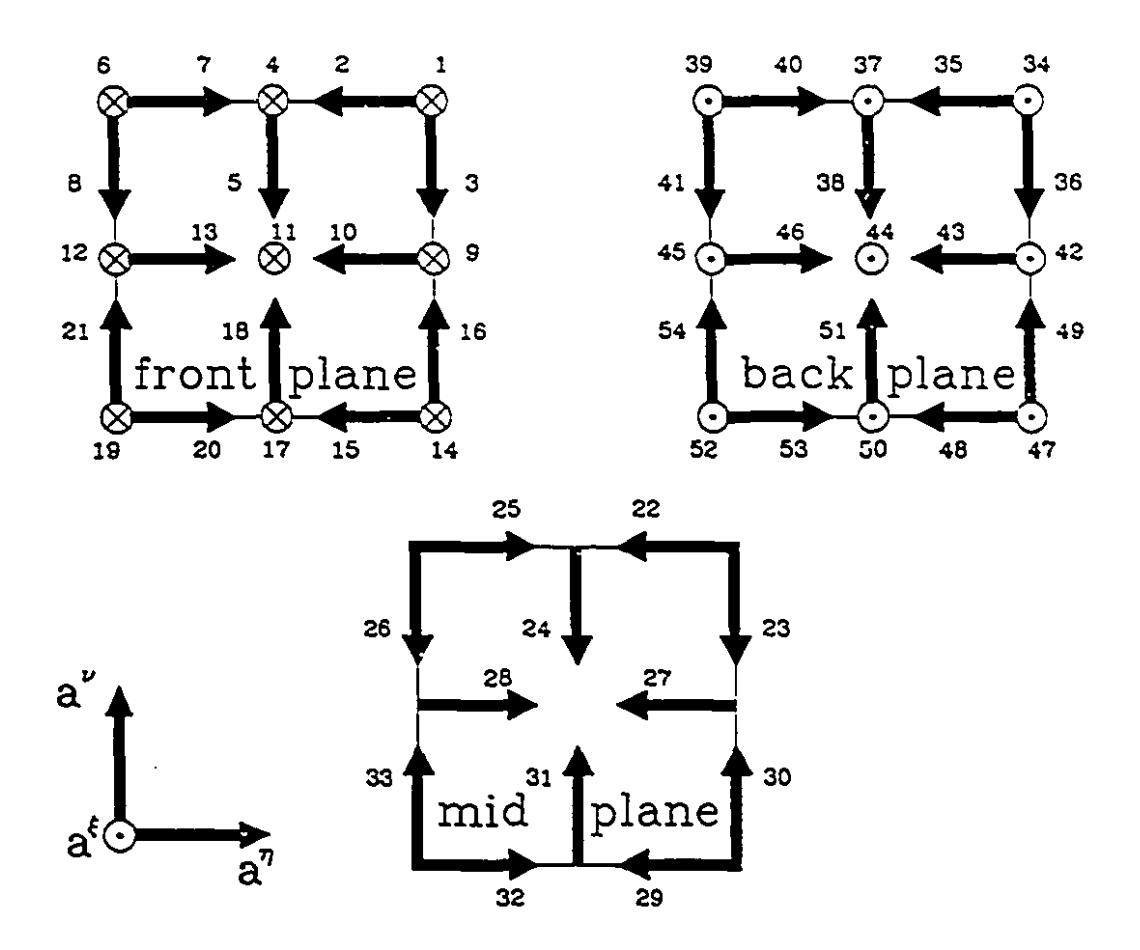


Figure B.3 The 54 field nodes and the corresponding 54 vector trial functions. There are 3 sets of 18 nodes, one set for each of the three coordinate directions. In each set, the trial functions are mixed order, first and second. Each geometric node may correspond to none, one, two or three field nodes. Trial functions in the at direction are first order in that direction and second order in the other two. For compatibility in imposing tangential field continuity across the elements, it was chosen that all vector trial functions point inwards.

### APPENDIX C

# Supplementary Vector Identities in Spherical Coordinates

$$H = H_{r}\bar{a}_{r} + H_{\theta}\bar{a}_{\theta} + H_{\bullet}\bar{a}_{\bullet}$$
 (C.1a)

$$- H_r + H_\theta + H_\bullet$$
 (C.1b)

$$- H_r + H_t$$
 (C.1c)

$$\mathbf{\hat{a}}_r \times \mathbf{H} = \mathbf{\hat{a}}_r \times \mathbf{H}_r \tag{C.2}$$

$$\hat{a}_r \times (\hat{a}_r \times H) = -H_t = H_r - H$$
 (C.3)

$$\nabla \times \mathbf{H} = \nabla \times \mathbf{H}_{t} + \nabla \times \mathbf{H}_{r}$$
$$= \nabla \times \mathbf{H}_{t} - \mathbf{a}_{r} \times \nabla \mathbf{H}_{r} \qquad (C.4)$$

$$\hat{\mathbf{a}}_r \times \nabla \times \mathbf{H} - \nabla_t \mathbf{H}_r = \hat{\mathbf{a}}_r \times \nabla \times \mathbf{H}_t$$
 (C.5)

$$\hat{\mathbf{a}}_r \times \nabla \times \mathbf{H}_t = -\frac{\mathbf{H}_t}{r} - \frac{\partial}{\partial r} \mathbf{H}_t \qquad (C.6)$$

$$\bar{a}_r \times \nabla \times H_r = \nabla_t H_r$$
 (C.7)

$$\hat{\mathbf{a}}_r[\hat{\mathbf{a}}_r \cdot (\nabla \times \mathbf{H})] = \frac{\hat{\mathbf{a}}_r}{r \sin(\theta)} \left[ \frac{\partial}{\partial \theta} (\mathbf{H}_{\bullet} \sin(\theta)) - \frac{\partial}{\partial \phi} \mathbf{H}_{\theta} \right]$$
 (C.8)

$$(\nabla \times \mathbf{H})_{t} = -\mathbf{a}_{r} \times \nabla \mathbf{H}_{r} + \mathbf{a}_{r} \times \frac{\mathbf{H}_{t}}{r} - \mathbf{a}_{r} \times \frac{\partial}{\partial r} \mathbf{H}_{t}$$
 (C.9)

$$\hat{\mathbf{a}}_r \times \nabla \times \frac{\mathbf{H}}{r} = \frac{1}{r^2} \mathbf{H}_t + \frac{1}{r} \hat{\mathbf{a}}_r \times \nabla \times \mathbf{H}$$
 (C.10)

$$\hat{\mathbf{a}}_r \times \nabla \times (\hat{\mathbf{a}}_r \times \nabla \times \mathbf{H}) = -\frac{1}{r} \hat{\mathbf{a}}_r \times \nabla \times \mathbf{H} - \frac{\partial}{\partial r} (\hat{\mathbf{a}}_r \times \nabla \times \mathbf{H}) \quad (C.11a)$$
$$= -\frac{1}{r} \hat{\mathbf{a}}_r \times \nabla \times \mathbf{H} - \hat{\mathbf{a}}_r \times \frac{\partial}{\partial r} (\nabla \times \mathbf{H}) \quad (C.11b)$$

$$\hat{\mathbf{a}}_r \times \nabla \times \nabla_t \mathbf{H}_r = -\nabla_t \left( \frac{\partial \mathbf{H}_r}{\partial r} \right) \tag{C.12}$$

### APPENDIX D

**D.1** The  $L_N(\nabla_t H_{ar})$  operator

(From Section 3.3)

$$L_N(\nabla_t H_{nr}) = L_N(\nabla_t \left\{ g \frac{H_{nr}(\theta, \phi)}{r^{n+1}} \right\}) =$$

using(3.6):

$$= \hat{\mathbf{a}}_r \times \nabla \times \nabla_t \left\{ g \frac{\mathbf{H}_{nr}(\theta, \phi)}{r^{n+1}} \right\} - \left( j k_0 + \frac{N}{r} \right) \nabla_t \left\{ g \frac{\mathbf{H}_{nr}(\theta, \phi)}{r^{n+1}} \right\}$$

using (C.6):

$$= -\frac{1}{r} \nabla_{t} \left\{ g \frac{H_{nr}(\theta, \phi)}{r^{n+1}} \right\} - \frac{\partial}{\partial r} \nabla_{t} \left\{ g \frac{H_{nr}(\theta, \phi)}{r^{n+1}} \right\}$$
$$- \left( j k_{0} + \frac{N}{r} \right) \nabla_{t} \left\{ g \frac{H_{nr}(\theta, \phi)}{r^{n+1}} \right\}$$

$$=-\frac{\partial}{\partial r}\nabla_{t}\left\{g\frac{H_{nr}(\theta,\phi)}{r^{n-1}}\right\} - \left(jk_{0} + \frac{N+1}{r}\right)\nabla_{t}\left\{g\frac{H_{nr}(\theta,\phi)}{r^{n-1}}\right\}$$

Considering the  $\frac{1}{r}$  term included in the  $\nabla_{r}$  operator:

$$-\left(jk_0 + \frac{n+2}{r}\right)\nabla_t\left\{g\frac{H_{nr}(\theta,\phi)}{r^{n+1}}\right\} - \left(jk_0 + \frac{N+1}{r}\right)\nabla_t\left\{g\frac{H_{nr}(\theta,\phi)}{r^{n+1}}\right\}$$

OI

$$L_{N}(\nabla_{t}H_{nr}) = (n+1-N)\nabla_{t}\left\{g\frac{H_{nr}(\theta,\phi)}{r^{n+2}}\right\}$$

D.2 The  $B_2(H)$  operator

#### (From Section 3.4.2)

The operator that annihilates the first two terms of the vector radiation function (3.3) is given by:

$$B_2(H) = (L_1)^2(H_t) + sL_2(\nabla_t H_r)$$
 (D.2.1)

$$(L_1)^2(\mathbf{H}_t) = \mathbf{a}_r \times \nabla \times (\mathbf{a}_r \times \nabla \times \mathbf{H}_t) - \left(\frac{1}{r} + 2jk_0\right) \mathbf{a}_r \times \nabla \times \mathbf{H}_t$$
$$-\mathbf{a}_r \times \nabla \times \frac{\mathbf{H}_t}{r} + \left(\frac{1}{r} + jk_0\right)^2 \mathbf{H}_t \qquad (D.2.2)$$

Using (C.10) on H, instead of on H and expanding we get:

$$(L_1)^2(\mathbf{H}_t) = \mathbf{a}_r \times \nabla \times (\mathbf{a}_r \times \nabla \times \mathbf{H}_t) - \left(\frac{2}{r} + 2jk_0\right)\mathbf{a}_r \times \nabla \times \mathbf{H}_t$$
$$+ \left(j\frac{2k_0}{r} - k_0^2\right)\mathbf{H}_t$$

Using (C.11) on H, instead of on H we get:

$$(L_1)^2(\mathbf{H}_t) = -\left(\frac{3}{r} + j2k_0\right) \bar{\mathbf{a}}_r \times \nabla \times \mathbf{H}_t - \bar{\mathbf{a}}_r \times \frac{\partial}{\partial r} (\nabla \times \mathbf{H}_t)$$

$$+ \left(j\frac{2k_0}{r} - k_0^2\right) \mathbf{H}_t \quad (D.2.3)$$

Applying the operator  $\hat{a}_r \times \frac{\delta}{\delta r}$  from the left of the vector identity (C.4) and using (C.3)

we get:

$$\tilde{\mathbf{a}}_r \times \frac{\partial}{\partial r} (\nabla \times \mathbf{H}) = \tilde{\mathbf{a}}_r \times \frac{\partial}{\partial r} (\nabla \times \mathbf{H}_t) + \frac{\partial}{\partial r} \nabla_t \mathbf{H}_r$$
 (D.2.4a)

or

$$\hat{\mathbf{a}}_r \times \frac{\partial}{\partial r} (\nabla \times \mathbf{H})_t = \hat{\mathbf{a}}_r \times \frac{\partial}{\partial r} (\nabla \times \mathbf{H}_t) + \frac{\partial}{\partial r} \nabla_t \mathbf{H}_r \qquad (D.2.4)$$

Applying the  $a_r \times$  operator from the left of the curl-curl equation (2.5), and using the vector identities (C.5) and (C.6) we get (see also C.8):

$$\mathbf{a}_r \times \nabla \times \nabla \times \mathbf{H} = \mathbf{a}_r \times k_0^2 \mathbf{H}$$

OL

$$-\frac{(\nabla \times \mathbf{H})_t}{r} + \nabla_t [\mathbf{a}_r \cdot (\nabla \times \mathbf{H})] - \frac{\partial}{\partial r} (\nabla \times \mathbf{H})_t = \mathbf{a}_r \times k_0^2 \mathbf{H} \qquad (D.2.5)$$

Applying the vector identity (C.6) on the vector  $\nabla_t H_r$  we get:

$$\hat{\mathbf{a}}_r \times \nabla \times \nabla_t \mathbf{H}_r = \frac{-\nabla_t \mathbf{H}_r}{r} - \frac{\partial}{\partial r} (\nabla_t \mathbf{H}_r)$$
 (D2.6)

Equation (D.2.4) through (D.2.5) and (D.2.6) gives:

$$\hat{\mathbf{a}}_{r} \times \frac{\partial}{\partial r} (\nabla \times \mathbf{H}_{t}) = \hat{\mathbf{a}}_{r} \times \nabla \times \nabla_{t} \mathbf{H}_{r} + \hat{\mathbf{a}}_{r} \times \nabla_{t} [\hat{\mathbf{a}}_{r} \cdot (\nabla \times \mathbf{H})]$$

$$-\hat{\mathbf{a}}_{r} \times \frac{(\nabla \times \mathbf{H})_{t}}{r} + \frac{\nabla_{t} \mathbf{H}_{r}}{r} + k_{0}^{2} \mathbf{H}_{t} \qquad (D.2.7)$$

Using (C.12), the above can be rewritten as:

$$\hat{\mathbf{a}}_r \times \frac{\partial}{\partial r} (\nabla \times \mathbf{H}_t) = -\nabla_t \left( \frac{\partial \mathbf{H}_r}{\partial r} \right) + \hat{\mathbf{a}}_r \times \nabla \times \nabla_t \mathbf{H}_r + \hat{\mathbf{a}}_r \times \nabla_t [\hat{\mathbf{a}}_r \cdot (\nabla \times \mathbf{H})]$$

$$-\hat{\mathbf{a}}_r \times \frac{(\nabla \times \mathbf{H})_t}{r} + \frac{\nabla_t \mathbf{H}_r}{r} + k_0^2 \mathbf{H}_t$$
(D.2.8)

From  $\nabla \cdot \mathbf{H} = 0$  we get that:

$$\frac{\partial H_r}{\partial r} = -\frac{2}{r}H_r - \nabla_i \cdot H_i$$

So.

$$\hat{\mathbf{a}}_r \times \nabla \times \nabla_t \mathbf{H}_r = \frac{2}{r} \nabla_t \mathbf{H}_r + \nabla_t (\nabla_t \cdot \mathbf{H}_t)$$
 (D.2.9)

and by substituting the above expression back to (D.2.8) we get:

$$\hat{\mathbf{a}}_{r} \times \frac{\partial}{\partial r} (\nabla \times \mathbf{H}_{t}) = \frac{2}{r} \nabla_{t} \mathbf{H}_{r} + \nabla_{t} (\nabla_{t} \cdot \mathbf{H}_{t}) + \hat{\mathbf{a}}_{r} \times \nabla_{t} [\hat{\mathbf{a}}_{r} \cdot (\nabla \times \mathbf{H})]$$
$$-\frac{1}{r} \hat{\mathbf{a}}_{r} \times (\nabla \times \mathbf{H})_{t} + \frac{\nabla_{t} \mathbf{H}_{r}}{r} + k_{0}^{2} \mathbf{H}_{t}$$

and using (C.5) we have:

$$\hat{\mathbf{a}}_{r} \times \frac{\partial}{\partial r} (\nabla \times \mathbf{H}_{t}) = \frac{2}{r} \nabla_{t} \mathbf{H}_{r} + \nabla_{t} (\nabla_{t} \cdot \mathbf{H}_{t}) + \hat{\mathbf{a}}_{r} \times \nabla_{t} [\hat{\mathbf{a}}_{r} \cdot (\nabla \times \mathbf{H})]$$

$$-\frac{1}{r} \hat{\mathbf{a}}_{r} \times \nabla \times \mathbf{H}_{t} + k_{0}^{2} \mathbf{H}_{t} \qquad (D.2.9)$$

Then the operator  $(L_1)^2(H_i)$  may be written as:

$$(L_1)^2(\mathbf{H}_t) = -2\left(\frac{1}{r} + jk_0\right) \hat{\mathbf{a}}_r \times \nabla \times \mathbf{H}_t - \frac{2}{r} \nabla_t \mathbf{H}_r - \nabla_t (\nabla_t \cdot \mathbf{H}_t)$$

$$- \hat{\mathbf{a}}_r \times \nabla_t [\hat{\mathbf{a}}_r \cdot (\nabla \times \mathbf{H})] + 2\left(j\frac{k_0}{r} - k_0^2\right) \mathbf{H}_t$$
 (D.2.10)

Using (3.8), the operator  $L_2(\nabla_t H_r)$  gives:

$$L_{2}(\nabla_{t}H_{r}) = \hat{a}_{r} \times \nabla \times \nabla_{t}H_{r} - \left(jk_{0} + \frac{2}{r}\right)\nabla_{t}H_{r}$$

$$(using (D.2.9): = \frac{2}{r}\nabla_{t}H_{r} + \nabla_{t}(\nabla_{t} \cdot H_{t}) - \left(jk_{0} + \frac{2}{r}\right)\nabla_{t}H_{r}$$

Then the  $B_2(H)$  operator is given by:

$$B_{N}(H) = (L_{1})^{2}(H_{t}) + sL_{2}(\nabla_{t}H_{r})$$

$$= -2\left(\frac{1}{r} + jk_{0}\right)\hat{a}_{r} \times \nabla \times H_{t} - \frac{2}{r}\nabla_{t}H_{r}$$

$$-\nabla_{t}(\nabla_{t} \cdot H_{t}) - \hat{a}_{r} \times \nabla_{t}[\hat{a}_{r} \cdot (\nabla \times H)]$$

$$+2\left(j\frac{k_{0}}{r} - k_{0}^{2}\right)H_{t} + s\frac{2}{r}\nabla_{t}H_{r}$$

$$+s\nabla_{t}(\nabla_{t} \cdot H_{t}) - s\left(jk_{0} + \frac{2}{r}\right)\nabla_{t}H_{r}$$

using (C.5):

$$= -2\left(\frac{1}{r} + jk_0\right)\hat{\mathbf{a}}_r \times \nabla \times \mathbf{H}_t - 2\left(\frac{1}{r} + jk_0\right)\nabla_t \mathbf{H}_r$$

$$+ j2k_0\nabla_t \mathbf{H}_r - \nabla_t(\nabla_t \cdot \mathbf{H}_t) - \hat{\mathbf{a}}_r \times \nabla_t[\hat{\mathbf{a}}_r \cdot (\nabla \times \mathbf{H})]$$

$$+ 2\left(j\frac{k_0}{r} - k_0^2\right)\mathbf{H}_t + s\nabla_t(\nabla_t \cdot \mathbf{H}_t)$$

$$- jsk_0\nabla_t \mathbf{H}_r$$

$$= -2\left(\frac{1}{r} + jk_0\right)\hat{\mathbf{a}}_r \times \nabla \times \mathbf{H} + (s-1)\nabla_t(\nabla_t \cdot \mathbf{H}_t)$$

$$- \hat{\mathbf{a}}_r \times \nabla_t[\hat{\mathbf{a}}_r \cdot (\nabla \times \mathbf{H})] + 2\left(j\frac{k_0}{r} - k_0^2\right)\mathbf{H}_t$$

$$+ (2-s)jk_0\nabla_t \mathbf{H}_r$$

and finaly using (C.4):

$$B_{2}(H) = -\frac{1}{\beta(r)}\hat{\mathbf{a}}_{r} \times \nabla \times \mathbf{H} + \frac{\alpha(r)}{\beta(r)}\mathbf{H}_{t}$$
$$+ \nabla \times \hat{\mathbf{a}}_{r}[\hat{\mathbf{a}}_{r} \cdot (\nabla \times \mathbf{H})] + (s-1)\nabla_{t}(\nabla \cdot \mathbf{H}_{t})$$
$$+ (2-s)\alpha(r)\nabla_{t}\mathbf{H}_{r}$$

where  $\alpha(r) = jk_0$  and  $\beta(r) = 1/(2jk_0 + 2/r)$ .

#### APPENDIX E

E.1 The functional for the second order ABC

(From Section 4.1)

For s = 2 the surface term of the functional is:

$$\int_{S} \mathbf{H} \cdot P_{2}(\mathbf{H}) dS =$$

$$= \int_{S} \{\alpha(r) \mathbf{H} \cdot \mathbf{H}_{t} + \beta(r) \mathbf{H} \cdot \nabla \times \hat{\mathbf{a}}_{r} [\hat{\mathbf{a}}_{r} \cdot (\nabla \times \mathbf{H})] + \beta(r) \mathbf{H} \cdot \nabla_{t} (\nabla \cdot \mathbf{H}_{t}) \} dS \qquad (E.1.1)$$

Using the vector identity  $\nabla \cdot (A \times B) = B \cdot \nabla \times A - A \cdot \nabla \times B$ , and for a spherical surface S of constant radius r = R, the second part of the surface integral in (E.1.1) may be rewritten as:

$$\int_{S} \mathbf{H} \cdot \nabla \times \hat{\mathbf{a}}_{r} [\hat{\mathbf{a}}_{r} \cdot (\nabla \times \mathbf{H})] dS = -\int_{S} \nabla \cdot \mathbf{H} \times \hat{\mathbf{a}}_{r} [\hat{\mathbf{a}}_{r} \cdot (\nabla \times \mathbf{H})] dS$$

$$+ \int_{S} \hat{\mathbf{a}}_{r} [\hat{\mathbf{a}}_{r} \cdot (\nabla \times \mathbf{H})] \cdot \nabla \times \mathbf{H} dS \qquad (E.1.2)$$

The first integral on the right side of (E.1.2) vanishes over a closed surface, see #18,#19 p. 501, and #42 p.503 in [Van Bladel-64]. The second integral on the right side of (E.1.2) can be rewritten as:

$$\int_{S} [\hat{\mathbf{a}}_{r} \cdot (\nabla \times \mathbf{H})]^{2} dS \tag{E.1.3}$$

Similarly, using the vector identity  $\nabla \cdot (\psi A) = A \cdot \nabla \psi + \psi \nabla \cdot A$  and for a spherical surface S of constant radius r = R, the third part of the surface integral in (E.1.1) may be rewritten as:

$$\int_{S} \mathbf{H} \cdot \nabla_{t} (\nabla_{t} \cdot \mathbf{H}_{t}) dS = \int_{S} \mathbf{H}_{t} \cdot \nabla_{t} (\nabla_{t} \cdot \mathbf{H}_{t}) dS$$

$$= \int_{S} \nabla_{t} \cdot (\mathbf{H}_{t} \nabla_{t} \cdot \mathbf{H}_{t}) dS - \int_{S} (\nabla_{t} \cdot \mathbf{H}_{t}) (\nabla_{t} \cdot \mathbf{H}_{t}) dS (E.1.4)$$

The first integral on the right side of (E.1.4) vanishes over a closed surface, see #18,#19 p.501, and #42 p.503 in [Van Bladel-64]. Also from the same reference:  $\nabla \cdot H_i = \nabla_i \cdot H_i$ . Thus, from (E.1.1), (E.1.2), (E.1.3) and (E.1.4) we have that:

$$\int_{S} \mathbf{H} \cdot P_{2}(\mathbf{H}) dS = \int_{S} [\tilde{\mathbf{a}}_{r} \cdot (\nabla \times \mathbf{H})]^{2} dS - \int_{S} (\nabla_{t} \cdot \mathbf{H}_{t})^{2} dS$$

E.2 The Absorbing Boundary Condition as a natural condition to the variation formulation

The stationary point of the functional F in (4.4), is given by:

$$\delta(F(H)) = 0 \Rightarrow$$

$$\delta \left( \int_{V} \{ (\nabla \times \mathbf{H})^{2} - k_{0}^{2} \mu_{r} \mathbf{H}^{2} \} dV + \int_{S} P_{n}(\mathbf{H}) \cdot \mathbf{H} dS \right) = 0 \qquad (E.2.1)$$

where n = 1 or 2 and it denotes the first or second order Absorbing Boundary Condition.

The volume part of (E.2.1) gives:

$$2\int_{V} \{\nabla \times (\delta H) \cdot \nabla \times H - k_{0}^{2}(\delta H) \cdot H\} dV \qquad (E.2.2)$$

The surface part of (E.2.1) gives:

$$\int_{S} \{H \cdot \delta(P(H)) + P_n(H) \cdot (\delta H)\} dS$$

Because of the linearity of the operator  $P_n$ , the above may be written as:

$$\int_{S} \{H \cdot P_{n}(\delta H) + P_{n}(H) \cdot (\delta H)\} dS$$

and because the operator  $P_n$  is symmetric, the above may be written as:

$$\int_{S} \{ (\delta H) \cdot P_n(H) + P_n(H) \cdot (\delta H) \} dS$$

ОΓ

$$2\int_{S} P_{n}(H) \cdot (\delta H) dS \qquad (E.2.3)$$

Using the vector identity  $A \cdot \nabla \times \nabla \times B = (\nabla \times A) \cdot (\nabla \times B) - \nabla \cdot (A \times \nabla \times B)$  and from (E.2.2) and (E.2.3), we have that (E.2.1) can be rewritten as:

$$\int_{V} \{ \nabla \cdot (\delta \mathbf{H}) \times \nabla \times \mathbf{H} + (\delta \mathbf{H}) \cdot \nabla \times \nabla \times \mathbf{H} - k_{0}^{2} (\delta \mathbf{H}) \cdot \mathbf{H} \} dV$$

$$+ \int_{S} (\delta \mathbf{H}) \cdot P_{n}(\mathbf{H}) dS = 0$$

Applying the divergence theorem above we get:

$$\int_{V} (\delta \mathbf{H}) \cdot (\nabla \times \nabla \times \mathbf{H} - k_{0}^{2} \mathbf{H}) dV$$

$$+ \int_{S} (\delta \mathbf{H}) \cdot (-\hat{\mathbf{a}}_{r} \times \nabla \times \mathbf{H} + P(\mathbf{H})) dS = 0 \qquad (E.2.4)$$

Since (E.2.4) holds for any  $\delta H$ , it is true that  $\nabla \times \nabla \times H - k_0^2 H = 0$  in volume V, and  $\delta_r \times \nabla \times H = P_n(H)$  on the spherical surface S.

### APPENDIX F

# Description of the Input Data Structure

(From Section 5.1)

This Section describes the input data structure of a two-element problem. The program reads the data from the file "input.dat", and such a file is illustrated in the following Section. The first two columns have been added extra to facilitate the explanation using markers (#1, #2, etc).

The marker ## denotes a single empty line where comments can be added. The line marked with #1, is a single line and contains two numbers: the first is the total number of elements and the second is the total number of geometric nodes (i.e. points) in the problem, (parameters nelmnt and gnodes in the program respectively).

Every element has 27 geometric nodes. When 2 elements have a common face they share 9 geometric nodes. So, for a two-element problem the total number of geometric nodes is 27+27-9=45. There is no restriction on the number of lines required for the geometric nodes. So, line #2 says that the first node of element 1 (local node numbering, see Appendix B.1) is geometric node 1, the second node is geometric node 6, etc. The coordinates of the geometric nodes are given later. At the end of the geometric nodes, there are 6 numbers (marker #3) which are intentionally in italics. Every number gives information on the boundary conditions for each of the 6 faces of the finite element. A positive integer means that the face is an excitation face. Every excitation face is characterized by a different positive integer. -3 means that the Absorbing Boundary Condition will be applied on that face, -2 means that the face is a magnetic wall and -1 means that the face is an electric wall. Thus, the first face of the first element is labeled as -2, the

second as -1 etc. For the local face numbering see subroutines face1-6. Markers #4 and #5 denote the beginning and the end for the geometrical information for the second element.

Marker #6 denotes the beginning of the cartesian coordinate information. The first column is the geometric node, and the next 3 columns are the x, y and z cartesian coordinates for that node.

The line marked with #8, gives the x, y and z coordinates of the centre of the ABC surface. Line marked with #9 gives the relative dielectric permittivity and relative magnetic permeability of the medium inside the first element, (parameters *smatrl* and *tmatrl* in the program respectively). The line right below gives the same information for the second element. These numbers may be complex. Line marked with #10 gives the normalized excitation frequency  $k_0$ .

Marker #11 marks the first line containing information on the problem's excitation. Each line has 5 columns. The first column gives the positive integer that characterizes each excitation face, discussed earlier. So, from line mark with #3, we see that element 1 has 2 excitation faces, and so does element 2. Back to line marked with #11, the second column gives the geometric node in local numbering (1-27). The next three columns have the x, y and z components of the excitation field. These numbers may be complex.

```
##
        nelmnt, gnodes
#1
        2
             45
        read the geometric nodes of the elements
##
                                                     13
#2
                               7
                                    12
                                           3
                                                8
                  11
                         2
                                22
                                                  23
        16
              21
                    26
                          17
                                      27
                                            18
                                                        28
                                37
                                      42
                                                        43
        31
              36
                    41
                          32
                                            33
                                                  38
#3
        -2
             -1
                    2
                          I
                               0
                                     0
#4
        3
             8
                  13
                         4
                               9
                                    14
                                           5
                                                10
                                                      15
        18
             23
                   28
                          19
                                24
                                      29
                                            20
                                                  25
                                                        30
        33
              38
                    43
                          34
                                39
                                      44
                                            35
                                                  40
                                                        45
#5
        -2
             -1
                    3
                         0
                               4
                                    -3
        gnode
                                                         coordinates
##
                  X
                                                    z
#6
                             0.0000000E+00
                                              9.9862951E-01
        1
            5.2335959E-02
        2
            6.5419950E-02
                            0.0000000E+00
                                              1.2482870E+0G
        3
                                              1.4979444E+00
            7.8503937E-02
                             0.0000000E+00
                                              1.7476016E+00
        4
            9.1587923E-02
                             0.0000000E+00
        5
            1.0467192E-01
                             0.0000000E+00
                                              1.9972590E+00
        6
            7.2537434E-01
                             0.0000000E+00
                                              6.8835455E-01
        7
            9.0671796E-01
                             0.0000000E+00
                                              8.6044323E-01
        8
            1.0880616E+00
                              0.0000000E+00
                                               1.0325319E+00
        9
             1.2694051E+00
                              0.0000000E+00
                                               1.2046205E+09
        10
            1.4507487E+00
                              0.0000000E+00
                                               1.3767091E+00
        11
            1.0000000E+00
                              0.0000000E+00
                                               7.5497901E-08
        12
            1.2500000E+00
                              0.0000000E+00
                                               9.4372375E-08
        13
            1.5000000E+00
                              0.0000000E+00
                                               1.1324685E-07
        14
            1.7500000E+00
                              0.0000000E+00
                                               1.3212133E-07
        15
            2.0000000E+00
                              0.0000000E+00
                                               1.5099580E-07
        16
            3.7007108E-02
                             3.7007112E-02
                                             9.9862951E-01
        17
            4.6258885E-02
                             4.6258889E-02
                                             1.2482870E+00
        18
            5.5510666E-02
                             5.5510666E-02
                                             1.4979444E+00
        19
            6.4762443E-02
                             6.4762443E-02
                                             1.7476016E+00
        20
                             7.4014224E-02
            7.4014217E-02
                                             1.9972590E+00
        21
            5.1291710E-01
                             5.1291716E-01
                                             6.8835455E-01
        22
            6.4114642E-01
                             6.4114642E-01
                                             8.6044323E-01
        23
            7.6937568E-01
                             7.6937574E-01
                                             1.0325319E+00
        24
            8.9760494E-01
                             8.9760500E-01
                                             1.2046205E+00
        25
            1.0258342E+00
                              1.0258343E+00
                                               1.3767091E+00
        26
            7.0710677E-01
                             7.0710677E-01
                                             7.5497901E-08
        27
            8.8388348E-01
                             8.8388348E-01
                                             9.4372375E-08
            1.0606601E+00
        28
                              1.0606602E+00
                                               1.1324685E-07
        29
            1.2374369E+00
                              1.2374369E+00
                                               1.3212133E-07
        30
            1.4142135E+00
                              1.4142135E+00
                                               1.5099580E-07
        31
             -2.2876774E-09
                             5.2335959E-02
                                              9.9862951E-01
        32
             -2.8595968E-09
                              6.5419950E-02
                                              1.2482870E+00
        33
            -3.4315162E-09
                             7.8503937E-02
                                              1.4979444E+00
```

```
-4.0034354E-09
                              9.1587923E-02
        34
                                               1.7476016E+00
        35
             -4.5753548E-09
                               1.0467192E-01
                                               1.9972590E+00
        36
             -3.1707120E-08
                              7.2537434E-01
                                               6.8835455E-01
        37
             -3.9633903E-08
                              9.0671796E-01
                                               8.6044323E-01
        38
             -4.75606S3E-0S
                               1.0880616E+00
                                                1.0325319E+00
             -5.5487462E-08
        39
                               1.2694051E+00
                                                1.2046205E+00
        40
             -6.3414241E-08
                               1.4507487E+00
                                                1.3767091E+00
        41
             -4.3711388E-08
                               1.0000000E+00
                                                 7.5497901E-0S
        42
             -5.4639237E-08
                               1.2500000E+00
                                                9.4372375E-08
        43
             -6.5567086E-08
                               1.5000000E÷00
                                                 1.1324685E-07
        44
             -7.6494935E-08
                               1.7500000E+00
                                                 1.3212133E-07
#7
             -8.7422777E-08
                               2.0000000E+00
                                                 1.5099580E-07
##
        x-y-z coordinates of the ABC spherical surface
#8
        0.0, 0.0, 0.0
##
        element no, material properties (smatrl,tmatrl)
#9
              (1.00,0.00) (1.00,0.00)
              (1.00,0.00) (1.00,0.00)
##
        Normalized frequency ko
#10
        1.88495E+00
##
        global constrained face number, local geometric node number and the x-y-z field constrains
#11
                 (0.00000E+00, 0.00000E+00) (2.00241E-02, 1.34107E-01) (0.00000E+00, 0.00000E+00)
        1
                 (0.00000E+00, 0.00000E+00) (4.98921E-02, 1.00411E-01) (0.00000E+00, 0.00000E+00)
        1
                 (0.00000E+00, 0.00000E+00) (7.10480E-02, 6.38286E-02) (0.00000E+00, 0.00000E+00)
        1
                 (-1.01182E-01,-6.70536E-02) (-8.11583E-02, 6.70536E-02) ( 9.72552E-02, 1.45216E-02)
        1
                 (-6.21214E-02,-4.81961E-03) ( 8.92659E-03, 5.90090E-02) ( 4.90322E-02,-3.69999E-02)
        1
              21 (8.84565E-09, 5.86201E-09) (-1.82341E-01, 1.53806E-09) (1.37540E-01, 2.05366E-02)
              24 (6.71801E-09, 2.55133E-09) (-1.03798E-01, 4.20430E-02) (1.03788E-01,-2.50282E-02)
        1
                 (5.43082E-09, 4.21344E-10) (-5.31948E-02, 5.41894E-02) (6.93420E-02,-5.23258E-02)
        1
        2
                 (0.00000E+00, 0.00000E+00)(-1.17327E-01, 1.13599E-01)(0.00000E+00, 0.00000E+00)
        2
                 (0.00000E+00, 0.00000E+00) (-5.37533E-02, 1.25404E-01) (0.00000E+00, 0.00000E+00)
        2
              7
                 (0.00000E+00, 0.00000E+00) (1.80095E-03, 1.16083E-01) (0.00000E+00, 0.00000E+00)
        2
              10 (-2.77150E-04,-1.83657E-04) (-1.17604E-01, 1.13415E-01) (-2.38873E-03,-4.19612E-03)
        2
                 (-1.70159E-04,-1.32013E-05) ( 1.63079E-03, 1.16070E-01) (-2.02541E-03,-2.29266E-03)
        2
              19
                 (2.42293E-11, 1.60561E-11) (-1.17881E-01, 1.13231E-01) (-3.37817E-03,-5.93421E-03)
        2
              22 (1.84012E-11, 6.98831E-12) (-5.41742E-02, 1.25245E-01) (-2.60068E-03,-4.36041E-03)
        2
              25 (1.48756E-11, 1.15371E-12) (1.46063E-03, 1.16056E-01) (-2.86437E-03,-3.24231E-03)
        3
                 (0.00000E+00, 0.00000E+00) (1.80095E-03, 1.16083E-01) (0.00000E+00, 0.00000E+00)
        3
                 (0.00000E+00, 0.00000E+00) (4.37281E-02, 9.06636E-02) (0.00000E+00, 0.00000E+00)
        3
                 (0.00000E+00, 0.00000E+00) (6.90155E-02, 5.56939E-02) (0.00000E+00, 0.00000E+00)
        3
              10 (-1.70159E-04,-1.32013E-05) ( 1.63079E-03, 1.16070E-01) (-2.02541E-03,-2.29266E-03)
        3
                (-9.50702E-05, 6.73173E-05) ( 6.89205E-02, 5.57613E-02) (-2.41841E-03,-5.30653E-04)
        3
                 (1.48756E-11, 1.15371E-12) (1.46063E-03, 1.16056E-01) (-2.86437E-03,-3.24231E-03)
        3
              22
                 (1.16897E-11,-3.02804E-12) (4.34607E-02, 9.07329E-02) (-3.26669E-03,-2.04988E-03)
        3
                 (8.31078E-12,-5.88529E-12) (6.88254E-02, 5.58286E-02) (-3.42015E-03,-7.50456E-04)
         4
                 (0.00000E+00, 0.00000E+00) (7.10480E-02, 6.38286E-02) (0.00000E+00, 0.00000E+00)
         4
                 (0.00000E+00, 0.00000E+00) (7.87649E-02, 2.63334E-02) (0.00000E+00, 0.00000E+00)
         4
                  (0.00000E+00, 0.00000E+00) (7.29818E-02, -7.64272E-03) (0.00000E+00, 0.00000E+00)
         4
              12 (-6.21214E-02,-4.81961E-03) ( 8.92659E-03, 5.90090E-02) ( 4.90322E-02,-3.69999E-02)
```

18 (-3.47083E-02, 2.45759E-02) ( 3.82735E-02, 1.69332E-02) ( 2.80843E-03,-4.48472E-02)

```
4 21 (5.43082E-09, 4.21344E-10) (-5.31948E-02, 5.41894E-02) (6.93420E-02, -5.23258E-02) 4 (4.26783E-09, -1.10526E-09) (-1.88715E-02, 5.16187E-02) (3.50849E-02, -6.44185E-02)
```

## F.2 The file "mesphe.dat" for the mesh generator

## (From Section 6.1)

The following file is read by the 3D mesh generator and it is self-explanatory - see also Fig.6.1 and discussion above. All elements are assumed to have the same material properties. The total number of elements in the produced mesh is  $12 \times 12 \times 6 = 864$ .

```
Number of elements in r, \theta, and \phi directions
12 12 6
D, D+R (in meters)
1.0 2.2
\theta_{min}. \theta_{max} (in degrees)
3 177
\phi_{min}. \phi_{max} (in degrees)
Boundary constrain labels for the two spherical surfaces defined by:
D and by D+R (integers)
Boundary constrain labels for the two surfaces defined by:
\theta_{min} and by \theta_{max} (integers)
21
Boundary constrain labels for the two surfaces defined by:
\phi_{min} and by \phi_{max} (integers)
-2 -1
material properties (parameters smatrl and tmatrl)
(1.0,0.0)
            (1.0,0.0)
Normalized frequency ko
1.88495
```

<sup>4 27 (3.03430</sup>E-09,-2.14849E-09) (3.56516E-03, 4.15090E-02) (3.97172E-03,-6.34236E-02)

### REFERENCES

- [AutoCAD-88] AutoCAD, REFERENCE MANUAL, Release 10, Autodesk Inc., 1988.
- [Balanis-89] Balanis C.A. Advanced Engineering Electromagnetics, John Wiley & Sons, 1989.
- [Balfour-79] Balfour A. and Marwick D.H. Programming in Standard FORTRAN 77, North Holland, 1979.
- [Bayliss-82] Bayliss A., Gunzburger M. and Turkel E. "Boundary Conditions for the Numerical Solution of Elliptic Equations in Exterior Regions", SIAM Journal on Applied Mathematics, vol.42, no.2, 430-451, April 1982.
- [Berk 56] Berk A.D. "Variational principle for electromagnetic resonators and wave-guides", IRE, Trans. on Antennas and Propagation, AP-4, 104-111, April 1956.
- [BCSLIB-EXT-89] The Boeing Extended Mathematical Subprogram Library, Boeing Computer Services, The Boeing Company, 1989.
- [Cangellaris-87] Cangellaris A.C., Lin C.C. and Mei K.K. "Point-Matched Time Domain Finite Element Methods for Electromagnetic Radiation and Scattering", *IEEE*, *Trans. on Antennas and Propagation*, AP-35, 1160-1173, October 1987.
- [Collins-90] Collins J.D., Jin J.M. and Volakis J.L. "A Combined Finite Element-Boundary Element Formulation for Solution of Two-dimensional Problems via CGFFT", Electromagnetics, 423-437, 1990.
- [Crowley-88a] Crowley C., Silvester P.P., Hurwitz H.Jr. "Covariant Projection Elements for 3D Vector Field Problems", *IEEE Trans. on Magnetics*, MAG-24, no.1, 397-400, January 1988.
- [Crowley-88b] Crowley C.W. Mixed Order Covariant Projection Finite Elements for Vector Fields. PhD Thesis, McGill University, Montréal, Canada, 1988.
- [D'Angelo-89] D'Angelo J. and Mayergoyz I.D. "On the Use of Local Absorbing Boundary Conditions for RF Scattering Problems", *IEEE Trans. on Magnetics*, MAG-25, no.4, 3040-3042, July 1989.

- [D'Angelo-90] D'Angelo J. and Mayergoyz I.D. "Finite Element Methods for the Solution of RF Radiation and Scattering Problems", *Electromagnetics*, vol.10, 177-199, 1990.
- [Dasgupta-84] Dasgupta G. "Computation of Exterior Potential Fields by Infinite Substraining", Computer Methods in Applied Mechanics and Engineering, vol.46, 295-305, 1984.
- [Engquist-77] Engquist B. and Majda A. "Absorbing Boundary Conditions for the Numerical Simulation of Waves", *Mathematics of Computation*, vol.31, no.139, 629-651, July 1977.
- [Emson-88] Emson C.R.I. "Methods for the Solution of Open-Boundary Electromagnetic-Field Problems", *IEE PROC*, vol.135, Pt.A, no.3, 151-158, March 1988.
- [Fusco-91] Fusco M.A., Smith M.V. and Gordon L.W. "A Three-Dimensional FDTD Algorithm in Curvilinear Coordinates", *IEEE Trans. on Antennas and Propagation*, AP-39, no.10, 1463-1471, October 1991.
- [GRAPHER-88] GRAPHER, REFERENCE MANUAL, version 1.79, Golden Software Inc., 1988.
- [Hagmann-86] Hagmann M.J. and Levin R.L. "Accuracy of Block Models for Evaluation of the Deposition of Energy by Electromagnetic Fields", *IEEE Trans. on Microwave Theory and Techniques*, MTT-34, no.6, 653-659, June 1986.
- [Hansen-81] Hansen R.C. Geometric Theory of Diffraction, IEEE Press, 1981.
- [Harrington-61] Harrington R.F. Time-Harmonic Electromagnetic Fields, McGraw-Hill, 1961.
- [Harrington-68] Harrington R.F. Field Computation by Moment Methods, Macmillan, 1968.
- [Irons-80] Irons B.M. "A Frontal Solution Program for Finite Element Analysis", Int. J. Num. Meth. Engng., vol.15, no.4, 519-536, 1980.
- [Iskander-83] Iskander M.F., Lakhtakia A. and Durney C.H. "A New Procedure for Improving the Solution Stability and Extending the Frequency Range of the EBMC", IEEE Trans. on Antennas and Propagation, AP-31, no.2, 317-324, March 1983.

- [Jin-91] Jin J.M. and Volakis J.L. "A Finite Element-Boundary Integral Formulation for Scattering by Three-Dimensional Cavity-Backed Apertures", *IEEE Trans. on Antennas and Propagation*, AP-39, no.1, 97-104, January 1991.
- [Kanellopoulos-91] Kanellopoulos V.N. and Webb J.P. "A Numerical Study of Vector Absorbing Boundary Conditions for the Finite-Element Solution of Maxwell's Equations", *IEEE Microwave and Guided Wave Letters*, vol.1, no.11, 325-327, November 1991.
- [Katz-91] Katz D.S., Piket-May M.J., Taflove A. and Umashankar K.R. "FDTD Analysis of Electromagnetic Wave Radiation from Systems Containing Horn Antennas", IEEE Trans. on Antennas and Propagation, AP-39, no.8, 1203-1212, August 1991.
- [Lee-87] Lee J.F. and Cendes Z.J. "Transfinite Elements: A Highly Efficient Procedure for Modeling Open Field Problems", J. Applied Physics, vol.61, no.8, 3913-3915, April 1987.
- [Linz-79] Linz P. Theoretical Numerical Analysis, John Wiley & Sons, 1979.
- [Lotus Manuscript-88] Lotus Manuscript, Reference Manual, release 2.1, Lotus Development Corporation, 1989.
- [Lynch-86] Lynch D.R., Paulsen K.D. and Strohbehn J.W. "Hybrid Element Method for Unbounded Electromagnetic Problems in Hyperthermia", *International Journal for Numerical Methods in Engineering*, vol.23, 1915-1937, 1986.
- [Marin-82] Marin S.P. "Computing Scattering Amplitudes for Arbitrary Cylinders Under Incident Plane Waves", *IEEE Trans. on Antennas and Propagation*, AP-30, no.6, 1045-1049, November 1982.
- [McDonald-80] McDonald B.H. and Wexler A. "Mutually Constrained Partial Differential and Integral Equation Field Formulations", Finite Elements in Electrical and Magnetic Field Problems, Chapter 9, (M.V.K. Chari and P.P. Silvester Eds.), John Wiley & Sons, 1980.
- [McDougall-89] McDougall M.J. and Webb J.P. "Infinite elements for the analysis of open dielectric waveguides", *IEEE Trans. on Microwave Theory and Techniques*, MTT-37, no.11, 1724-1731, November 1989.
- [Mei-74] Mei K.K. "Unimoment Method of Solving Antenna and Scattering Problems", IEEE Trans. on Antennas and Propagation, AP-22, no.6, 760-766, November 1974.

- [Meunier-86] Meunier G., Coulomb J.L., Salon S.J. and Krahenbul L. "Hybrid Finite Element Boundary Element Solutions for Three Dimensional Scalar Potential Problems", *IEEE Trans. on Magnetics*, MAG-22, no.5, 1040-1042, September 1986.
- [Miniowitz-91] Miniowitz R. and Webb J.P. "Covariant-Projection Quadrilateral Elements for the Analysis of Waveguides with Sharp Edges", *IEEE Trans. on Microwave Theory and Techniques*, MTT-39, no.3, 501-505, March 1991.
- [Mittra-89] Mittra R., Ramahi O., Khebir A., Gordon R. and Kouki A. "A Review of Absorbing Boundary Conditions for the Two and Three-Dimensional Electromagnetic Scattering Problems", *IEEE Trans. on Magnetics*, MAG-25, no.4, 3034-3039, July 1989.
- [Mohammadian-91] Mohammadian A.H., Shankar V. and Hall W.F. "Application of Time-Domain Finite-Volume Method to Some Radiation Problems in Two and Three Dimensions", *IEEE Trans. on Magnetics*, MAG-27, no.5, 3841-3844, September 1991.
- [Morse-53] Morse P.M. and Feshbach H. Methods of theoretical physics, part 1, McGraw-Hill, New York, 1953.
- [NDP Fortran-90] NDP Fortran USER'S MANUAL, MicroWay, Inc, April 1990.
- [Orikasa-83] Orikasa T., Honma T., Fukai I. and Washisu S. "Finite Element Method for Unbounded Field Problems and Application to Two-dimensional Taper", *International Journal for Numerical Methods in Engineering*, vol.19, 157-168, 1983.
- [Pearson-89] Pearson L.W., Whitaker R.A. and Bahrmasel L.J. "An Exact Radiation Boundary Condition for the Finite-Element Solution of Electromagnetic Scattering on an Open Domain", *IEEE Trans. on Magnetics*, MAG-25, no.4, 3046-3048, July 1989.
- [Peterson-88] Peterson A.F. "Absorbing Boundary Conditions for the Vector Wave Equation", Microwave and Optical Technology Letters, vol. 1, no. 2, 62-64, April 1988.
- [Peterson-89a] Peterson A.F. "A Comparison of Integral, Differential and Hybrid Methods for TE-Wave Scattering from Inhomogeneous Dielectric Cylinders", Journal of Electromagnetic Waves and Applications, vol.3, no.2, 87-106, 1989.

- [Peterson-89b] Peterson A.F. and Castillo S.P. "A Frequency-Domain Differential Equation Formulation for Electromagnetic Scattering from Inhomogeneous Cylinders", *IEEE Trans. on Antennas and Propagation*, AP-37, no.5, 601-607, May 1989.
- [Pinchuk-88] Pinchuk A.R. Spectrally Correct Finite Element Analysis of Electromagnetic Fields. PhD Thesis, McGill University, Montréal, Canada, 1988.
- [Rahman-84] Rahman B.M.A. and Davies J.B. "Finite Element Analysis of Optical and Microwave Problems", *IEEE Trans. on Microwave Theory and Techniques*, MTT-32, no.1, 20-28, January 1984.
- [Ramahi-89] Ramahi O.M. and Mittra R. "Finite-Element Analysis of Dielectric Scatterers Using the Absorbing Boundary Condition", *IEEE Trans. on Magnetics*, MAG-25, no.4, 3043-3045, July 1989.
- [Ramahi-91a] Ramahi O.M. and Mittra R. "Finite Element Solution for a Class of Unbounded Geometries", *IEEE Trans. on Antennas and Propagation*, AP-39, no.2, 244-250, February 1991.
- [Ramahi-91b] Ramahi O.M., Khebir A. and Mittra R. "Numerically Derived Absorbing Boundary Condition for the Solution of Open Region Scattering Problems", *IEEE Trans. on Antennas and Propagation*, AP-39, no.3, 350-353, March 1991.
- [Rheingold-91] Virtual Reality, New York: Summit books, 1991.
- [Richmond-65] Richmond J.H. "Digital computer solutions of the rigorous equations for scattering problems", *Proc. IEEE*, vol.53, 796-804, August 1965.
- [Schaubert-84] Schaubert D.H., Wilton D.R. and Glisson A.W. "A Tetrahedral Modeling Method for Electromagnetic Scattering by Arbitrarily Shaped Inhomogeneous Dielectric Bodies", *IEEE Trans. on Antennas and Propagation*, AP-32, no.1, 77-85, January 1984.
- [Silvester-77] Silvester P.P., Lowther D.A., Carpenter C.J. and Wyatt E.A. "Exterior Finite Elements for 2-dimensional Field Problems With Open Boundaries", *PROC. IEE*, vol.124, no.12, 1267-1270, December 1977.
- [Silvester-90] Silvester P.P and Ferrari R.L. Finite Elements for Electrical Engineers, Second Edition, Cambridge University Press, 1990.
- [Spiegel-68] Spiegel. M.R. Mathematical Handbook of Formulas and Tables, Schaum's Outline Series, McGraw-Hill, 1968.

- [Stratton-41] Stratton J.A. Electromagnetic theory, Chapter 1, McGraw-Hill, New York, 1941.
- [Sumbar-91] Sumbar E., Vermeulen F.E. and Chute F.S. "Implementation of Radiation Boundary Conditions in the Finite Element Analysis of Electromagnetic Wave Propagation", *IEEE Trans. on Microwave Theory and Techniques*, MTT-39, no.2, 267-273, February 1991.
- [Umanshankar-82] Umanshankar K. and Taflove A. "A Novel Method to Analyze Electromagnetic Scattering of Complex Objects", *IEEE Trans. on Electromagnetic Compatibility*, EMC-24, no.4, 397-405, November 1982.
- [Van Bladel-64] Van Bladel J. Electromagnetic Fields, McGraw-Hill, 1964.
- [Webb-81] Webb J.P. Developments in a Finite Element Method for Three-Dimensional Electromagnetic Problems. PhD Thesis, Cambridge University, England, 1981.
- [Webb-83] Webb J.P., Maile G.L. and Ferrari R.L. "Finite Element Solution of Three-Dimensional Electromagnetic Problems", *IEE PROC*, vol.130, Pt.H, no.2, 153-159, March 1983.
- [Webb-89] Webb J.P. and Kanellopoulos V.N. "Absorbing Boundary Conditions for the Finite Element Solution of the Vector Wave Equation", *Microwave and Optical Technology Letters*, vol.2, no.10, 370-372, October 1989.
- [Webb-90] Webb J.P. "Absorbing Boundary Conditions for the Finite-Element Analysis of Planar Devices", *IEEE Trans. on Microwave Theory and Techniques*, MTT-38, no.9, 1328-1332, September 1990.
- [Wilcox-56a] Wilcox C.H. "A generalization of theorems of Rellich and Atkinson", *Proc. Amer. Math. Soc.*, 271-276, April 1956.
- [Wilcox-56b] Wilcox C.H. "An Expansion Theorem for Electromagnetic Fields", Communications on Pure and Applied Mathematics, vol.9, 115-134, 1956.
- [Wolfram-88] Wolfram S. Mathematica: A System for doing Mathematics by Computer, Addison-Wesley, 1988.
- [Zienkiewicz-77] Zienkiewicz O.C. The Finite Element Method, McGraw-Hill, London 1977.